

Electronic Theses and Dissertations, 2004-2019

2018

Flutter Stability of Shrouded Turbomachinery Cascades with Nonlinear Frictional Damping

Alex Torkaman

 Part of the [Mechanical Engineering Commons](#)
Find similar works at: <https://stars.library.ucf.edu/etd>
University of Central Florida Libraries <http://library.ucf.edu>

This Doctoral Dissertation (Open Access) is brought to you for free and open access by STARS. It has been accepted for inclusion in Electronic Theses and Dissertations, 2004-2019 by an authorized administrator of STARS. For more information, please contact STARS@ucf.edu.

STARS Citation

Torkaman, Alex, "Flutter Stability of Shrouded Turbomachinery Cascades with Nonlinear Frictional Damping" (2018). *Electronic Theses and Dissertations, 2004-2019*. 6169.
<https://stars.library.ucf.edu/etd/6169>

FLUTTER STABILITY OF SHROUDED TURBOMACHINERY
CASCADES WITH NONLINEAR FRICTIONAL DAMPING

by

ALEX TORKAMAN

Bachelor of Science in Mechanical Engineering, Florida Atlantic University, 1996
Master of Science in Mechanical Engineering, University of Florida, 1997

A dissertation submitted in partial fulfillment of the requirements
for the degree of Doctor of Philosophy
in the Department of Mechanical and Aerospace Engineering
in the College of Engineering and Computer Science
at the University of Central Florida
Orlando, Florida

Fall Term
2018

Major Professor: Jeffrey L. Kauffman

© 2018 Alex Torkaman

ABSTRACT

Prediction of flutter in shrouded turbomachinery cascades is difficult due to i) coupling of aerodynamic drivers and structural dynamics of the cascade through shrouds, and ii) presence of nonlinear dry friction damping as a result of relative motion between adjacent shrouds. An analytical framework is developed in this dissertation to determine flutter stability of shrouded cascades with consideration of friction damping. This framework is an extension to the well-established energy method, and it includes all contributing factors affecting stability of the cascade such as aerodynamic excitation and the stabilizing effects of dry friction damping caused by nonlinear contact forces between adjacent blades.

This framework is developed to address a shortcoming in current analytical methods for flutter assessment in the industry. The influence of dry friction damping is typically not included due to complexity associated with nonlinearity, leading to uncertainty about exact threshold of flutter occurrence. The new analytical framework developed in this dissertation will increase the accuracy of flutter prediction method that is used for design and optimization of gas turbines.

A hybrid time-frequency-time domain solution method is developed to solve aeroelastic equations of motion in both fluid and structural domains. Solution steps and their sequencing are optimized for computational efficiency with large scale realistic models and analytical accuracy in determining nonlinear friction force. Information exchange between different domains is used to couple aerodynamic and structural solutions together for a comprehensive and accurate analysis of shrouded cascade flutter problem in presence of nonlinear friction.

Example application to a shrouded IGT blade shows that the influence of nonlinear friction damping in flutter suppression of an aerodynamically unstable cascade is significant. This is in line with previous research that has found stabilizing effects of friction damping in forced response applications. Comparison with limited engine test data shows that at observed vibration amplitudes in operation friction

damping is sufficient to overcome aerodynamic excitation of this aerodynamically unstable cascade, resulting in overall cascade stability.

Development of this method is significant because it allows analytical prediction of flutter stability in presence of nonlinear friction damping. This capability will improve design and optimization process of gas turbine critical components, leading to more efficient and robust designs that ultimately increase engine efficiency and improve durability.

I would like to dedicate this work to my family.

ACKNOWLEDGMENTS

I would like to thank my professors at University of Central Florida who constantly strive to provide the best learning experience for their students. I would like to specifically thank my advisor Dr. Kauffman for his support, advice, and working with me on the difficult problem of turbomachinery flutter. I would also like to thank Dr. Subith Vasu who taught me the science of Combustion, Dr. Seetha Raghavan who taught me the science of Aeroelasticity, and Dr. Jayanta Kapat who taught me the science of Turbine Aerodynamics. With the deep learning experience provided by them and other professors at UCF, I have gained new and significant insight in the field of turbomachinery.

I would like to acknowledge that this research was made possible by financial support from Power Systems Mfg., an Ansaldo Energia Company. Without PSM's financial support and technical prowess in the field of Industrial Gas Turbines, this research would not have been possible. Specifically I would like to thank Dr. Gregory Vogel, Lonnie Houck, and Chris Johnston for their support, and Steven Fiebiger and Ron Washburn (from Agilis Measurement Systems) for their technical insight and collaboration.

TABLE OF CONTENTS

LIST OF FIGURES	xi
LIST OF TABLES	xiv
LIST OF ABBREVIATIONS, SYMBOLS AND SUBSCRIPTS	xv
CHAPTER ONE: INTRODUCTION	1
1.1 Turbomachinery Flutter	3
1.2 Aerodynamic Work Interaction	7
1.3 Friction in Turbomachinery Applications	8
1.4 Motivation	10
1.5 Objectives	13
CHAPTER TWO: LITERATURE REVIEW	17
2.1 History of Flutter	17
2.2 Fundamental Influencing Factors	24
2.3 Computational Approach for Unsteady Pressure and Validation	25
2.3.1 Unsteady Euler Based Methods	27
2.3.2 Navier Stokes Based Methods	28
2.3.3 Validation with Standard Configurations	29
2.4 Fluid Domain Solution Methods	30
2.4.1 Time Domain Solution	31
2.4.2 Coupled Solutions of Fluid Structure Interaction	31

2.4.3 Mesh Morphing or One-Way Interaction.....	32
2.4.4 Frequency Domain Solution	32
2.4.5 Fourier Decomposition Method	33
2.4.6 Phase Lagged Boundary Condition.....	33
2.5 Structural Domain Solution Methods	34
2.6 Friction and Nonlinear damping	36
2.6.1 Friction Models in Turbomachinery Applications	37
2.6.2 Friction Damping Applications.....	38
2.7 Cyclic Symmetric Influence	41
2.7.1 Aerodynamic Coupling	42
2.7.2 Shrouded Blade Vibration.....	42
2.8 Hybrid Solution Methods.....	45
CHAPTER THREE: METHODOLOGY	47
3.1 Aeroelastic Formulation.....	48
3.1.1 Solution Methodology	50
3.1.2 Separation of Structural and Aerodynamic Drivers	51
3.1.3 Mass / Stiffness vs. Damping Terms	53
3.2 Solution Form	55
3.2.1 Aerodynamic Work Interaction	57
3.2.2 System Response with Aerodynamic Damping Only	57

3.3 Mechanical Work Dissipation.....	59
3.3.1 Viscous Damping.....	60
3.3.2 Non Viscous (Frictional) Damping.....	60
3.4 Nonlinear Damping Due to Dry Friction	61
3.4.1 General Friction Law	62
3.4.2 Three Step Time-Frequency-Time Domain Solution Sequence	63
3.4.3 Contact Condition Transitions from Stick to Slip.....	69
3.4.4 Work Dissipation Due To Friction.....	72
3.4.5 Equivalent Log-Decrement Damping	73
3.5 System Response with Nonlinear Damping.....	74
3.6 Cascade Stability.....	77
CHAPTER FOUR: FINDINGS	79
4.1 Application to IGT Blade.....	79
4.2 Nonlinear Damping Results	84
4.3 Stability Prediction.....	89
4.4 Trade Studies	92
4.5 Engine Test and Data Analysis	95
CHAPTER FIVE: CONCLUSION.....	103
5.1 Dissertation Contributions	103
5.2 Future Research	106

LIST OF REFERENCES 108

LIST OF FIGURES

Figure 1: a) Cantilevered compressor blades b) Shrouded turbine blades	5
Figure 2: Analytical framework for flutter analysis of shrouded cascades	15
Figure 3: 2D pitch and heave flutter model	18
Figure 4: Aeroelasticity triangle	19
Figure 5: Shrouded blade geometric features	20
Figure 6: Picture of nodal diameter patterns	21
Figure 7: Sector model using phase-lagged boundary condition	34
Figure 8: Frequency of first and second family modes	43
Figure 9: Typical analytical work flow for flutter analysis.....	49
Figure 10: Analytical framework expanded with friction damping	50
Figure 11: Force diagram of sinusoidal vibrating motion on real-imaginary plane.....	53
Figure 12: Time domain response of cascade with periodic and exponential components with only aerodynamic damping (-5% aerodynamic damping, $\omega n = 400\text{Hz}$).....	59
Figure 13: Nonlinear friction with variable normal load	63
Figure 14: Solution sequence and information exchange flow chart	64
Figure 15: Full cycle of vibration and time step division	66
Figure 16: Vibrating motion of cascade.....	67
Figure 17: In plane trajectory of relative motion with stick mode shape.....	69
Figure 18: Friction force vs. distance from steady state position	70
Figure 19: Transition from stick to slip condition.....	70
Figure 20: (a) In plane trajectory with slip mode shape, (b) Hysteresis loop	72
Figure 21: Algorithm for determining system response and stability	76

Figure 22: System response with linear damping and total damping	77
Figure 23: FEM model of one blade/disk sector	80
Figure 24: First torsional sixth nodal diameter mode shape of the coupled cascade with shrouds interlocked under operating loads	81
Figure 25: Typical aerodynamic log-decrement damping vs. nodal diameter	82
Figure 26: In plane relative motion for multiple values of γ	83
Figure 27: Out of plane motion and contact normal load for multiple values of γ	83
Figure 28: (a) Friction force (b) Incremental distance (c) Incremental work dissipation with small amplitude	85
Figure 29: (a) Friction force (b) Incremental distance (c) Incremental work dissipation with large amplitude	86
Figure 30: Hysteresis loop for (a) Small (b) Medium (c) large amplitudes	87
Figure 31: Non-viscous or frictional work per cycle as a function of amplitude.....	87
Figure 32: non-viscous mechanical damping as a function of amplitude	88
Figure 33: Total system damping as a function of amplitude	89
Figure 34: Cascade stability map for case C.....	91
Figure 35: Cascade response with perturbation amplitude in C1, C2 and C3 sub-cases	92
Figure 36: Total system damping with three aerodynamic damping values	93
Figure 37: Total system damping with three tangential stiffness values	94
Figure 38: Total system damping with three coefficient of friction values	95
Figure 39: Tip timing instrumentation with multiple probes around the cascade.....	96
Figure 40: Cascade response at maximum power.....	96
Figure 41: Cascade time domain response.....	98
Figure 42: Frictional damping with observed engine amplitude	99

Figure 43: Contact surface condition after removal from engine	99
Figure 44: Comparison of numerical results with experimental data	101
Figure 45: Novel aspects of flutter analysis framework	105

LIST OF TABLES

Table 1: Percentage difference between numerical results and mean engine data	101
---	-----

LIST OF ABBREVIATIONS, SYMBOLS AND SUBSCRIPTS

Abbreviations

CFD	Computational fluid dynamics
CO	Carbon Oxide
DOF	Degrees of freedom
EPFL	Ecole Polytechnique Federale de Lausanne
FEM	Finite element modeling
FFT	Fast Fourier transfer
FSI	Fluid-structure interaction
HCF	High cycle fatigue
IBPA	Inter-blade phase angle
IGT	Industrial gas turbine
KE	Kinetic energy
NO _x	Nitrogen Oxide(s)
RPM	Rounds per minute
SDOF	Single degree of freedom
STCF	Standard test configuration

Symbols

a	Distance between aerodynamic center and shear center divided by chord length b
b	Chord length
c	Viscous damping for a SDOF system
$[C]$	Viscous damping matrix
ΔE_{pc}	Change in cascade energy per cycle of vibration
f	Frequency of vibration
$\{F_{AD}\}$	Complex aerodynamic force vector
$\{F_{Con}\}$	Nonlinear contact force vector
$\{F_{StSt}\}$	Steady state force vector
F_{Nor}	Total contact normal load
F_{Fri}	Total contact in plane friction load
h	Plunge motion
i	$\sqrt{-1}$
k	Reduced frequency
$[K]$	System stiffness matrix

K_e	Kinetic energy
K_{Tan}	Contact tangential stiffness
L	Characteristic length
$[M]$	System mass matrix
N	Number of time steps for third solution step
N_b	Number of blades in the cascade
N_{cyc}	Number of vibration cycles
N_d	Nodal diameter
s	Distance along contact path in plane trajectory
δs	Incremental distance along the contact trajectory
S_t	Strouhal number
T	Period of oscillation
t	Time variable
Δt	Time step duration for third solution step
V	Fluid velocity
ΔW_k	Incremental work dissipation during time step k
W_{pc}	Total mechanical work per cycle
x	Peak amplitude of SDOF system

$\bar{\alpha}$	Global amplitude parameter
α_0	Initial perturbation amplitude
β	Log-decrement damping valid for one cycle only
$\bar{\gamma}$	Amplitude parameter
δ	Log-decrement damping
ξ	Critical damping ratio
$\{\eta\}$	Displacement variable vector
θ	Mode shape vector
μ	Friction coefficient
ρ	Fluid density
σ	Slip condition indicator
$\{\varphi\}$	Natural mode shape
ω	Angular frequency

Subscripts

aer	Aerodynamic
cn	Cycle number
cri	Critical
exp	Exponential

fri	Frictional
l	Index of time step in solution step 3
n	Natural
per	Periodic
pre	Prestressed
slp	Slip mode shape
sta	Static
stk	Stick mode shape
tot	Total
vis	Viscous

CHAPTER ONE: INTRODUCTION

Gas turbines are used extensively in aerospace and power generation industries to convert large amounts of fossil fuels into usable mechanical power to propel airplanes and power electrical generators. Due to their extensive use, even a small increase in the rate of conversion efficiency can have large impact on overall consumption of fossil fuels.

Associated technologies such as internally cooled components and advanced materials and coatings have developed at an accelerated rate over the past 70 years since the inception of first generation gas turbines. Advances in analytical and design methods have also taken place, made possible by emergence of computers and near exponential increase in computational power. Modern day gas turbines feature much higher efficiency and durability compared to their predecessors, made possible by usage of analytical and computational methods such as CFD and FEM during design process.

Despite all advances to date, both aerospace and power generation industries face continuous market demand for increased efficiency, higher output, and lower costs. Recent awareness about the effects of greenhouse gases such as CO₂ on the earth atmosphere has increased the demand for more efficient gas turbines, in an attempt to reduce production of greenhouse gases. Increased environmental regulations have placed strict caps on emissions of harmful byproducts of combustion such and NO_x and CO, requiring advanced combustion system technologies to meet these regulations.

With the above considerations, the focus of gas turbine industry is to cost effectively optimize and improve current and future designs to achieve even higher efficiency and lower emissions. Gas turbine optimization at cycle level and component level is an ongoing effort, with major OEM's historically offering improved designs in 10-15 year long cycles. Several strategies are used for increasing engine efficiency and output, such as increase in turbine inlet temperature, increase in compressor and turbine efficiency, and increase in mass flow through the engine. Each stage of compressor and turbine is comprised of a static and a rotating cascade, and it is optimally designed to achieve highest possible

aerodynamic efficiency and flow capacity. However, design of turbomachinery cascades is a delicate multi-constrained problem that is often over constrained. Each parameter affecting aerodynamic efficiency also has an impact on structural integrity or other design requirements, therefore making the design function of multiple competing considerations. As an example, stage maximum solidity (maximum metal to air ratio) is a well known parameter that impacts both aerodynamic and structural objectives. Reducing solidity provides aerodynamic benefits by reducing flow blockage; however, it also reduces cross sectional area and stiffness of a rotating component, adversely affecting multiple structural issues. Therefore optimization of aerodynamic efficiency is directly (and often adversely) related to optimization of structural and durability requirements.

Multiple issues play a prominent role in structural design and durability of turbomachinery cascades, such as creep and plasticity, vibration and dynamics, and thermally induced fatigue and crack growth. Most of these phenomena have been researched over many years of gas turbine development and are well understood. By correlating test data from laboratory measurements with analytical models simulating the physics of the problem, methods have been developed and are currently available to properly design cascades and avoid most of these failure modes. Vibration and dynamics is one of the more difficult issues in design of new cascades, and itself includes two major categories: forced response (or engine order vibration), and self-induced vibration also known as flutter. Cascade instability due to flutter is amongst the least understood and most difficult phenomenon to predict, mostly due to coupling and interaction between aerodynamic and structural forces and difficulty in reproducing a fully representative environment for testing. It is also a substantially consequential issue in case of an unsuccessful design that can adversely affect development cycle of a new product due to cost and schedule impact associated with redesign or an engine failure.

Therefore proper design for (avoidance) of flutter is a high priority design objective in development of new turbomachinery cascades. While many tools have been developed over years with varying levels

of sophistication and computational efficiency, there is still a need to increase the accuracy of current flutter analysis methods for shrouded cascades.

In addition to design of new engines, another method to meet market demands of the future is to upgrade and optimize existing engines. This method is less capital intensive due to the large investment required for construction of new engines, especially in the IGT field. A typical path to more power output and more efficiency with minimal investment in new casting tooling is to increase engine mass flow and / or turbine inlet temperature of an existing engine, without major aerodynamic redesign of the cascades. Increase in turbine inlet temperature, however, is contradictory to emissions objectives since increasing flame temperature leads to increased NO_x production and regression on environmental objectives. Increase in engine air flow remains one viable path to achieving market demands for cleaner and more efficient power, but challenges with accurate prediction of flutter and aeroelastic instability of shrouded cascades remain. These challenges relate to destabilizing effect of increased mass flow on flutter boundaries, and accurate prediction of these boundaries which is the primary focus of this dissertation.

1.1 Turbomachinery Flutter

Aeroelasticity is the science of studying the interaction between aerodynamic forces and elasticity of the structure, i.e., deflection due to applied force. There are three major branches in aeroelasticity that have significantly contributed to understanding the underlying physical phenomenon and resolving associated design issues in aerospace structures and turbomachinery. This classification is mainly based on the nature of the applied aerodynamic loads.

- i) Static aeroelasticity is the interaction between static (steady state or zero-frequency) aerodynamic forces (such as steady state lift and moment on an aircraft wing), and the structure's response (bending, twist, or deflection in general). In-flight mean deflection of an aircraft wing due to lift and moment of a steady air stream is an example of static

aeroelasticity problem. Static aeroelasticity is also concerned with the feedback loop between control surfaces, structural deflections, and “as deflected” lift and moment. These issues can cause flight control anomalies such as control reversal of wing ailerons.

- ii) Dynamic aeroelasticity or flutter is the interaction between dynamic (unsteady or time variable) aerodynamic, inertia, and elastic forces. In-flight vibration of an aircraft wing, or buffeting, is an example of dynamic aeroelasticity phenomenon. Since flutter can result in catastrophic failure of aerospace structures, significant analytical efforts are spent to understand and avoid it. Due to complexity of flutter, it has been an on-going research field in aerospace structures.
- iii) Turbomachinery flutter is a subset of dynamic aeroelasticity that is concerned with flutter of compressor and turbine cascades in turbomachines. Such cascades are typically comprised of a number of identical airfoils assembled on a rotating flexible disk. The airfoils may be cantilevered style supported only at the root as shown in Figure 1 (a), or they may feature part span and/or full span shrouds as shown in Figure 1 (b). The shrouds provide additional contact between airfoils at part span or full span. The nature of aerodynamic loads in turbomachinery flutter is harmonic (repeating pattern) due to continuous passing of rotating airfoils, known as blades or buckets, in front of repeating passages formed by upstream stationary airfoils, known as vanes or nozzles.



Figure 1: a) Cantilevered compressor blades b) Shrouded turbine blades

There are many similarities and differences between aeroelastic characteristics of an isolated aircraft wing and a cascade of airfoils. Therefore the science of turbomachinery flutter has grown in parallel, but separate from the science of aircraft wing flutter.

Similarities include flexible airfoil(s) in a high velocity fluid stream where unsteadiness and turbulence associated with the fluid interacts with structural dynamics of the structure by exciting one or more of the structure's natural mode shapes.

The differences include multiple aspects than mainly relate to repeating passages and annulus nature of the flow in turbomachinery applications. One is the difference between incoming airstream in isolated wing versus the flow in cascades. An isolated wing is typically subjected to a steady airstream as an input boundary condition. This steady air stream may interact with motion of the wing, but it is steady before reaching airfoil leading edge. In a cascade, incoming air stream is inherently unsteady and turbulent due to flow passing through upstream passages. This unsteady flow is in form of repeating waves of velocity and pressure profiles that oscillate between minimum and maximum values, associated with trailing edge and center of upstream passages as the rotor turns and airfoil moves from one passage to the next.

Another differences between turbomachinery flutter versus wing flutter is the aerodynamic and structural influence of neighboring airfoils in the cascade. In shrouded cascade, coupling caused by contacting shrouds and traveling wave pattern of vibration are a major influencing factor. Nonlinear friction

and contact between adjacent blades introduce additional difficulty in shrouded cascade flutter. Friction related problems are typically researched in forced response applications due to relative simplicity compared to flutter.

While forced response and flutter have many commonalities as aeroelastic instabilities, there are also distinctive differences. Forced response is response of a structure to an external forcing function. Therefore, frequency and magnitude of the excitation (forcing function) are external to the structure. They are either known or can be readily calculated. Accurate prediction of natural frequency is the most important aspect of the analysis in a forced response analysis because of sharp slope of response in the vicinity of resonance, where the ratio of forcing frequency to natural frequency determines margin to resonance. Flutter is response of a structure due to self-induced excitation. Therefore it always happens at the resonance and margin to resonance is by definition zero (forcing frequency = natural frequency). In a flutter analysis, total system damping is the most important parameter that determines system stability and response. Total system damping is related to imaginary forces in equations of motion, and is associated with work interaction within the system. If a system has a total damping that is negative in value, in a mathematical sense it is equivalent to an ever expanding exponential function. Therefore such a system would be mathematically unstable. In practice, value of damping is not a constant number and it depends on instantaneous work interaction within the system. Total system work interaction can be attributed to aerodynamic work interaction caused by energy exchange between the fluid and the structure, and mechanical dissipation within the structure as a result of vibrating motion. Therefore sum of both components of total work interaction and not any single one of them alone determines overall cascade response and stability.

As the primary focus of this dissertation is overall stability of shrouded cascade, both components of work interaction are explored in detail to aid in development of a new analytical framework for flutter stability. Aerodynamic work interaction is briefly discussed in section 1.2 and in more details in 2.3 and

2.4. Similarly, mechanical dissipation due to friction is discussed briefly in sections 1.3 and in details in 2.6 and 2.7.

1.2 Aerodynamic Work Interaction

The most prominent indicator of aeroelastic instability in turbomachinery cascades is the work interaction between the fluid and the structure. If the fluid extracts work from the structure, any motion resulting from an initial perturbation of the structure will be damped by combination of work extraction by the fluid and work dissipation within the structure. Therefore, there are no concerns regarding self-excitation and such a cascade is fully stable.

If the structure extracts work from the fluid, on the other hand, any small perturbation has the potential of becoming an uncontrolled catastrophic failure due to the following mechanism. After a small vibrating motion initiates as a result of an initial perturbation, small amount of energy is extracted by the structure from the fluid over one full cycle of oscillation. The fluid has near infinite supply of energy due to moving stream of the flow; therefore impact on the fluid from this phenomenon is minimal and unnoticeable. On the structure side, the system has a limited capacity for storing energy in form of vibrating motion and associated kinetic and elastic energies. During each half cycle of vibration, this stored vibratory energy in the structure undergoes transformation from kinetic energy (associated with mass and velocity of the structure) to elastic energy (associated with spring like elastic deflection of the structure). When small amount of work is extracted from the fluid over a full vibration cycle, this work adds to the existing system energy and carries over to the next cycle such that the subsequent cycle will have slightly more energy stored in the system. As a result, velocities and deflections associate with the vibrating motion increase slightly in amplitude. Since aerodynamic work interaction is itself a function of amplitude of motion, increase in amplitude over previous cycle results in slightly more energy extraction during each subsequent cycle. This trend continues with each cycle and not only the initial vibrating motion due to perturbation

does not die down, its amplitude increases over each cycle as more energy gets extracted from the fluid and stored in the structure with increasing vibration amplitude. If the energy continues to accumulate within the structure as the vibration amplitude increases by each cycle, eventually vibratory stresses that are related to vibration amplitude will exceed the material HCF capability and result in premature blade failure during operation.

Blade failure in turbomachinery is a catastrophic event and its avoidance is a first tier design requirement above and beyond any other design objective. Any single blade failure is immediately accompanied by failure of the entire cascade and any downstream cascades due to restricted spacing between components and large inertia associated with the rotor assembly and high operating RPM. This event will likely result in loss of the engine or some of its major components, catastrophic damage to nearby components and structures, and loss of propulsion power in case of aerospace engines.

Therefore significant engineering effort is invested in making flutter free turbomachines. Accurate prediction of the aeroelastic interaction between the fluid and the structure and aerodynamic stability of cascade has been the subject of much research and progress, which will be outlined in section 2.2 through 2.4. Despite this progress, difficulties still exist in predicting accurate flutter boundaries in shrouded cascades due to complexity associated with friction and nonlinearity. Another difficulty is lack of a fully representative test rig that includes all complicated and influencing factors associated with shroud contact and vibrating pattern of the rotating cascade during operation.

1.3 Friction in Turbomachinery Applications

Underlying physical phenomenon that causes flutter can be summarized as energy (or work) extraction by the structure from the fluid. However, aerodynamic work interaction is not the only determining factor in occurrence of flutter. In practice, some cascades may have a slight amount of negative

work interaction with the fluid (aerodynamic excitation), but have enough mechanical damping present to overcome the energy extracted from the fluid and dampen the motion associated with an initial perturbation.

A mechanical system in absence of any fluid interaction is always self-damping. When fluid interaction is introduced in a vibrating airfoil, work on the structure by unsteady pressure and surface velocity of the airfoil maybe either negative or positive. If aerodynamic work interaction is negative (i.e., the structure does not extract but dissipates energy into the fluid), net aerodynamic effect over a full cycle is dissipative. In this case, aerodynamic damping is positive and it increases damping effects of the mechanical damping. This condition is obviously the most desirable in a cascade design but due to multiple other design objectives it is not always possible. Such competing objectives may include aerodynamic efficiency of the cascade, weight target, or other specific design requirements.

In the case of such aerodynamically unstable cascade, the outcome of cascade stability in addition to aerodynamic work interaction depends on the magnitude of mechanical work dissipation as a result of vibrating motion of the structure. If the magnitude of mechanical dissipation exceeds the magnitude of aerodynamic excitation resulting from an initial perturbation, the vibrating motion will be damped and eventually die out. If the magnitude of aerodynamic excitation exceeds the magnitude of mechanical dissipation, energy begins to accumulate within the structure and the amplitude of motion increases by each cycle. As energy is stored and vibration amplitude increases, eventually vibratory stresses that are related to vibration amplitude will result in blade failure.

Therefore when a cascade design is aerodynamically unstable, mechanical damping and its magnitude is the determining factor in cascade stability. Two sources of mechanical damping are identified in literature.

- i) Internal material damping is known as viscous damping and it is treated as an inherent property of material. This component of mechanical damping is represented by linear damping matrix $[C]$ in equations of motion. In a SDOF system, damping ratio is defined

as the ratio of system damping to critical damping where a vibrating system transitions to fully damped system.

- ii) Dry friction damping is the result of relative rubbing motion and friction between surfaces that are in contact, also known as non-viscous or Coulomb damping. This component of mechanical damping is much more complicated and it is a property of contact interface material as well as operating conditions such as loads acting on the contact. Furthermore, due to inherent nonlinearity of friction, dry friction damping is a nonlinear function of displacement and amplitude of vibration. Introducing nonlinearity significantly complicates all aspects of already complicated aeroelastic equations of motion, to the point that nonlinear friction damping is typically omitted from flutter related analytical work flow or approximated by a constant value. Neither representation is adequate in fully predicting cascade stability boundaries, as it will be shown in this dissertation.

1.4 Motivation

To meet future market demands, current turbine design trends are towards higher cycle efficiency and power output by means of increased mass flow through the engine and more efficient turbine stages. These trends are therefore moving towards taller, thinner, and highly loaded blade designs. All of these design trends also have destabilizing effects on cascade flutter stability. Design challenges are always exacerbated on the last stage turbine blade since the expansion path of the primary flow through the turbine naturally makes the last stage the tallest blade with the lowest natural frequency. Last stage also has a high pressure ratio, which provides for a highly loaded blade with transonic exit velocity. Due to low natural frequency and high fluid velocity, last stage turbine and first stage compressor blades have historically been susceptible to aerodynamic instabilities such as flutter and limit cycle oscillation. Most significant design and operating parameters influencing flutter boundaries are natural frequency of the blade, and fluid

velocity. Therefore, with taller (lower frequency) and highly loaded blades (higher exit velocity), current industry trends constantly approach (and sometimes exceed) experimentally established flutter limits.

Over many years of gas turbine development, tools and methods have been developed and used extensively to design for (avoidance) of aerodynamic instabilities. However, major issues still exist with these tools since they are mostly empirical based and cannot definitively predict occurrence of flutter. Existing tools are based on linearized structural and aeroelastic equations, and they only consider aerodynamic work interaction. Mechanical damping is a major complicating factor that is not included in current flutter analysis methods. Full consideration of mechanical damping requires analysis of cyclic symmetrical cascade structure with nonlinear shroud friction force and time varying shroud contact normal force, which is not possible for large scale models with methods currently available. Therefore current flutter analysis methods lack fidelity in accurately predicting flutter boundaries with consideration of all influencing parameters.

Due to the catastrophic nature of an engine failure resulting from flutter (with capital loss associated with a single event often in tens of millions of dollars, in addition to redesign costs, brand damage, etc.), there is an overriding design requirement to avoid any such event. Since current analytical tools and methods cannot fully predict flutter boundaries and the associated risk of high cycle fatigue, validation of new designs is typically accomplished in the operating environment of an engine via costly instrumentation and testing campaigns. At this stage of project, when the new design is developed and tested in an engine, major expenses associated with engineering and procurement cycle have already been incurred in design and manufacturing of the hardware. If flutter problems are discovered at this stage, major schedule impact and redesign expenses are involved. Therefore, there are strong financial incentives in the industry to detect and diagnose any potential flutter issues in design stage of a project (when changes can be made much more cost effectively) and not during the validation phase.

With cascade design trends approaching and sometimes exceeding experimentally established flutter boundaries, there is a need for an accurate analytical tool to achieve the above goal and avoid large expenses associated with a non-successful product. Such tool must be capable of considering all factors involved in this complex phenomenon and ensure flutter free operation of the cascade while simultaneously allowing for optimization of all other objectives and requirements.

Despite this need, there is much complexity associated with flutter prediction of shrouded turbine blades that has prevented development of a fully inclusive analytical tool. From aerodynamic perspective, there are many challenges associated with accurate prediction of unsteady pressure around the vibrating blade and the mutual effects of the structure and the fluid on each other and on the work relationship between the two domains. With most of research in flutter focused on aerodynamic aspects, many of these challenges have been overcome over past 20 years and currently there are reliable and computationally efficient methods available to determine aerodynamic work interaction.

In case of shrouded blades (full or part span) another complexity that affects stability of the cascade is presence of the shrouds which form a continuous, interlocked ring around the blades during operation. The resulting cyclic symmetric structure created by the disk, blades, and the ring of the interlocked shrouds is subject to traveling wave phenomenon and vibration in distinct nodal diameter patterns (see Figure 6). Aerodynamic and mechanical aspects of the cascade flutter are related to the particular nodal diameter mode of vibration and can mutually affect each other through frequency, mode shape, and amplitude of vibration. There are also the complexities associated with nonlinear friction forces between neighboring blades in the cascade. Inclusion of nonlinearity in equations of motion presents a great difficulty in solving these equations since most available methods for solving vibration and aeroelastic problems are linear.

In addition to general nonlinearity caused by friction, there are other complexities with shrouded cascade flutter that need to be considered for a complete formulation of the physical phenomenon. These factors include the following:

- Contact interface loads acting on contact surfaces, their variations during the vibration cycle and effects on friction force
- Stick-slip condition at the contact interface between adjacent shroud tips and its influence on cascade mode shape
- Influence of variations in contact parameters (such as tangential stiffness and coefficient of friction) on cascade stability

While there has been much recent research and progress in the science of flutter prediction, most have focused on aerodynamic work interaction. Mechanical damping is either entirely ignored or represented by a constant value in flutter application. Mechanical damping in turbomachinery has been mostly researched in the context of forced response analysis, which is a simpler problem than flutter because frequency and amplitude of external drivers are known. It has been shown in forced response research that mechanical damping is not constant and system response varies based on amplitude of drivers.

Therefore, full consideration of nonlinear mechanical damping in a flutter application will enable more accurate prediction of cascade stability, which is not possible with current analytical method. The objective of this dissertation is to create an analytical framework that eliminates this limitation with current method, as discussed in details in section 1.5.

1.5 Objectives

Considering the shortcomings of current state of the art flutter prediction method for shrouded cascades, there is a strong benefit in developing a more advanced method that is capable of including all of the complicating factors affecting the overall cascade stability.

Overall objective of this dissertation is to create a framework of analysis for determining cascade stability with consideration of aerodynamic work interaction, shroud coupling, nonlinear friction damping,

and related factors. However, due to enormous complexities associated with this problem, the overall objective is divided into four related objectives which collectively enable the above goal.

Objective 1: Develop a method to evaluate mechanical work dissipation associated with friction forces at the shroud during a single vibration cycle for arbitrary amplitude. This method must take into consideration nonlinear stick-slip condition at the interface which is amplitude dependent, in addition to time variability of contact forces between the adjacent blades during the vibration cycle. Development of this method enables calculation of work dissipation within the cascade during one cycle and increase in kinetic energy of next cycle. Details of development of this method are discussed in section 3.4.

Development of this method is also one novelty aspect of this dissertation. While flutter problem with nonlinear friction has been researched before with under-platform dampers and SDOF models, no prior research is conducted with effects of friction damping on shrouded cascade flutter and with large scale models. Under-platform damper is a simpler problem because operating loads on the dampers are constant (centrifugal loads due to rotation). Shrouded blade friction is more complicated problem as it will be discussed in section 2.7, with variations of contact normal load during the cycle of vibration and contact condition effects on the mode shape.

Objective 2: Develop a framework for calculation of flutter stability based on combined time and frequency domain solutions to fluid and structural models, and overall work exchange of the system. This framework considers both aerodynamic work interaction and mechanical damping as calculated in objective 1 to evaluate amplitude of vibration during multiple cycles based on net energy in or out of the cascade and determine cascade stability.

This objective is another novelty aspect of present dissertation. While the aeroelastic analysis aspect of this method is currently available, the existing method can only consider linearized system damping for shrouded cascades. Novelty aspect in this dissertation is that the additional work flow

highlighted in red box in Figure 2 enables consideration of nonlinear frictional damping, which is shown to be significant.

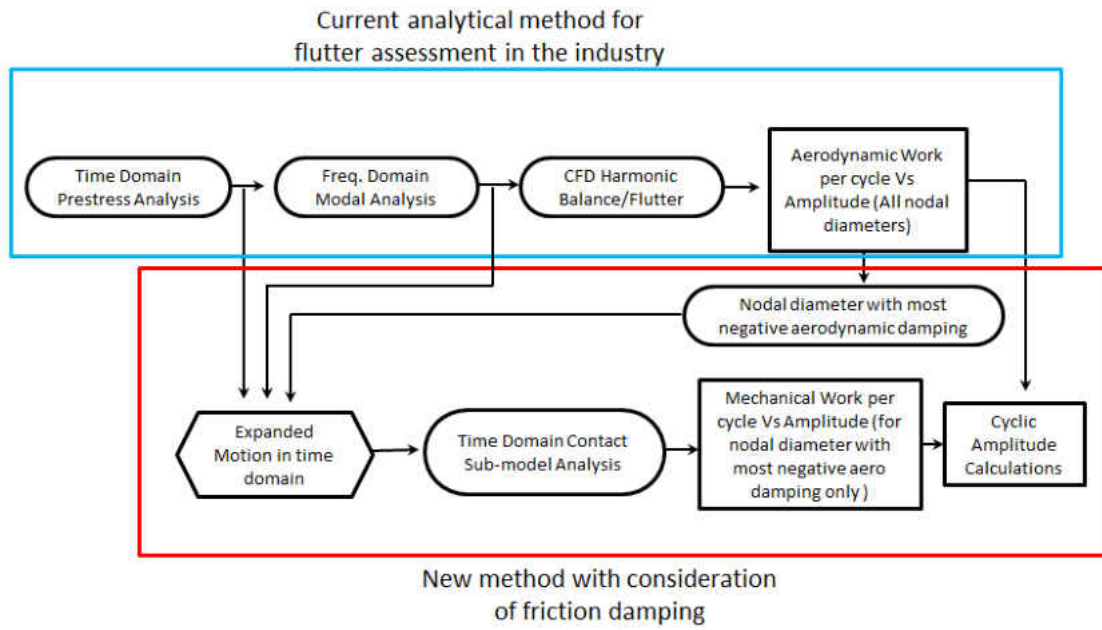


Figure 2: Analytical framework for flutter analysis of shrouded cascades

This objective is discussed in detail in chapter 3.5.

Objective 3: Apply this method to a large scale, full fidelity analytical model of an actual IGT component. Show information exchange and intermediate steps that are involved to illustrate inputs and outputs of each step. Purpose of this objective is to demonstrate applicability of this method to a real life case with reasonable computational time, and it is discussed in detail in section 4.

Addressing this objective requires use of a blade design for computational domain since all analytical steps are numerical and highly dependent on geometry. A model of an actual last stage IGT blade, proprietary of Power Systems Mfg. has been used for this purpose. Tip timing data of engine validation testing of this blade are available, however an organized flutter response was not observed in the operating range of the engine during the test. Therefore the data is of limited use for establishing exact

stability limit since cascade was always stable. Despite limitations, data will be used as much as possible to correlate with analytical predictions.

Objective 4: Conduct trade study of contact interface parameters such as tangential stiffness and coefficient of friction to demonstrate impact of each on overall aeroelastic stability of the system. Prior research into contact interface parameters shows that a wide tolerance band can be expected, and its influence on the response is often significant. Purpose of this objective is to allow cascade designers to understand contact parameter effects and make adjustments in the design phase as desired by proper selection of interface material and coating.

CHAPTER TWO: LITERATURE REVIEW

Flutter is a complex interaction between aerodynamic and structural forces, resulting in excessive vibration amplitude and catastrophic failure in some instances. Much research has been conducted to understand this phenomenon in general and in turbomachinery applications in particular. A major complicating factor in flutter research is the unsteady and nonlinear nature of underlying physics. Another factor is the difficulty in producing fully representative conditions in laboratory environment for research. Despite difficulties, much progress has been made in developing and expanding the collective understanding of this phenomenon within the research community and the turbomachinery industry, which is explored in this section.

2.1 History of Flutter

An oscillating object in a moving flow field was first studied in details in 1878 when Vincenc Strouhal experimented with wires vibrating in the wind [1]. Based on his observations, he developed a non-dimensional parameter known as Strouhal number, which is still used today as a trending parameter for flutter evaluation [2].

$$St = \frac{fL}{V} \quad (1)$$

Where St is the Strouhal number, f is the frequency of oscillation, L is the characteristic length of the object such as diameter of a cylinder, and V is the fluid velocity.

Earliest occurrences of flutter phenomena in modern machinery were observed in early days of aviation, where air plane wings or control surfaces would vibrate violently at high air speeds resulting in premature failure. Many experiments and studies were conducted to understand and prevent flutter of aerospace structures, which was a major barrier to achieving higher air speeds. Simplified 1D torsional and

2D “pitch and heave” aeroelastic models (Figure 3) were developed to study single mode or coupled bending torsion flutter.

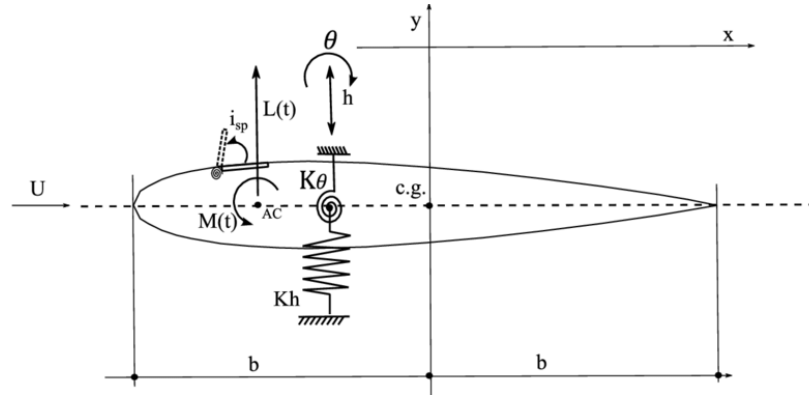


Figure 3: 2D pitch and heave flutter model

Theodorsen developed a general relationship between airfoil motion and unsteady lift and pitching moment as a derivation of Bessel function solutions [3]. Resulting equations correlate unsteady lift and moment on the airfoil with its pitch and heave motions and their derivatives as follows [4]:

$$Lift = \pi \rho b^2 [\dot{h} + V \dot{\theta} - b a \ddot{\theta}] + 2 \pi \rho V b C(k) [\dot{h} + V \theta + b \left(\frac{1}{2} - a\right) \dot{\theta}] \quad (2)$$

$$Moment = \pi \rho b^2 \left[b a \ddot{h} - V b \left(\frac{1}{2} - a\right) \dot{\theta} - b^2 \left(\frac{1}{8} + a^2\right) \ddot{\theta} \right] + 2 \pi \rho V b^2 \left(a + \frac{1}{2}\right) C(k) [\dot{h} + V \theta + b \left(\frac{1}{2} - a\right) \dot{\theta}] \quad (3)$$

Where θ and h are pitch and heave motion and their derivatives, ρ is fluid density, V is air speed, b is half chord, product of $b.a$ is the distance between half chord and shear center of the airfoil, and $C(k)$ is a complex function known as Theodorsen's function. Development of Theodorsen's equation was an important milestone in flutter research since it created a closed form function of the unsteady forces acting on the airfoil for use in future research.

Flutter was formally defined by Collar [5] as the interaction between aerodynamic, inertial and structural forces. This definition is still widely in use today. Figure 4 shows this interaction as a triangle

where corners represent those forces and its sides represent mechanical disciplines concerning the forces on either end of it. Flutter, also known as dynamic aeroelasticity, is represented by the area of the triangle as it involves all three corners and sides.

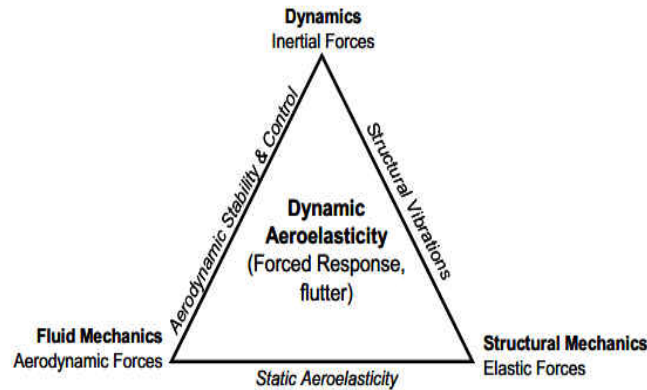


Figure 4: Aeroelasticity triangle

Turbomachinery flutter is a branch of flutter that involves rotating or static airfoils in a turbine or compressor cascade. This phenomenon is often encountered during testing of tall and slender airfoils such as first stage fan blades and last stage turbine blades [6, 7]. While much research has been conducted to understand and predict turbomachinery flutter, this research is still an on-going effort due to complexities associated with this phenomenon. There are multiple complicating issues that historically make turbomachinery flutter more complex than aircraft wing flutter.

One issue is the interaction between different airfoils in the cascade that makes determination of total unsteady forces much more difficult than an isolated airfoil. In addition to unsteady lift and moment acting on the airfoil as a result of its own vibrating motion, combined effects of motion of all other airfoils in the cascade must also be considered for a complete understanding of the system.

Whitehead [8] developed classical methods for derivation of unsteady loads in a cascade, with the influence of each individual airfoil on itself and all others in the cascade. Isolated airfoil theories were used in conjunction with cascade relationships to develop unsteady forces on vibrating blades using potential

flow theories. Influence matrices were developed later on to account for effects of each blade on every other blade in the cascade and will be discussed in section 2.7.1.

Another complexity in turbomachinery flutter is the complicated shape of the blade due to radial twist. This twist is required for proper aerodynamic design of the blade due to radial vortex, and it prevents application of simplistic 2D aeroelastic models. A picture of a turbine blade and its geometric features including airfoil twist is shown in Figure 5. Due to this complexity, simplified models cannot be successfully applied and generally numerical methods must be used with sufficient grid density to describe complicated geometry and the flow around it.

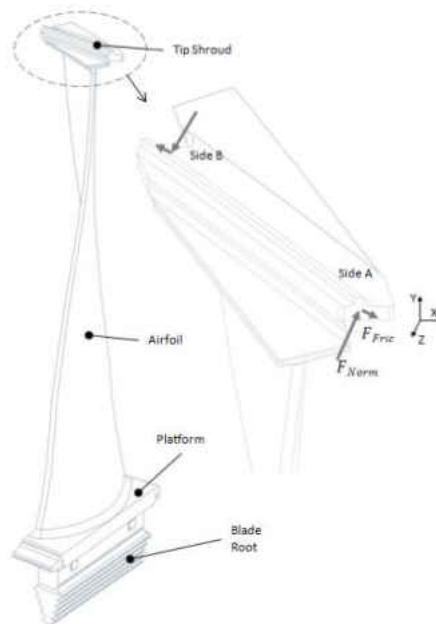


Figure 5: Shrouded blade geometric features

Another issue specific to shrouded cascades is the coupling between multiple blades during operation and resulting cyclic nature of vibration around the wheel. This phenomenon was first researched by Lane [9] and a mathematical formulation was developed to describe the relationship between nodal diameter patterns of the vibrating wheel as shown in Figure 6:

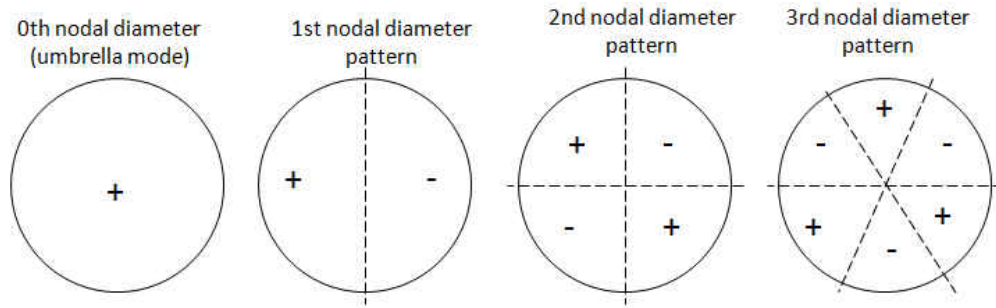


Figure 6: Picture of nodal diameter patterns

Another issue was recognition of stalled vs. unstalled flutter, and understanding the different operating conditions where each phenomenon occurred. Stalled flutter is much more likely to occur in cascade designs and operating conditions with high incident angles (higher than stall angle), where much more turbulence and vortex shedding is present due to turbulent nature of stalled flow over an airfoil. Stalled flutter is not an issue with low to moderate incident angles where flow remains attached to the airfoil over the entire suction side. Cascades with low (or moderate in some cases) incident angle are also preferred designs from aerodynamic efficiency standpoint. With proper design of airfoil aerodynamic shape and alleviating off-design conditions with techniques such as start-up bleed, modern cascades are designed to avoid operating in stall conditions where stalled flutter is likely to be a concern. Therefore unstalled flutter emerged as the major focus of industry as it remains the flutter mode that could not be avoided by simple control of airfoil incident angle.

A major breakthrough in the field of unstalled flutter research was achieved when Carta [10] researched vibrating patterns of coupled blade-disk-shroud assemblies. He used classical models of unsteady lift and moment developed by [8] and evaluated differential work over a small time step done by the fluid on the structure as a result of unsteady aerodynamic forces and vibrating motion of the airfoil. Integral of this differential work over the full cycle of vibration, or work per cycle, was interpreted as the measure of energy exchange between the fluid and the structure. Flutter initiates when sign of work per cycle integral is positive (work is extracted by the structure), or aerodynamic damping is negative. This

theory fit well with experimental observations [11], and it has since been used for flutter prediction in the industry as the “energy method”. Work extracted by the blade over each cycle is assumed to accumulate in the structure over many cycles and add to existing cascade energy which exchanges between kinetic and elastic energies twice per cycle.

While the aerodynamic energy exchange is assumed for simplicity to be the only work interaction of the cascade in [10], some energy is also dissipated over the cycle of vibration due to mechanical damping. Theoretically, the cascade is unstable with any amount of negative aerodynamic damping as the amplitude of vibration will continue to build up indefinitely. In practice, the system may stabilize slight amount of negative aerodynamic damping due to positive mechanical damping. This effect can be demonstrated by an example of a car that is accelerating by a constant force. In absence of friction, all the work done by the force would convert to kinetic energy, resulting in perpetual acceleration of the car. In presence of friction, only some of the work will convert to kinetic energy and the rest is converted to heat due to irreversible losses associated with dissipative work caused by friction. If friction force becomes equal to the constant force at some velocity, acceleration will stop and the car will reach an equilibrium velocity. The influence of mechanical work dissipation on the threshold of flutter stability is the primary focus of present dissertation and it will be fully explored in section 3.

Another major breakthrough occurred when Bolcs and Fransson [12] developed standardized airfoil geometries and test conditions for flutter research. These standards, known as STCFs, cover various cascade geometries and flow regimes (fan, compressor, turbine, subsonic, transonic, supersonic, etc.), and allow for various research teams to share and make use of other teams’ experimental and analytical results by conducting research on identical geometries and conditions. Prior to the inception of STCF, it was difficult to collaborate and use other research results due to differences in geometries and operating conditions used by different teams.

With the availability of mathematical models and experimental data, a research mechanism was established for flutter studies. Using energy method and cascade theories, total system work could be numerically determined as the sum of each blade's work due to unsteady pressure from each blade in the cascade. This work could then be compared with experimental data obtained from electro-mechanically driven, pitch only motion in a linear or annular test rig. This research mechanism has enabled great progress in improving analytical models to accurately determine aerodynamic work interaction by correlating analytical and experimental results. However, limitations still exist between motion induced in the rig test that can only be pitch motion (rotation about an axis) and the actual 3D vibrating motion of a flexible blade in the engine. Additionally, replication of exact flow conditions and traveling wave phenomenon of an actual cascade in a test rig is not quite possible. In an engine, traveling wave has endless number of passages around the full wheel and over many rotations to develop and strengthen. This phenomenon cannot be replicated in a sector rig with limited number of passages. Operating temperature and mass flow of an actual turbine stage is also nearly impossible to replicate in laboratory. Therefore, experimental research in the field of flutter is conducted using many simplifications and restrictions.

Finally, stability criterion with consideration of mechanical damping was researched by Khalak [13]. System variables were re-arranged to non-dimensionalized parameter to represent operational and design related parameters. Stability criterion was established as the ratio of mechanical damping to density parameter being larger than aerodynamic work input into the system. Mechanical damping represented in [13] is total mechanical damping from all sources, and it is assumed constant in that paper. In reality, non-viscous portion of mechanical damping is not constant when considering nonlinear nature of friction force, and it will be explored in detail in section 2.6.

2.2 Fundamental Influencing Factors

Historically, a non-dimensional parameter known as reduced frequency (similar to Strouhal Number) has been used to quantitatively assess turbomachinery airfoils for flutter.

$$k = \frac{b \cdot \omega}{V} \quad (4)$$

Therefore three major influencing factors in flutter are angular frequency of the cascade ω , semi-chord of the airfoil b , and fluid velocity V . It is well known that decrease in reduced frequency has a destabilizing effect on flutter [14]. However, this dependency is a general trend and the exact threshold where flutter occurs depends on many other parameters.

Operational aspects of the system in reduced frequency are represented by fluid velocity, which relates to cascade operating conditions such as mass flow and pressure ratio. Design aspects are represented by semi chord and natural frequency, which is itself a function of mass and stiffness characteristics of the cascade. There are other major influencing factors both operational and design related that influence flutter stability. Therefore limits based on reduced frequency approach are empirically based and are often too conservative. In other words, going over established limits does not necessarily lead to flutter initiation at all times because there are many more parameters involved that are not represented in this non-dimensional parameter.

Research by Nowinski [15] carried out at the annular rig facility at EPFL shows that in addition to reduced frequency, the location of torsional axis (in a simplified pitch only motion) plays a significant role. Three locations of torsional axis were included as a variable in experimental testing, and the results show strong correlation of aeroelastic stability with location of the torsion axis.

Follow up work by Panovsky [16] created a design method to decompose any 2D mode shape into three fundamental in-plane motions (axial, flex, and torsion) and calculate aerodynamic damping as a linear superposition of individual elements corresponding to the fundamental motions. In other words, any 2D mode shape can be decomposed into a linear combination of axial, flex, and torsional components.

Aerodynamic work per cycle can be evaluated for unit axial, flex, and torsional motions and then multiplied by corresponding coefficients of the mode shape motion components. For small magnitudes of motion, sum of aerodynamic work corresponding to three components is equal to aerodynamic work of the original mode shape. Follow up work by Kielb et. al [17] expanded this design method to cyclic symmetric applications.

Based on this work, a plot known as Tie-Dye plot [14] can be created for any particular airfoil shape and can be used as a design tool to evaluate the critical value of reduced frequency based on the location of torsion axis of the mode shape. This critical value is the value of reduced frequency below which aerodynamic damping becomes negative and flutter may initiate, depending on magnitude of mechanical damping.

Research by Waite et. al [18] shows the effects (independent from reduced frequency) of steady state operational conditions such as blade loading on flutter boundaries, which is related to thermodynamic flow conditions at the throat. Reduced frequency is kept constant in that research by artificially manipulating cascade natural frequency.

All of above progress concerns aerodynamic aspects of flutter. Mechanical aspects are mostly studied in structural dynamics and forced response analysis, as discussed in sections 2.5 through 2.7. As it will be shown, for an aerodynamically unstable airfoil mechanical damping is the most important influencing factor in determining cascade stability, and will be discussed in details in section 3.4.

2.3 Computational Approach for Unsteady Pressure and Validation

Much of flutter related research over the last decades has focused on developing accurate and computationally efficient methods to determine unsteady aerodynamic pressure around an oscillating airfoil. While steady flow assumption is often used in static aeroelasticity such as lift and drag on a wing

to simplify governing equation, unsteady flows and associated aerodynamic forces are distinguishing characteristics of turbomachinery flutter and must be fully considered for a meaningful analysis.

The nature of unsteady aerodynamic forces acting on the blade is in the form of pressure waves propagating through the fluid domain, and the resulting surface static pressure on the suction side and pressure side of the airfoil. Pressure waves on two sides of the airfoil are not always in-phase, meaning maximum magnitude of peaks and valleys on pressure side and suction side may not coincide along the chord. Therefore, at any given time instance there is a net imbalance of aerodynamic forces acting on the subject blade [19]. The magnitude and direction of this force and resulting moment about the shear center of the airfoil can be determined from magnitude and phase information of unsteady pressure acting on pressure side and suction side of the airfoil at any given time instance.

The source of unsteady aerodynamic pressure may be external to the cascade, such as blade passing frequency of an upstream cascade. In this case, the excitation frequency is predetermined by operating conditions of the engine (i.e. rotor speed and number of blades in upstream cascade). Resulting vibration patterns are referred to as “Engine Order” or synchronous vibration. Unsteady aerodynamic forces may also be the result of subject blade’s oscillating motion, or the oscillating motion of a neighboring blade in the same cascade. This type of unsteady aerodynamic load and its interaction with the structure is known as self-excitation or asynchronous vibration.

Regardless of the source, various analytical methods have been used to evaluate unsteady pressure. Most of these methods are based on Euler or Navier-Stockes equations, and they are discussed in more details in chapters 2.3.1 and 2.3.2 respectively. Classical methods based on Theodorsen’s derivations were used early on for self-excitation type problems, but these methods have many restrictions in transonic passages where turbulent flow and shock effects are dominant [20]. Since highly loaded transonic cascades are typical in modern day turbomachinery, classical methods are not used extensively in the industry due to limitations and will not be discussed here.

The time relationship between unsteady pressure and motion is known as unsteady pressure phase. While magnitude of unsteady pressure is an important parameter in determining net unsteady aerodynamic force, phase angle of unsteady pressure is recognized as an even more important parameter in [21]. The reason is that if the phase angle is favorable, even an unsteady pressure wave of large magnitude would neutralize itself by acting simultaneously in opposite directions on suction side and pressure side of the airfoil. The phase information is therefore critical in determining the unsteady force, whereas a non-desirable phase would lead to a large “net” force and aerodynamic excitation of the blade. Flutter can therefore be summarized as a result of unfavorable phase of unsteady pressure acting on the blade. Capability of any analytical method in accurately predicting phase angle distribution of unsteady pressure, especially in transonic regimes where shock location strongly affects pressure distribution along the airfoil suction side, is therefore an important consideration.

2.3.1 Unsteady Euler Based Methods

The Euler equations are a set of conservation of mass, momentum and energy equations, and they are used extensively to describe adiabatic and inviscid flows. The Euler equations are applied to both compressible and incompressible flows; however, since they are inherently inviscid their application is limited to flow regimes where viscosity effect does not play an important role.

Methods based on steady or unsteady Euler method have been developed to calculate unsteady pressures and determine aerodynamic loads with computationally efficiency. One such method is described by Marshall and Giles [22] which uses time linearized unsteady Euler equations and assumes unsteady flow to be a small perturbation to the steady flow. Unsteady flow can then be broken into different frequencies and computed individually at each frequency with a pseudo time marching algorithm. Due to its computational efficiency, this method is used in industrial applications using the aeroelastic analysis code SliQ. This code has been used to develop, validate, or compare various turbomachinery applications [23].

Another method using unsteady Euler equations is described by Ning and He [24], which also decomposes the flow into a steady and harmonic unsteady portion. This method is capable of including some nonlinear effects by strong coupling of perturbation equations and time averaged flow equations.

Despite computational efficiency of the Euler based models, their limitations in accurately predicting nonlinear aspects of transonic flow associated with vorticity and shock effects requires use of better computational technique to improve accuracy in transonic conditions which are typical in first stage compressors and last stage turbine blades.

2.3.2 Navier Stokes Based Methods

The Navier-Stokes equations are the most complex and comprehensive governing fluid equations available. They consist of conservation equations of mass, energy, and three components of momentum with full viscous and time dependent effects such as turbulence. Since the flow is too complex to solve turbulent problems from first principles even with advanced computational tools, turbulence is modeled using one of a number of turbulence models and coupled with a flow solver that assumes laminar flow outside a turbulent region. Viscosity effects can often be neglected in turbomachinery flows, as high Reynolds numbers indicate that the inertial forces are more significant than the viscous forces. However, even in high Reynolds number regimes, certain problems require that viscosity be included for better accuracy. In particular, use of viscous equations is required in problems involving calculation of net forces on bodies such as the vibrating airfoils in a cascade. Additionally, in highly turbulent flows dominated by recirculation, eddies, and randomness, viscosity effects become significant and must be included.

The Navier-Stokes equations are in general too complicated to be solved in a closed form, even for simplified airfoil geometry. Therefore they are solved using numerical methods that require large grid sizes and are computationally expensive. While methods based on Euler equations are more computationally effective, the accuracy of Navier-Stokes-based models is superior relative to the former, especially in

transonic flow regions where the effects of flow separation and shock related phenomena such as oscillation shock and shock boundary layer interaction play an important role.

Therefore many advanced studies in flutter use the Navier-Stokes equations which despite computational costs offer better accuracy. Research by Thermann and Niehuis [21] uses the Navier-Stokes equations along with algebraic transition models on a compressor blade cascade to calculate unsteady pressure at transonic near stall conditions. Research by Srivastava [25] uses unsteady Navier-Stokes equations for aeroelasticity analysis of a fan blade.

2.3.3 Validation with Standard Configurations

Since multiple solution methods [26] with varying simplification levels can be used for calculation of steady and unsteady flow conditions and may yield different results, relative accuracy and applicability of each method must be clearly understood to conduct a meaningful analysis. Validation of analytical results with experimental data is also required to determine accuracy and applicable range of each method. However, due to unsteady nature of surface pressure and vibrating motion of the airfoil at high frequencies, experimental measurements are difficult to obtain.

In fact, one could argue that creating an exact representative environment for flutter with true 3D vibrating motion of the airfoil is nearly impossible in a test set up. Creating the best possible representative environment with simplifications has been one of the primary focus areas of flutter research. Various researchers have used linear sector cascades or scaled annular cascades to measure both steady and unsteady conditions with 1D pivoting motion. Electromagnetic driving mechanisms are used to induce a rigid body airfoil motion approximating true vibrating motion of the airfoil [27].

Initially, different research groups used different set ups, operating conditions, and cascade geometries to conduct their work, making comparison of results and data impossible.

Bolcs and Fransson [12] modernized the field of turbomachinery flutter research by compiling standardized airfoil geometries and operating conditions for flutter studies. These STCFs allow for various research teams to conduct their work on identical geometries and conditions and make comparison with other analytical and experimental results on an equivalent basis. Prior to the inception of STCF, it was difficult to collaborate and use various other research results due to incompatibility.

Since the implementation of STCFs, there have been many advances in the field of modeling and prediction of aerodynamic instability. With unsteady pressure measurements made possible (with simplifications) by rig testing and standard configurations, aerodynamic studies have been conducted to predict and validate with experimental data the unsteady pressure distribution on airfoil as a result of airfoil motion [28]. Specifically in the field of unsteady pressure prediction, many analytical tools have been developed and calibrated with experimental results.

McBean et al. [29] compared results from multiple analytical methods with experimental measurements. This research shows 3D Navier-Stokes solution has a better capability than 2D and 3D Euler methods to predict flow conditions, including unsteady pressure phase angle on airfoil suction side which is an important parameter in overall flutter solution. Also, the importance of flow separation, shock waves and 3D modeling effects are discussed in detail which leads to the conclusion that modeling technique and grid size requirements of CFD model must be such that high fidelity solution is obtained to yield accurate flutter result.

2.4 Fluid Domain Solution Methods

Various solution methods have been used to solve governing fluid domain equations, which are discussed in this section. Since there is a wide spectrum of blade configurations and flow regimes in turbomachinery applications, each method has particular advantages and disadvantages that justify their use in a particular application. For instance, some methods have better accuracy in transonic regions where

shock-boundary layer interaction effects are significant, while others have computational time advantages where a linearized harmonic flow may be adequate to describe the unsteady flow.

2.4.1 Time Domain Solution

Time domain solution has been historically used as the standard solution method for computational fluid problems. It has been used extensively for solving 2D and 3D Euler and Navier-Stokes based solutions with explicit and implicit algorithms. Due to complexity of the transonic flow around moving objects, multiple categories of flow such as steady, transitional and turbulent flows must be accurately modeled to yield an accurate result. Historically time linearized methods have been used due to their (relative) computational efficiency. With improvements in computational power over the years, time accurate methods are used to better model nonlinear aspects associated with unsteady and turbulent flows.

Other important considerations are boundary layer effects, flow separation, and shock-boundary layer interactions. Prediction of transitional boundary layer development in a transonic cascade is improved in research by [21] using an algebraic transition model, leading to better prediction of aerodynamic damping. While time domain solution offers advantages in accurate prediction of turbulent and viscous flows, it is computationally expensive. Various parallel block and memory distribution techniques can be used to decrease computational time to manageable amount.

2.4.2 Coupled Solutions of Fluid Structure Interaction

To fully simulate the interaction between the fluid and the structure, coupled solutions have been developed which are also referred to as two-way fluid structure interaction (FSI). Fluid and structural governing equations are solved simultaneously in a coupled solution method in time domain. At each time step, structural deflections are accounted for in fluid equations and changes in fluid conditions are

accounted for in structural equations. Multiple problems using this method have been researched in self-excited vibration [30, 31] and similar work in blade row interaction [32, 33].

While a fully coupled, two-way FSI is a highly accurate method, its application in realistic large scale models is computationally prohibitive due to small time steps and slow rate of convergence. Many iterations are required before final stability trends can be determined since only small amount of system damping is present in turbomachinery applications.

2.4.3 Mesh Morphing or One-Way Interaction

Due to great computational expense of fully coupled aeroelastic solutions, a simpler method has been used to include only effects of structural displacement on the fluid field. This method is also known as one way FSI, since structural deflection is pre-imposed and it does not include effects of changes in surface pressure on the structure. To implement this method, computational nodes associated with geometry of the airfoil are moved at multiple time steps, representing airfoil motion over a full cycle of vibration. In addition to governing equations of fluid motion, various flux equations are also solved for each element in the computational domain to account for change in its volume and surfaces at each time step.

Due to (relative) computational efficiency, this method is used extensively to simulate moving airfoil in a computational fluid domain with airfoil motion prescribed as harmonic function with a known mode shape and amplitude.

2.4.4 Frequency Domain Solution

The most common method of solving governing aerodynamic equations is direct integration in time domain. However, due to the computational expense of predicting unsteady flow using time domain method, frequency domain solution method has been developed that requires considerably less

computational resources. Method developed by Hall et al. [34] is a frequency domain solution based on Fourier Decomposition method and periodicity assumption which are described in sections 2.4.5 and 2.4.6. Unsteady flow is assumed to be the sum of harmonically varying components, which can be individually calculated in the frequency domain.

2.4.5 Fourier Decomposition Method

Various Fourier-based methods have been developed for use in both time and frequency domain solutions to take advantage of periodicity of flow in turbomachinery applications. In a time domain solution, the advantage of using Fourier Decomposition method is that only Fourier coefficients of the flow field need to be retained therefore substantially reducing memory requirements of the computational grid [35]. In a traditional direct integration time marching analysis, flow conditions at all grid locations for multiple time steps must be retained in the memory to proceed to the next iteration. The need to retain all of this information requires large amounts of memory space and increases computational costs.

The main advantage of Fourier Decomposition method is that it enables application of frequency domain solution method for computation of unsteady pressure, which is much more computationally efficient than direct integration time marching method. Fourier based methods are further reviewed by He [36] where various applications of this approach, their assumptions, and effectiveness are discussed.

2.4.6 Phase Lagged Boundary Condition

Another major advancement that significantly reduces the required numerical domain size to describe a cyclic symmetric flow is the concept of phase lagged boundary condition method [35]. The main advantage of this method is that it enables simulation of the entire cascade by modeling only one sector, therefore significantly reducing the required domain size and computational costs.

This method may be applied in both time and frequency domain solutions and it assumes boundary conditions on one side of the cyclic symmetric structure are a time transition from the opposite side. This time transition is the time required for the “wave” to travel from one side of the cyclic sector to the other. In effect, the same boundary conditions are applied from one cyclic sector face to the other with a time shift, which is determined from natural period of vibration, sector angle, and prevailing nodal diameter of the cascade. Figure 7 shows a sector flow model with phase shift boundary conditions.

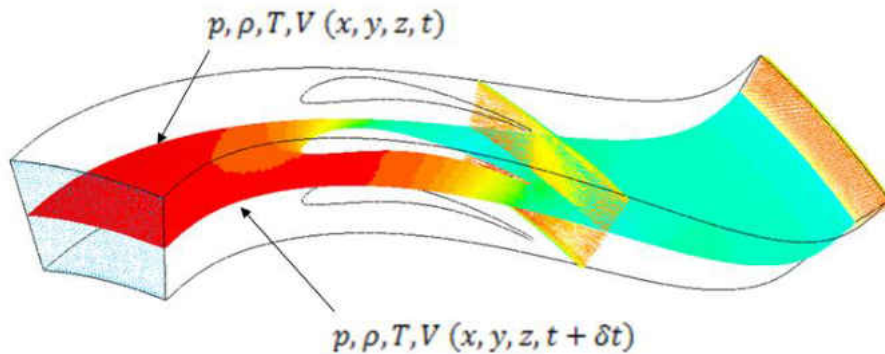


Figure 7: Sector model using phase-lagged boundary condition

2.5 Structural Domain Solution Methods

Solution methods for structural dynamics problems related to turbomachinery cascades have been well established [37]. FEM based methods are commonly used to numerically access complicated turbine components. Steady state problems arising from quasi-static (or steady state) operating loads such as centrifugal loads and thermal expansion mismatch loads are typically solved in time domain by various matrix inversion methods. Vibration and dynamics problems arising from inertia-stiffness interactions are solved in frequency domain using eigenvalue method. Inclusion of a linearized system damping is possible by assuming a proportional damping matrix.

Introduction of nonlinearities into structural models increases complexity and computational cost of such systems depending on the solution method and nature of nonlinearity. Material nonlinearity such

as plasticity and creep can be solved in time domain by modeling the system as a piecewise linear system in either amplitude incremental or time marching method. In a typical analysis of this sort, mechanical loads are ramped up in multiple solution steps and material properties are assessed at each step according to the strain state. Element stiffness matrices are subsequently updated and used for the next solution step. Material properties and system matrices are iteratively updated based on applied loads until full loads are applied and various convergence criteria are met. Geometrical nonlinearities such as gaps and interferences are solved similarly by evaluating system stiffness matrix based on displacements at multiple steps. With nonlinear considerations, multiple solutions must be performed which increases computational time many folds compared to a single solution linear problem. Research by [38, 39] shows significant influence of nonlinearity in aeroelastic and vibratory problems.

Friction is another major source of nonlinearity that significantly affects system's response. Presence of friction in turbomachinery applications is a major influencing factor which is discussed in detail in section 2.6.

Nonlinear systems present much more challenge in frequency domain solutions. The eigenvalue problem can only be solved with linear matrices; therefore direct modeling of nonlinearity in frequency domain is not possible. Hybrid and iterative solutions have been developed using numerical FFT methods where some level of nonlinearity can be taken into account by iteratively solving frequency domain and time domain solutions and exchanging information between domains at each iteration. Highlights of hybrid type solutions are presented in chapter 2.8.

Researchers also use reduced order or simplified mass-spring models to solve many iterations in time domain and include a very simplified representation of nonlinearities [40, 41]. These models are an excellent source for identifying overall response trends, but they are overly simplistic to be used for detailed studies. Large scale models are required to fully define various geometric features and SDOF or reduced order models do not have the necessary accuracy for detailed studies due to limitations with resolution.

2.6 Friction and Nonlinear damping

Friction plays an important role in reducing resonant stresses in gas turbine components by providing energy dissipation and additional mechanical damping (in addition to material dependent viscous damping) during vibration motion. This type of dry friction damping provided by rubbing motion of contacting parts is also referred to as non-viscous or Coulomb damping in literature. Most of the research in nonlinear friction effects and dry friction damping applications in turbomachinery has been conducted in the context of forced response analysis because of relative simplicity of experimental set up in forced response compared to flutter. While force response and flutter have many commonalities as aeroelastic instabilities, there are also distinctive differences.

Forced response is the response of a structure to an external forcing function. Therefore, frequency and magnitude of the excitation forces are external to the structure, and they are typically known in this type of problem. Furthermore, external source is not affected by the response of the system, so frequency and magnitude of the excitation are constants regardless of magnitude and phase shift of the response. Therefore, equations of motion can be solved with frequency and magnitude of the driver as constants and structure's response as the only variable. Accurate prediction of natural frequencies of the structure is of primary importance for a forced response analysis because of sharp nonlinearity when frequency ratio is close to unity. Damping is typically a secondary factor because cascades are designed to operate at a margin with resonance conditions.

In case of flutter, the magnitude and phase shift of unsteady aerodynamic forces are not known in advance because they both depend on the aeroelastic coefficients of the equations of motion. Flutter is the result of imbalance and fluctuations of internal inertial and structural forces with the unsteady pressure field caused by the motion of subject cascade itself. Therefore calculation of magnitude and phase of unsteady pressure is a major complexity in flutter and self-excitation problems. Frequency of vibration is typically close to one of fundamental "in-vacuum" natural frequencies of the structure. However, in case of shrouded

turbine blades, frequency and mode shape of the system response depends on shroud contact condition due to nonlinearity in friction force and transition from stick to slip condition.

Therefore in a flutter-friction problem there are multiple interdependencies of relevant variables. Response of the structure, frequency of the vibration, magnitude of the drivers, contact conditions at the shroud, and prevailing nodal diameter all influence each other and overall stability of the cascade. Furthermore, creating fully representative test condition for this type of problem is nearly impossible. Only engine testing or large scale rotating rig can be used to fully capture all aspects of structural dynamics and self-induced aerodynamics of the cascade with representative shroud damping.

By comparison, research of nonlinear friction is much simpler in forced response type studies. It requires a shaker table set up that allows conducting frequency sweep at multiple amplitudes, which is significantly less burdensome than an engine test or a rotating rig. Therefore most of friction related research in various aspects of blade vibration has been conducted to forced response and is outlined in section 2.6.1.

2.6.1 Friction Models in Turbomachinery Applications

Generic dry friction has been researched extensively in many engineering applications and there are many models available with varying levels of complexity. Most commonly used model is Coulomb model [42], which is nonlinear but relatively simple. Other friction models are available such as Dahl model [43] which offers more accuracy but is also more complicated. A nonlinear but continuous model is developed by Petrov et al. [44] that uses a trigonometric function to approximate nonlinearity in friction force with a continuous function. This formulation is especially attractive for use in time integration methods where the derivative of the friction force is calculated based on contact parameters and is then integrated in time domain to determine friction force at any desired time due to an arbitrary 1D or 2D motion.

While multiple methods are available for simulation of friction, Coulomb based models are mostly used in turbomachinery research due to their (relative) simplicity. These friction models have been combined with contact models to represent a “flexible contact” by including normal stiffness and tangential stiffness values in a contact interface.

One example of a generic contact friction model is model by Petrov et al. [45] that calculates contact forces at interfacing surfaces while taking into account influence of tangential and normal stiffness as well as variable normal load. This model is capable of considering initial gaps and interferences. Various other penalty based or Lagrange based algorithms are utilized in commercial FEM software to solve the contact-friction problem [46, 47].

Research is also conducted to characterize generic contact parameters such as tangential stiffness, coefficient of friction, and influence of their scatter in vibration response of the system. Research by Schwingshackl et al. [48] uses a high temperature friction rig to evaluate friction parameters for various material combinations at various operating temperatures. Influence of operating temperature on contact parameters is noteworthy in this research as the wide range of data scatter at room temperature converges to a narrower band at elevated temperatures. Other research by Petrov et al. [49, 50, 51] evaluate the influence of variability of contact parameters on system response, and illustrate that due to the large scatter inherent to friction parameters there could be significant difference in system response.

2.6.2 Friction Damping Applications

There are multiple sources of contact between adjacent components in a typical bladed disk assembly that provide mechanical damping or work dissipation. Blade root is in contact with the disk and any relative motion results in work dissipation and damping. Research in blade root damping conducted by Allara [52] develops a model to evaluate the oscillating contact force versus relative tangential displacement for various geometries and calculated Hertzian contact stress. Dissipated work at the contact

is subsequently calculated for various amplitudes of forced response drivers. This model uses contact interface geometry and related parameters to evaluate the characteristic hysteresis curves and associated energy dissipation. However, in most applications the amount of damping in the blade root is small compared to other sources of friction damping because the root is where the blade is attached to the disk and there is little relative motion in the mode shapes of the cascade between blade root and disk.

Another source of mechanical work dissipation is under-platform dampers that are placed under platforms of adjacent blades and sometimes referred to as Coulomb dampers. Griffin [53] researched resonance response of a turbine airfoil with under-platform damper, demonstrating experimentally that the damper can substantially influence the blade response. This research concluded that an optimal normal load at the contact interface can minimize the response of the entire blade. Sinha et al. [54] studied effects of static friction on forced response as a function of ratio of static to dynamic friction coefficients. System response was found to be essentially harmonic, but at some transition point it turned into more complex periodic wave forms.

Research by Breard et al. [55] outlines an integrated analytical method that includes effects of nonlinear friction forces in the FEM solution. Nonlinear friction force is solved in a time domain solution and represented as a harmonic correction term to the linear modal equations. Modal forcing function consists of an aerodynamic load vector and an additional friction damping vector, which are both nonlinear in nature. System equations are integrated in time domain where at each time step a new modal forcing vector is generated based on the state of variables in previous time step. A similar integrated method was developed by [56, 57] for forced response applications.

Other research by Petrov et al. [58] implements advanced modeling of damper pins where contact stick-slip transition, inertia force acting on the dampers, and the effects of normal load variations during the vibration cycle are taken into account. In this method the equations of motion are solved in frequency domain using multi harmonic balance method to obtain a steady state solution to the nonlinear bladed disk

system. Similar research is conducted in under platform [59] and internal damping of hollow blades [60, 61] and influence of friction damping on mistuning [62].

Work by Sinha et al. [63] examined influence of under-platform friction dampers on torsional blade flutter using classical cascade aerodynamic theory [8] for calculation of unsteady aerodynamic loads. Rotor stage was represented by mass spring damper elements for this study, as well as nonlinear friction elements between adjacent blades. This research identified margin to flutter condition by calculating allowable increase in fluid velocity before flutter condition is mathematically predicted. While the classical aerodynamic model used in this study has many restrictions (especially in compressible and transonic regions [20]), this study concluded that flutter margin can be substantially increased by incorporating friction dampers. Similar research by [64] on under-platform dampers also indicates stabilizing effects of mechanical damping in flutter, and it corroborates with similar findings from forced response research.

While damping provided by blade root and under-platform are substantial in some applications, their overall influence is a strong function of geometry and mode shape of the blade. In short and cantilevered front stage turbine blades, where root shank is an appreciable portion of the overall blade height and platform motion in the mode shape is substantial, damping effects from root and under platform dampers are important sources of frictional damping. In case of tall last stage shrouded blades, where the mode shape is dominated by motion of slender airfoil and the shroud tip, negligible amount of relative motion exists in platform and root resulting in minimal damping contribution from these sources. Majority of friction damping in shrouded cascades is related to shroud relative motion, which is discussed in section 2.7.2.

Limitation of existing research in friction damping is that it mainly focuses on forced response applications. Few flutter related research are related to application of under platform dampers with constant normal load, and use simplified SDOF model which are not sufficient for accurately representing complex geometry and mode shape of a typical blade.

2.7 Cyclic Symmetric Influence

The interlocking shrouds in a shrouded cascade form a continuous outer ring around the bladed disk assembly during operation. This ring, along with the disk and the airfoils, creates a flexible cyclic symmetrical structure that vibrates in certain nodal diameter patterns (see Figure 6) and is subject to both standing wave and traveling wave phenomena (also referred to as synchronous and non-synchronous vibration respectively).

The significance of cyclic symmetric configuration of shrouded cascade is that the prevailing nodal diameter of the cascade and corresponding mode shape influences both aerodynamic and mechanical work interaction and associated damping. Aerodynamic damping is a nonlinear function of IBPA, which is related to the nodal diameter of vibration by the following expression [65]:

$$IBPA = \frac{360^{\circ} * Nd}{Nb} \quad (5)$$

Where Nd is the nodal diameter pattern of vibration and Nb is the number of blades in the disk. Mechanical damping is function of mode shape, as relative motion between adjacent shroud tips depends on the specific mode shape of vibration in addition to overall amplitude. Since each nodal diameter has unique fundamental mode shapes, mechanical damping is also function of the prevailing nodal diameter. Therefore aerodynamic damping and mechanical damping are coupled to each other in a shrouded cascade through the nodal diameter pattern of vibration.

Concepts of nodal diameter, traveling wave and standing wave are major influencing factors in forced response and flutter studies and have been used by researchers to formulate various phenomena. Research by Lee et al. [66] represents vibration of mistuned bladed disk using standing wave formulation and a two dimensional unsteady vortex lattice method to simulate higher engine order aerodynamic excitation sources. Another research that outlines the concept of aerodynamic damping versus nodal diameter pattern of vibration is by Rice et al. [19]. This research was conducted to experimentally measure

combined system damping of a bladed disk assembly using magnetic excitation sources and measurement of the response decay.

2.7.1 Aerodynamic Coupling

A major complicating factor in determining aerodynamic interactions in a cascade as opposed to isolated wing is the influence of neighboring blades on each other. In case of shrouded cascades, the phase relationship between adjacent blades is constant due to shroud coupling. Therefore an aerodynamic influence matrix can be formulated using the repeating pattern of the IBPA to account for aerodynamic influence of each blade on every other blade in the cascade [18].

Experimental research by [16] measured response of a blade in a cascade to vibration of neighboring blades, which led to experimental evaluation of an influence matrix. Aerodynamic work interaction is sum of the work interaction of each blade in the wheel assembly, accounting for the influence of unsteady pressure caused by its own motion and the motion of all other blades on it. This research experimentally demonstrates that the aerodynamic influence of neighboring blade is most significant for the first adjacent blades on pressure side and suction sides, and this influence dies out rapidly for the blades farther out as the distance with subject blade increases.

2.7.2 Shrouded Blade Vibration

An important aspect of shroud coupling around the wheel is the organization and patterns of aerodynamic and structural forces. Since flutter is sustained by self-excitation as opposed to engine order excitation, the structural response and aerodynamic drivers must be synchronized with each other and organize into a traveling wave pattern. This traveling wave pattern is the primary coupling factor between aerodynamic drivers and structural dynamics of the cascade by relating IBPA (aerodynamic influencing factor) to nodal diameter (structural influencing factor).

In case of shrouded blades, mode shapes and natural frequencies of a rotating cascade (with locked shrouds) depend on nodal diameter as each nodal diameter has a unique stiffness matrix associated with it. Figure 8 shows normalized natural frequencies of second family modes (first torsion) for a particular blade design as a function of nodal diameter. Motions of the airfoil and the shroud in each mode shape are different for each nodal diameter as each nodal diameter has a unique mode shape associated with it.

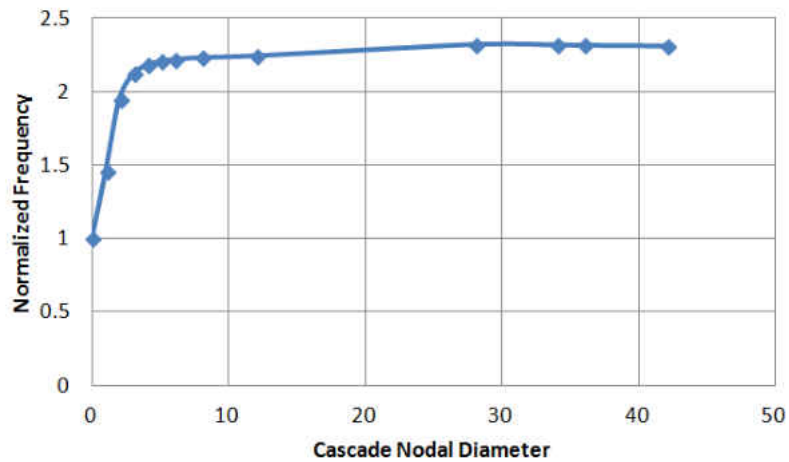


Figure 8: Frequency of first and second family modes

Another influencing factor in vibration characteristics of the cascade is stick or slip condition at the shroud tip contact. This influence is due to difference in contact tangential stiffness between stick and slip conditions. In addition to contact condition, contact normal load has a substantial effect on mechanical work dissipation and associated damping due to rubbing motion between adjacent blades. The effects of shroud contact and associated parameters have been researched mostly in forced response studies. Srinivasan [67] conducted experimental and analytical studies using macro slip model and frequency sweep induced forced response on a shrouded fan blade. He observed slip resonance responses at low sweep rates that had distinct flat tops, indicating sliding energy dissipation due to slip prevented higher response amplitudes. He also noted that critical shank vibratory stress at resonance is related to normal load at the

contact interface. This is an important observation as it confirms the critical role that operating contact normal load has on life critical alternating stress on the Goodman diagram.

Another consideration in system response is the complex vibrating mode shape of a shrouded blade, and its effects on the contact surfaces. Contact load and by derivation slip load varies during the cycle of vibration as a result of this complex motion, affecting the system response. Menq et al. [68] researched variable contact normal load and its influence on forced vibration response. He concluded that to minimize response an optimal preload exists which can be achieved by selecting appropriate design parameters. Yang et al. [69, 70, 71] researched variable normal load in shrouded blade forced response vibration that is also out of phase with the cycle of vibration due to the cascade IBPA. This research demonstrated that complex hysteresis curves in multi-dimensional space result from out of phase normal load and transition between stick and slip motion of the friction interface.

Above studies were in forced response applications. Research in flutter related friction damping is much more limited due to complexity associated with determining driver strength and simultaneously solving for the nonlinear system response. There are also limitations on experimental testing of shrouded cascade under realistic flutter conditions where both aerodynamic and mechanical parameters are sufficiently represented.

Martel [41] studied shrouded cascades using a mass-spring blade / disk model with combined effects of aerodynamic excitation and friction damping. While the model is simplistic due to limited number of DOF, two aspects of this work are significant. First, the study concluded that only the most unstable traveling wave (with most negative aerodynamic damping) is susceptible to being excited and all other traveling waves die out faster than the most unstable one. Second significant aspect of [41] is the conclusion that system response can be recognized as a large time scale exponential response imposed on a small time scale harmonic motion. These findings will be leveraged in present dissertation to enable computationally efficient solutions to this complex problem.

Limitation of work by [41] is that time domain solution method it used with a simplistic mass-spring model to enable many iterations. This level of model fidelity is sufficient to understand general response trends, but it cannot be applied to realistic applications and large scale models.

2.8 Hybrid Solution Methods

A major consideration in solving aeroelastic system equations is computational efficiency of the solution, which is an issue with large scale models required to fully describe complicated geometry of a blade. Time domain solution can predict nonlinear friction effectively but small time steps and many iterations are required for convergence. Most of forced response studies of friction damping mainly use simplified SDOF models to enable time domain solutions. For flutter applications, coupled aeroelastic time marching methods [30, 31] are available for direct time integration. However, direct time domain methods are computationally cost prohibitive with large models since many iterations are required for convergence due to small amount of overall damping in turbomachinery applications.

HBM method can be used in frequency domain analysis to approximate nonlinear friction by an equivalent harmonic term. Research by [72] develops a simple method based on a single harmonic assumption which assumes only the first Fourier term in equations of motion is significant. HBM method was applied by Wang et al. [73] to a SDOF model of blade with under platform damper. This work shows that multiple harmonic terms are required to accurately represent nonlinearity in frequency domain. With additional terms, computational cost with large models approach time marching methods.

Alternating frequency/time (AFT) method was developed by Cameron, et al. [74] to address shortcomings of both time and frequency domain solution methods by iterating between domains and exchanging information at each iteration. A similar hybrid method was developed by Guillen et al. [75] based on variations to the alternating method.

While computationally efficient, existing hybrid and HBM methods are based on approximation in deriving equivalent forcing function with FFT analysis and require multiple harmonic terms to accurately describe non-sinusoidal friction force. This is the main source of error in traditional HBM and hybrid methods that is especially problematic with single harmonic problem such as flutter, where a single harmonic term is insufficient to accurately include net effects of a non-sinusoidal force at an arbitrary phase angle relative to motion. Energy method, on the other hand, can include the full effects of damping associated with friction because it is based on total work dissipation over the full cycle. There is no approximation in this respect and the phase angle of friction force does not adversely affect accuracy as it does with the single harmonic FFT analysis.

Existing HBM and hybrid methods also do not consider influence of cascade static response and contact preload due to operational loads, which is an essential consideration for flutter analysis of shrouded cascades due to its effects on exponential damping term and overall stability of the response.

Present dissertation utilizes a novel three step hybrid time-frequency-time domain solution sequence based on energy method to address these shortcomings of existing methods and provide a comprehensive solution method for flutter-friction and cyclic symmetric type problems. Details and development of this method are discussed in section 3.

CHAPTER THREE: METHODOLOGY

A flexible cascade commonly used in turbomachinery applications includes a flexible disk, multiple blades assembled on the disk, and associated sealing and assembly hardware. Unshrouded or cantilevered cascades have free standing blades that only interface with the disk at the root (see Figure 1 a). Shrouded cascades feature blades that interface with the disk and are also in contact with each other at the shroud (see Figure 1 b). Extremely precise manufacturing methods are utilized to ensure proper fit of shrouded blades due to complexity in design and assembly of shroud interfaces. Parameters influencing assembly gaps and shroud to shroud contact in such design have substantial influence on response and structural integrity of the entire cascade, as do engine operating parameters and boundary conditions. Therefore proper consideration of all of aerodynamic and structural parameters is required for a comprehensive analytical solution to flutter, and this solution has to be computationally efficient to enable application to real life components.

The overall objective of present dissertation is to develop a comprehensive analytical framework for flutter analysis of shrouded cascades that considers both aerodynamic work interaction and friction related work dissipation within the cascade, while considering all influencing factors. A hybrid, three-step solution method is developed to utilize best aspects of time and frequency domain solutions while accounting for all of the influencing factors. Various steps of the framework utilize geometrical and operational parameters that have aerodynamic and structural impact and create detailed information regarding contact load, motion, frequency, and overall response characteristics of the cascade. Exchange of this information between multiple domains is used to couple all equations and solve iteratively based on an efficient, energy based method and converge on a global flutter condition that satisfies all constraints and requirements. This global flutter condition includes prevailing mode shape and nodal diameter of the cascade, corresponding frequency and amplitude of the motion, and amplitude trends over many cycles of vibration which determine cascade stability.

This framework is an energy-based method that includes the influence of both aerodynamic excitation and mechanical dissipation in determining system response as a function of many variables such as aerodynamic and flow conditions, geometric features of the cascade, and shroud contact parameters. Mechanical and aerodynamic work per cycle calculations are used to determine gross accumulation or dissipation of energy in the system starting from an initial condition. Nonlinearity associated with change in contact conditions at the shroud and its effect on system mode shapes is included in the analytical scope.

Development and rational of the analytical framework for flutter is divided in multiple sections for clarity, and it is described in detail in sections 3.1 through 3.6.

3.1 Aeroelastic Formulation

Equations of motion for a flexible blade-disk-shroud system in Finite Element domain with the consideration of aerodynamic and nonlinear contact loads are represented as:

$$[M]\{\ddot{\eta}\} + [C]\{\dot{\eta}\} + [K]\{\eta\} = \{F_{AD}\} + \{F_{Con}\} \quad (6)$$

Here, $[M]$ is the mass matrix, $[C]$ is the viscous damping matrix, $[K]$ is the stiffness matrix, $\{F_{AD}\}$ is the complex aerodynamic load vector, and $\{F_{Con}\}$ is the nonlinear shroud force vector. There are multiple issues that prevent a direct solution to this system such as dependence of aerodynamic loads on motion and its derivatives, nonlinear nature of shroud contact loads, and dependence of system stiffness matrix on contact stick / slip condition. Despite complexity with analytical solution of equations of motion, experimental observations show that flutter in physical sense is similar to free (unforced) vibration. Therefore simplifications have been used in previous research and in the industry to reduce complexity of the analytical models and enable approximate solutions. Current flutter prediction work flow in the industry (Figure 9) is based on analysis of aerodynamic work interaction using in-vacuum (or structure-only) mode shapes. This work flow is based on many aspects of the research and progress discussed in section 2.

This work flow consists of a static solution to calculate pre-stressed stiffness matrix and account for shroud contact and structural stiffening under significant operational loads, followed by modal analysis of the cascade in frequency domain to take advantage of computational efficiency. After mode shapes are determined from the structure-only modal analysis, a time domain or frequency domain aero-elastic analysis of a single passage is conducted, where periodic boundary conditions are used to impose flow periodicity condition corresponding to cascade nodal diameter. This process is repeated for all nodal diameters of the cascade to obtain a map of unsteady pressure distribution around the oscillating airfoil for each nodal diameter of the cascade. Energy method similar to [10] is subsequently used to determine resulting fluid-structure work interaction and aerodynamic stability vs nodal diameter. Due to repetition of large scale CFD solution with fine grid to sufficiently resolve transonic flow features, this step of the analysis is computationally expensive. A comparison of several available methods and their relative computational efficiency is discussed in [76]. While this analytical work flow is complicated and computationally expensive, it is necessary for proper design of highly loaded cascades and is performed as standard design practice.

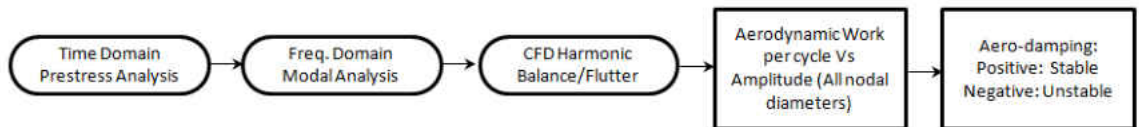


Figure 9: Typical analytical work flow for flutter analysis

The current work flow does not include stabilizing effects of mechanical damping or uses a constant value for mechanical damping as an approximation, which is not sufficient to describe the highly nonlinear friction damping.

The analytical framework developed in present dissertation expands the current energy based methodology to include frictional work dissipation associated with vibrating motion of flutter. Effects of contact nonlinearity and transition from stick to slip condition are included in the analytical method as this nonlinear transition affects system mode shapes and friction damping. Shroud contact load variations

during cycle of vibration are included in this framework by evaluating relative motion of contact surfaces associated with mode shape and using this information in a subsequent contact force analysis through the cycle.

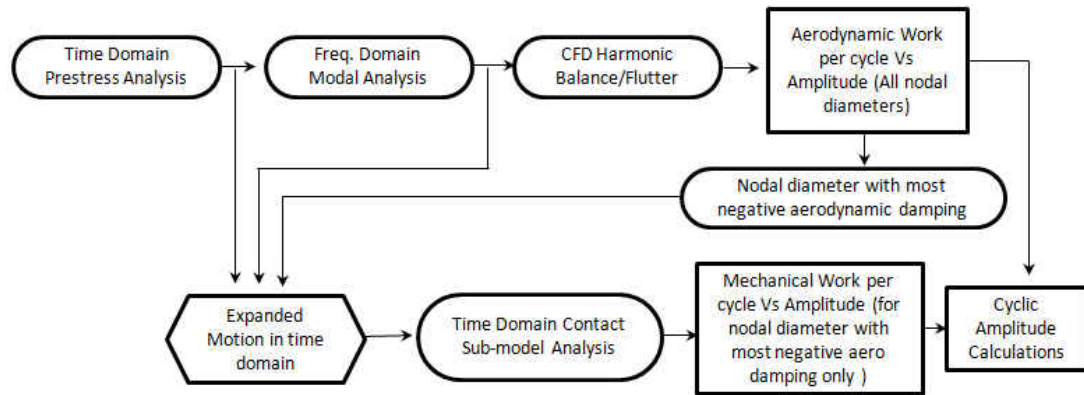


Figure 10: Analytical framework expanded with friction damping

This analytical framework is shown in Figure 10 and is discussed in detail in the following sections. For illustration, the analysis method is first demonstrated on a cascade with linear damping in section 3.3. It is then expanded to a nonlinear cascade in section 3.4.

3.1.1 Solution Methodology

Known characteristics of flutter have been used in previous research and in the industry to develop solutions for this complex phenomenon based on simplifications. Similar simplifications will be used in present work, while still maintaining effects of nonlinear friction that is not currently considered. First simplification similar with current analytical method in the industry is the use of a single harmonic natural mode shape and frequency of the system for periodic response of the system. This is based on observations [10] that system response is in agreement with structural dynamics prediction, indicating that one of natural mode shapes of the cascade is the primary system response. It is also noted in previous research that second

family mode shape (first torsion) is typically associated with flutter issues due to interaction with passage throat and shock wave [18, 14].

Another simplification is related to traveling wave phenomenon associated with flutter. Research by [41] shows that while multiple traveling waves may initiate as a result of a perturbation, an organized response that continuous and may build strength is associated with a single traveling wave pattern with the most negative aerodynamic damping.

Therefore a single harmonic, single nodal diameter motion associated with the most negative aerodynamic damping is the most susceptible to an organized flutter response in shrouded cascades and is studied in present dissertation. It is also known that flutter response can be recognized as a large time scale exponential response imposed on a small time scale harmonic motion [41]. This is associated with high frequency (100-1000 Hz range) free vibrating motion that is similar to natural resonance, and exponential increase of amplitude over many cycles due to energy exchange with the fluid.

These characteristics of flutter response will be utilized in present work along with the energy method to develop a flutter analysis framework that is comprehensive and computationally efficient, while using large scale, full fidelity analytical models that are required to fully describe complex geometry of a shrouded blade.

3.1.2 Separation of Structural and Aerodynamic Drivers

Classical methods for airplane wing flutter have been well developed. Using a classical pitch-heave method and unsteady lift and moment equations, influence of airspeed on natural frequency and mode shape of the wing can be determined [4]. Typical mechanism for wing flutter is known as the mode-coalescence flutter, where first and second modes of natural vibration coalesce together and create a self-induced instability at a frequency that is different from in-vacuum (or zero air speed) frequencies of both

elastic mode shapes. It is also well known in aeroelastic methods that the level of aeroelastic mode coupling is a strong function of mass ratio.

Therefore for a flexible light weight airplane wing the influence of aeroelastic coupling is strong, and aerodynamic mass and stiffness matrices are important factors in calculations of system frequencies and mode shapes. For a rigid turbomachinery blade, aeroelastic coupling is not a dominant factor due to much higher mass ratio, and it is a common practice in the industry to neglect effects of aeroelastic coupling and assume harmonic motion comprised of “in-vacuum” or “structure-only” as the systems frequencies and mode shapes [20]. Furthermore, it is known that in shrouded cascades, typically first torsional mode of the system (typically 2nd family mode) is of most concern due to strong interaction with throat area and shock wave in a choked passage [18, 20].

While a combination of nodal diameters may be present in a system’s response to an initial perturbation, it is known that for flutter to occur all nodal diameters coalesce and form a coherent, fully organized, single traveling wave pattern that is prone to extracting energy from the fluid as it travels endlessly through the cascade. Therefore to analytically predict occurrence of flutter, a single mode, single nodal diameter in-vacuum mode shape of the system is evaluated aerodynamically in a moving flow field to evaluate aerodynamic work interaction and damping.

Following the method of separation of structural versus aerodynamic forces that is used in the industry, it is assumed in this dissertation that natural frequency of the system is only a function of structural and steady state contact forces. Influence of aerodynamic forces and unsteady (or alternating) contact forces is assumed to be negligible on natural frequency. Despite this simplification, nonlinear effect of shroud contact transition on mode shape is included as it will be discussed in section 3.4. While not influencing natural frequency, aerodynamic forces and unsteady contact forces play an essential role in cascade stability by adding (or dissipating) small amount of energy over each cycle of vibration, which will be included in formulation of the problem.

3.1.3 Mass / Stiffness vs. Damping Terms

With the assumptions described in section 3.1.2, small time scale flutter motion in general can be described as a sinusoidal vibratory motion. Force diagram representation of this sinusoidal vibratory motion in real-imaginary plane is shown in Figure 11 to examine fundamental influencing forces and determine large time scale exponential component. Motion is represented as a rotation set of vectors with influencing inertial, stiffness and damping forces. Two groups of forces are identified in the instantaneous angle of rotational frame which are perpendicular to each other and therefore mutually exclusive. Third group is the static force which is shown as an offset on the real axis relative to the origin.

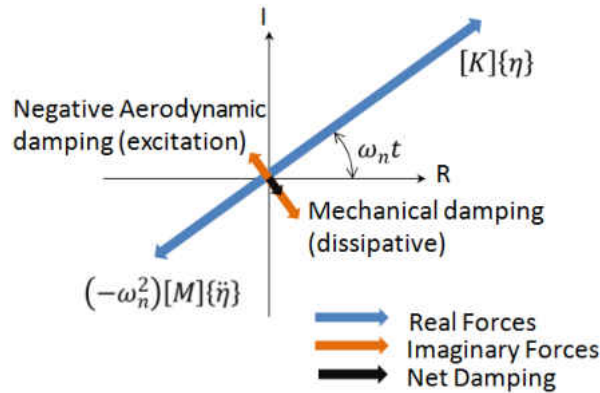


Figure 11: Force diagram of sinusoidal vibrating motion on real-imaginary plane

First group are the real forces consisting of inertia and stiffness forces, and they are at an angle of $\omega_n t$ relative to the real axis. These forces primarily determine frequency of vibration, and they are in phase (or 180° out of phase) with motion. Energies associated with real forces are kinetic and elastic energies, which convert from one form to another twice over the full cycle of vibration.

Second group consist of imaginary forces and are at angle of $\omega_n t \pm 90^\circ$ relative to the origin. Amplitude of imaginary forces is typically much smaller than real forces for systems with large mass ratio. While their influence on natural resonance characteristics is negligible, they do play a critical role in stability of the system by adding or dissipating small amount of energy over each cycle. While the amount

of energy associated with imaginary forces is much smaller than either kinetic or elastic energies, its net effect is essential over many cycles of vibration as it leads to either dissipation or accumulation of energy in the cascade.

Structural damping terms are always dissipating because the direction of friction force is always opposite of the motion. Therefore imaginary force associated with structural damping is always at a 90° lag of the motion. Aerodynamic damping may be dissipative or exciting depending on phase angle of aerodynamic force relative to the motion. If the resultant aerodynamic force lags the motion (similar to structural damping force) then aerodynamic damping is dissipative similar to structural damping. On the other hand, if aerodynamic force leads the motion then it is exciting and its net effect is addition of small amount of energy during each cycle of vibration. Source of this energy is the moving fluid, which offers unlimited kinetic energy. The energy associated with aerodynamic excitation over one cycle is very small compared to cascade kinetic and elastic energies, but its accumulation over many cycles can cause instability.

For the system, net effects or the resultant damping force determines stability. Resultant damping force is the algebraic sum of mechanical and aerodynamic forces projected on the rotating imaginary axis. Mechanical damping force is always dissipative. However, with consideration of nonlinear frictional damping, total value of mechanical damping is amplitude dependent as it will be discussed in section 3.4.

Static forces are the third group and act as an offset in non-rotating real coordinate. While static forces typically do not affect vibratory response, they play a substantial role in shrouded cascade stability by indirectly influencing system imaginary forces through contact friction load as it will be discussed.

A proper response form should therefore account for the influence of all three groups of forces, and it is developed in section 3.2.

3.2 Solution Form

A constitutive displacement model is utilized for total cascade response to properly account for the influence of each group of forces. This response is assumed to contain three major terms corresponding to each force group: a static (zero frequency or mean) term, an exponential term, and a periodic (or alternating) term as shown in equation 7.

$$\{\boldsymbol{\eta}\} = \{\boldsymbol{\eta}_{sta}\} + \bar{\alpha}_{exp} \cdot \{\boldsymbol{\eta}_{per}\} \quad (7)$$

A solution sequence is developed next to determine each term of the response, taking into account computational efficiency and the ability of solution method to accurately determine nonlinear forces. For the purpose of clarity in demonstration, this method is first applied to a system with only aerodynamic damping in present section and expanded to a fully nonlinear mechanical damping of the system in section 3.4.

Static component of the response is obtained using a time domain solution from application of centrifugal and steady state gas and thermal loads on the structure. Due to presence of contact interface which has no stiffness for gaps but only allows penetration of surfaces with contact normal stiffness, this is a nonlinear problem and therefore must be solved in time domain. This solution step is presented in matrix format as:

$$[\mathbf{K}]\{\boldsymbol{\eta}_{sta}\} = \{\mathbf{F}_{StSt}\} \quad (8)$$

Shroud contact parameters are included in this step as inputs that influence cascade stiffness matrix. Shroud tips of adjacent blades come into contact as a result of deflection associated with substantial operational loads, and a significant normal load develops between the contact surfaces. While this force is variable during the vibrating motion, its static (zero frequency or mean) value can be determined from static component of the response. Iterative methods are used to solve this problem by various matrix inversion methods and determine the static displacement vector according to equation 9.

$$\{\boldsymbol{\eta}_{sta}\} = [\mathbf{K}]^{-1} \{\mathbf{F}_{StSt}\} \quad (9)$$

System periodic response is generally harmonic because real forces are much larger in magnitude than imaginary forces. Therefore a homogenous companion equation can be solved to closely approximate periodic characteristics of the response, regardless of its instantaneous peak amplitude.

$$[M]\{\dot{\eta}_{per}\} + [K]\{\eta_{per}\} = \{0\} \quad (10)$$

Viscous damping matrix $[C]$ is omitted here for simplicity, however a linearized representation of $[C]$ may be included as linear combination of $[M]$ and $[K]$ matrices and considered in the modal analysis.

In case of shrouded blades, the boundary condition provided by the shroud at the end (or upper span) of a slender airfoil is fundamentally important in determining cascade vibration characteristics. Therefore a pre-stressed stiffness matrix is used in equation 11 to account for these influencing factors. Pre-stress stiffness matrix is calculated during the static solution and does not require an additional solution. This pre-stressed analysis concept is very similar to vibration analysis of a guitar string, where string tension influences frequency.

$$[M]\{\ddot{\eta}_{per}\} + [K_{pre}]\{\eta_{per}\} = \{0\} \quad (11)$$

Periodic response of the system is represented by a single harmonic period function that is the eigenvalue solution to equation 11.

$$\{\eta_{per}\} = \{\varphi\}e^{i\omega_n t} \quad (12)$$

Where $\{\varphi\}$ and ω_n are eigenvector and frequency of vibration and can be obtained using FEM software. Any of the fundamental modes of Equation 11 may be analyzed for susceptibility to flutter. In modern shrouded cascades with transonic or supersonic flow regimes, first torsional mode shape is often reported as the most likely mode to be excited due to its interaction with passage throat and shock wave [18] and is considered in present dissertation.

After determining mode shape and frequency of periodic response, the next step is to determine the effects of imaginary forces on the response. While imaginary forces do not significantly affect the periodic response due to their small magnitude, by the virtue of their $\pm 90^\circ$ phase angle they influence total energy

input into the system and slow build up or die down of amplitude over many cycles. Imaginary forces can be evaluated by substituting the assumed periodic motion into fluid and structural domains with known amplitude.

3.2.1 Aerodynamic Work Interaction

Aerodynamic study of the mode shape of interest involves evaluating unsteady pressure distribution that is caused by motion of the airfoil and motion of all other airfoils in the cascade. Multiple methods are available as detailed in section 2.4, and typically the most accurate and computationally efficient method used in the industry is frequency domain 3D Navier-Stokes based solver [29]. Using the unsteady pressure field and the energy method, aerodynamic work interaction with the fluid is determined by integrating the incremental work done by unsteady pressure field and airfoil motion over the full cycle.

Methods to evaluate aerodynamic energy exchange are well established and will not be discussed in details here. Aerodynamic Work per cycle is typically normalized to kinetic energy to obtain log-decrement aerodynamic damping which is assumed constant (amplitude independent) for small amplitudes.

$$\delta_{aer} = - \frac{W_{pc_aer}}{4.K_e} \quad (13)$$

3.2.2 System Response with Aerodynamic Damping Only

System response with energy based solution approach is first demonstrated for simplicity for a system with consideration of aerodynamic damping only. Total energy into the cascade during one cycle of vibration is the work interchange between the fluid and the structure:

$$\Delta E_{pc} = W_{pc_aer} \quad (14)$$

Assuming system energy during a flutter response is predominantly associated with the corresponding flutter mode shape, this total work per cycle can be normalized to system kinetic energy

using equation 13 to determine log-decrement damping coefficient. From definition of log-decrement function:

$$\delta_{aer} = \ln \frac{x_{cn}}{x_{cn+1}} \quad (15)$$

Or:

$$x_{cn+1} = x_{cn} e^{-\delta_{aer}} \quad (16)$$

Therefore the influence of linearized aerodynamic work input into the system is exponential increase in each cycle's peak amplitudes. For a system with circular frequency of ω_n the corresponding exponential component can be expressed as:

$$\bar{\alpha}_{exp_aer} = e^{-\delta_{aer} \frac{\omega_n t}{2\pi}} \quad (17)$$

Total system response for a system with only aerodynamic damping, starting from initial amplitude α_0 , is therefore as follows:

$$\{\eta\} = \{\eta_{sta}\} + \alpha_0 \{\varphi\} e^{(-\frac{\delta_{aer}}{2\pi} + i)\omega_n t} \quad (18)$$

Where $\{\eta_{sta}\}$ is the static response to operational loads at corresponding engine speed and operating condition, α_0 is the amplitude of initial perturbation, $\{\varphi\}$ and ω_n are mode shape and frequency of the system with consideration of pre-stress effects, and δ_{aer} is aerodynamic log-decrement damping. Figure 12 shows time domain representation of both periodic and exponentially growing response for a system with negative aerodynamic damping. Hypothetical value of -5% aerodynamic damping is used in this graph for clear illustration of the response.

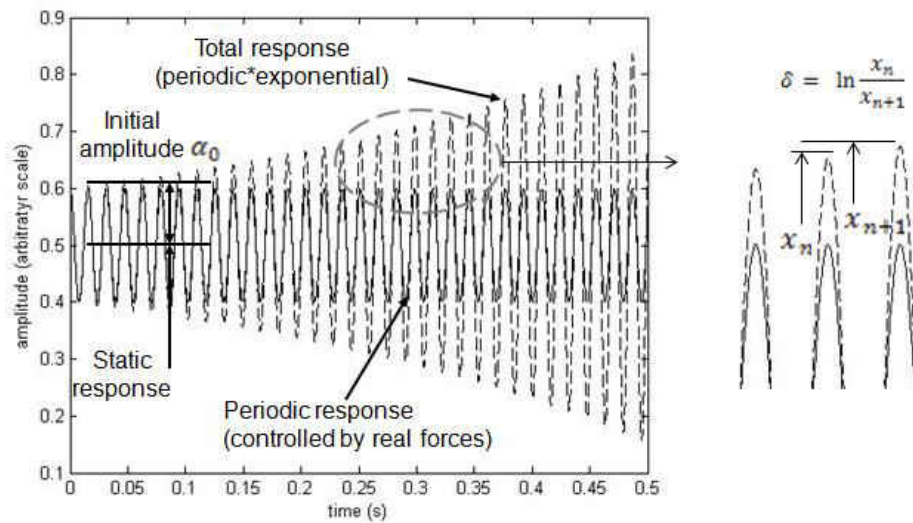


Figure 12: Time domain response of cascade with periodic and exponential components with only aerodynamic damping (-5% aerodynamic damping, $\omega_n = 400\text{Hz}$)

3.3 Mechanical Work Dissipation

Inclusion of mechanical work dissipation and associated damping in cascade stability calculations is a major contribution of present dissertation to the science of turbomachinery flutter. Current energy method based on positive aerodynamic damping criteria assumes all of the energy extracted by the structure from the fluid is accumulated in the structure during each cycle, leading to flutter instability. Therefore energy input over each cycle is calculated from equation 14, with consideration of aerodynamic work interaction only.

Present dissertation adds consideration of energy dissipation within the structure as a result of vibrating motion, in addition to aerodynamic work interaction. To accurately determine energy dissipation within the cascade, both viscous (linear) and non-viscous (nonlinear) portions of mechanical damping are included. Energy accumulated in the structure during each cycle is therefore the energy extracted by the structure from the fluid plus energy dissipated within the structure (which is always a negative work value) due to viscous and frictional effects.

$$\Delta E_{pc} = W_{pc_aer} + W_{pc_vis} + W_{pc_fri} \quad (19)$$

3.3.1 Viscous Damping

Viscous damping is characteristic of blade material and can be measured experimentally in a ping test. It is typically assumed constant (not a function of amplitude) and is represented in a SDOF system as critical damping ratio ξ , or log-decrement damping δ_{vis} .

$$\xi = \frac{c}{c_{cri}} \approx \frac{\delta_{vis}}{2\pi} \quad (20)$$

Energy dissipation due to viscous damping can be calculated using linear SDOF vibration equations

$$W_{pc_vis} = \pi c \omega x^2 \quad (21)$$

It can be shown that:

$$\delta_{vis} = - \frac{W_{pc_vis}}{4.K_e} \quad (22)$$

Non-viscous damping is much more difficult to determine due to nonlinearity, and it is further discussed in section 3.3.2.

3.3.2 Non Viscous (Frictional) Damping

Non viscous damping, also referred to as dry friction damping in literature, is the result of relative slipping motion between adjacent shrouds and associated dissipative work. Due to nonlinearity this type of damping is typically researched in forced response studies [53, 67], where frequency sweep method is used along with known excitation amplitude to experimentally study system response. In a self-excited problem, excitation amplitude is itself an unknown. With the additional unknown, study of flutter problems with friction becomes much more difficult than forced response friction problem.

While there are multiple sources of work dissipation due to friction, shroud tip contact contributes the most to non-viscous damping in shrouded cascades and is considered in present research. Dominant influence of shroud tip work dissipation compared to other contributors such as root and under platform

dampers is due to large relative displacement between adjacent shrouds and significant contact normal load at the tip. Relative displacement is a function of contact tangential stiffness and mode shape, which are in turn functions of shroud contact condition and prevailing nodal diameter. Contact condition and friction force are themselves functions of contact normal load which is caused by multiple factors such as blade untwist due to centrifugal load, thermal growth of the shrouds, and difference in operating temperature of the disk and the blade.

Contact normal load is itself an unknown in this problem and can only be determined analytically since experimental measurement of this force under operating condition is not practical due to compact nature of the shroud tip geometry and extreme centrifugal load and temperature during operation (often exceeding 1.0×10^5 g and 1000°F). Further complexity is time variability of this force during a vibration cycle. Yang [69] researched dynamics of shrouded fan blade vibration, demonstrating that as a result of 3D motion of adjacent blades contact normal load between part-span shrouds is not constant during the cycle of vibration. This consideration adds further complexity in determining contact status transition from stick to slip condition and non-viscous mechanical damping in general.

To address these complexities and determine non-viscous mechanical damping with consideration of all relevant parameters, an analytical method is developed by de-coupling system damping from amplitude of response. This method is discussed in full details in section 3.4.

3.4 Nonlinear Damping Due to Dry Friction

Work dissipation associated with nonlinear friction force is known as dry friction or Coulomb damping. Due to inherent nonlinearity of friction, this type of damping is amplitude dependent. This causes a coupling between nonlinear friction and aeroelastic equations of motion in a flutter problem, which cannot be readily solved. To enable a solution, de-coupling technique is used in this dissertation where friction damping is first evaluated as function of amplitude over one cycle of vibration and amplitude is then

determined based on total energy into the system over many cycles. In this section, work dissipation associated with friction damping is determined as function of amplitude. This is effectively a structural problem without any consideration of aerodynamic loads, with assumed values for amplitude to determine motion of the structure, friction forces acting on contact surfaces, and resulting incremental work dissipation. Work dissipation is then evaluated for a single cycle of periodic motion by integrating incremental values over the full cycle. Details of this method and consideration of nonlinear effects on mode shape are described in sections 3.4.1 through 3.4.6. Development of this method satisfies the first objective of this dissertation.

Work per cycle dissipation associated with friction damping can be calculated for multiple values for amplitude and expressed as a function of amplitude from this exercise. With this function available, aeroelastic equations can be solved with consideration of both aerodynamic work interaction and mechanical dissipation to determine total energy input and system response, as it will be discussed in section 3.5.

3.4.1 General Friction Law

Multiple friction models have been proposed [42, 43, 44], with trade-off between accuracy and simplicity. Coulomb friction law and contact stiffness model similar to [47] are used in present dissertation due to relative simplicity. According to this model, nonlinear friction force at the contact interface can be expressed as:

$$F_{Fri}(S) = \begin{cases} S \cdot K_{Tan} , & S < \frac{\mu \cdot F_{Nor}}{K_{Tan}} \\ \mu \cdot F_{Norm} , & S \geq \frac{\mu \cdot F_{Nor}}{K_{Tan}} \end{cases} \quad (23)$$

It must be noted that F_{Norm} is a not constant in this application involving shrouded blades, with implications that are discussed in [68]. Figure 13 shows nonlinear behavior of friction interface with

constant and oscillating normal load. Contact tangential stiffness and slip threshold force are shown for reference as they will be referred to throughout this section.

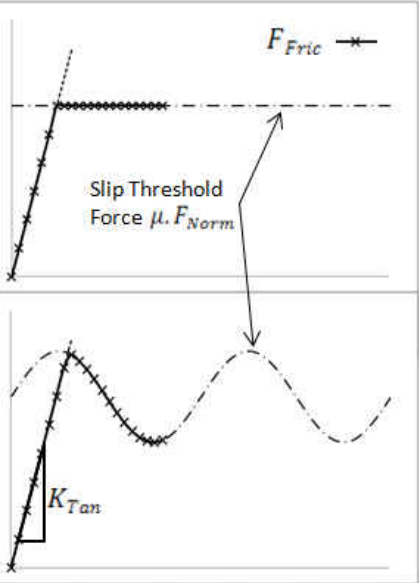


Figure 13: Nonlinear friction with variable normal load

3.4.2 Three Step Time-Frequency-Time Domain Solution Sequence

A solution sequence is developed next using computationally efficient solution techniques to solve system equations in multiple domains and evaluate work dissipation for known amplitude. The solution sequence and information exchange flow chart for this hybrid time-frequency-time domain method is shown in Figure 14 and discussed in detail in this section.

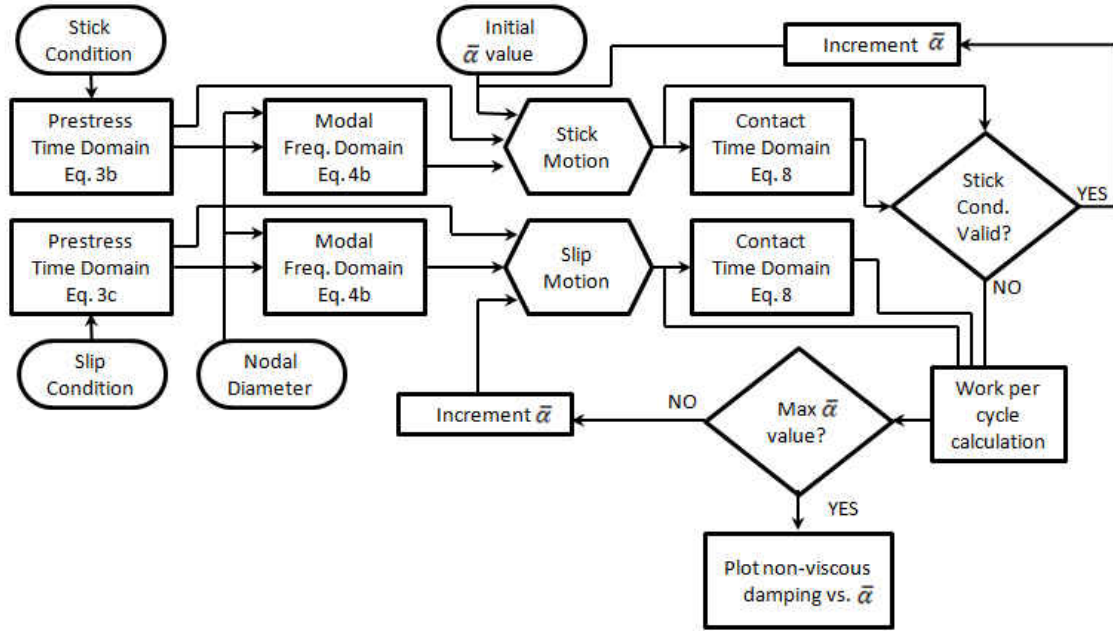


Figure 14: Solution sequence and information exchange flow chart

The first solution step is a time domain solution to determine contact normal load which is a nonlinear function of many design and operational parameters. This step is performed using equation 8 with all steady state centrifugal, thermal, and pressure loads to determine airfoil untwist and resulting contact normal load under steady state operating condition. This solution step also calculates stiffness terms associated with steady state components of $\{F_{AD}\}$ and $\{F_{Con}\}$ that will be used in prestressed stiffness matrix.

To account for nonlinearity associated with contact stick-slip condition, equation 8 is initially solved with both conditions according to equations 24 and 25, resulting in two sets of displacement fields and prestressed stiffness matrices to be used in subsequent analyses.

$$\{\eta_{sta_stk}\} = [K_{stk}]^{-1} \{F_{StSt}\} \quad (24)$$

$$\{\eta_{sta_slp}\} = [K_{slp}]^{-1} \{F_{StSt}\} \quad (25)$$

The second solution step is a frequency domain modal solution to determine cascade natural frequencies and mode shapes of vibration. A common assumption is made here that is typical in energy

based flutter analysis. It is assumed that frequencies and mode shapes of the system are dominated by oscillating inertial and structural forces. Oscillating aerodynamic and contact forces do not significantly influence mode shapes and frequencies, and they only dissipate small amounts of energy over each cycle. Note that the influence of steady state portion of contact forces is still accounted for in the analysis by using prestressed stiffness matrix. To incorporate this assumption, a companion equation representing a linear homogenous representation of the system is solved in frequency domain using equation 10 and prestressed stiffness matrix from the first solution step.

As noted, stick-slip condition at the shroud tip influences mode shapes and frequencies of the system due to difference in contact tangential stiffness. To account for this influence, two companion models are initially solved with K_{pre_stk} and K_{pre_slp} as system prestressed stiffness matrices corresponding to shroud contact in stick and slip condition respectively.

Assuming a response in form of equation 11, corresponding frequencies and mode shapes of each contact condition are obtained such that the following equations are satisfied:

$$(-\omega_{n_stk}^2)[M]\{\varphi_{stk}\} + [K_{pre_stk}]\{\varphi_{stk}\} = \{0\} \quad (26)$$

$$(-\omega_{n_slp}^2)[M]\{\varphi_{slp}\} + [K_{pre_slp}]\{\varphi_{slp}\} = \{0\} \quad (27)$$

Any of the system's mode shapes may be analyzed to determine mechanical damping associated with them. Focus of present dissertation is the first torsional mode which is typically associated with flutter issues in shrouded blades. Similarly, any nodal diameter of the cascade for that mode family can be analyzed. Least stable nodal diameter as determined from aerodynamic damping calculations is used in present dissertation since it is known that this is the nodal diameter most susceptible to flutter and will be excited before any other nodal diameter.

To determine non viscous work dissipation, relative in-plane displacement and friction force at the contact interface must be known. Due to nonlinearity and amplitude dependence, friction force must be determined in time domain as a function of amplitude of vibration. Implementing this rational requires the

addition of another solution step after the modal solution to evaluate friction force at the tip in time domain and as a function of known vibration amplitude. This can be done over a single cycle of vibration since all parameters are only functions of amplitude for a given mode shape and nodal diameter.

For the third solution step, full period of vibration is divided into N equal time steps to be used for the time domain expansion of the response.

$$\Delta t = \frac{T}{N} \quad (28)$$

Time domain division scheme of one full period is shown in Figure 15. The number of time steps along the cycle is arbitrary, although using more time steps will better capture details of the contact behavior along the peaks and valleys of the harmonic motion.

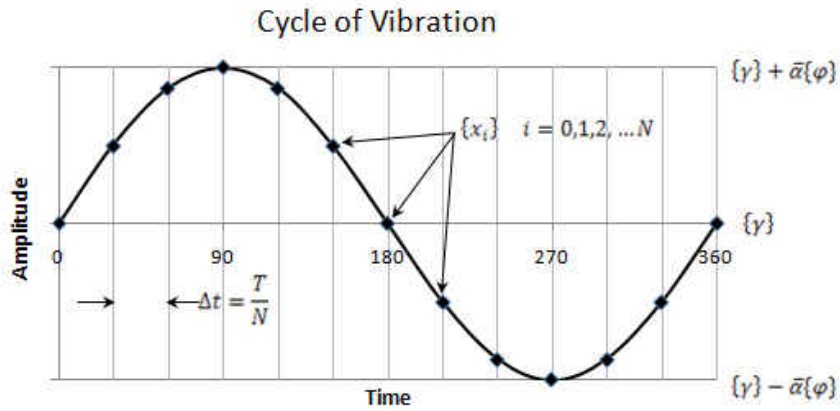


Figure 15: Full cycle of vibration and time step division

Next a value of \bar{y} is assumed as the instantaneous amplitude of vibration and system response is expanded in time domain at all time steps using equation 29:

$$\{\eta_l\} = \{\eta_{sta}\} + \bar{y}\{\varphi\}e^{i\omega_n l \Delta t} \quad l = 0, 1, 2, \dots, N \quad (29)$$

This results in N sets of displacement fields $\{\eta_l\}$ representing incremental motion of the blade through one full cycle of vibration. This is essentially the time domain representation of vibrating motion for given input amplitude \bar{y} . This vibrating motion visually exhibits a phenomenon that is known as traveling wave, caused by regular phase angle between adjacent blades in the cascade. This phenomenon

is shown in Figure 16 over a half cycle of periodic motion. As each blade vibrates in the prescribed nodal diameter pattern, peaks and valleys of the outer ring appear to move gradually to the right even though individual blades are stationary in this picture. When rotation at operating RPM is considered, observed traveling wave is the sum of actual traveling wave plus rotational speed of the cascade.

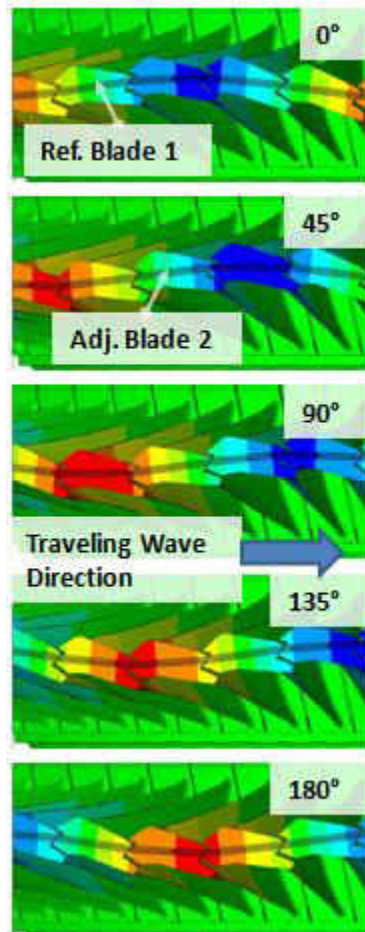


Figure 16: Vibrating motion of cascade

This traveling wave vibrating pattern results in relative motion between adjacent shroud tip surfaces, which is related to initial assumptions made for contact parameters such as tangential stiffness and coefficient of friction. To fully study the effects of this relative motion on contact forces, a subsequent time domain problem is solved at each time step of the cycle to determine solution to contact surfaces as a result of the imposed displacements. To minimize computational time, small subset of the original system

containing only shroud tip region and associated contact elements is used in this solution step since displacement is already known and values of contact loads are of interest.

This solution is repeated for each time step in a series of time domain solutions using Eq. 30.

$$\{\mathbf{F}_{con,l}\} = [\mathbf{K}_{con}]\{\boldsymbol{\eta}_l\} \quad l = 0, 1, 2, \dots N \quad (30)$$

Purpose of this solution step is to utilize detailed motion of contact surfaces at each time step through one full cycle of vibration and evaluate parameters affecting work dissipation. These parameters include relative in-plane displacement, contact normal load, and friction load. Contact relative displacements are used in both normal to contact surface and parallel to contact surface directions to determine the contact force vector acting on the shroud. This step of the solution also takes into consideration changes in the relative angle between adjacent contact surfaces and resulting cubic stiffening effects that may occur. It must be noted that all of these parameters are functions of amplitude, and they are calculated at this point for a given value of $\bar{\gamma}$.

Solution step 3 is repeated similar to steps 1 and 2 for both stick and slip conditions. Starting from small values of $\bar{\gamma}$, in plane friction force is evaluated using the stick response and corresponding contact normal force. A validity check is performed next to determine contact condition based on calculated relative displacement and friction force. For stick condition to be valid:

$$\mathbf{s} \cdot \mathbf{K}_{tan} < \boldsymbol{\mu} \cdot \mathbf{F}_{norm} \quad (31)$$

If the condition is not valid, smaller value of $\bar{\gamma}$ is used to find a response that satisfies stick condition.

Once a valid solution for stick condition is established next step is to determine transition from stick to slip condition as discussed in section 3.4.3.

3.4.3 Contact Condition Transitions from Stick to Slip

To study mechanics of shroud contact, amplitude of motion is assumed to gradually increase from small amplitudes associated with stick mode shape to larger amplitudes associated with slip mode shape. Assuming motion initiates from an original equilibrium position (relative displacement corresponding to static solution), vibrating motion of the cascade results in relative motion between adjacent shroud contact surfaces. For a given amplitude, trajectory of this relative motion in plane of contact with stick condition is in form of a tilted ellipse comprised of two in plane components that may be out of phase with each other. Figure 17 shows series of these trajectories with multiple small and increasing values of $\bar{\gamma}$.

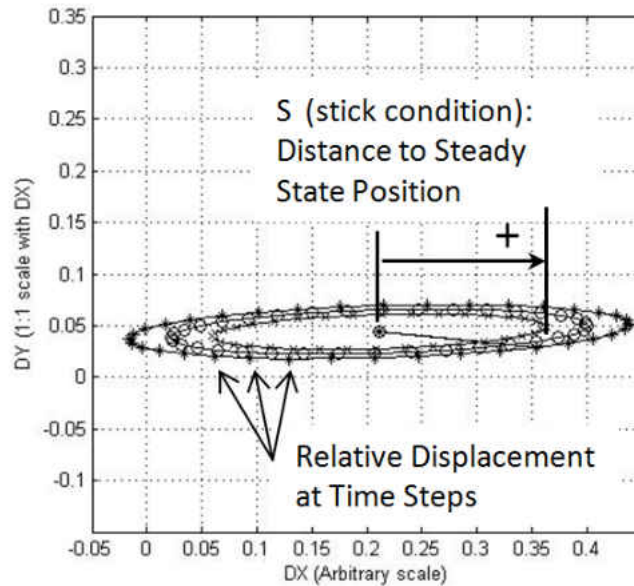


Figure 17: In plane trajectory of relative motion with stick mode shape

Distance S along the trajectory relative to static position is used in equation 23 to calculate in plane friction force during contact stick condition with corresponding mode shape. As long as in plane friction force remains smaller than slip threshold value $\mu \cdot F_{Norm}$ as shown in Figure 18, its value is the product of the distance from steady state position and contact tangential stiffness. Friction force in this amplitude

range is linear and there is no hysteresis loop, so no work dissipation is taking place (according to the simplified Coulomb friction model).

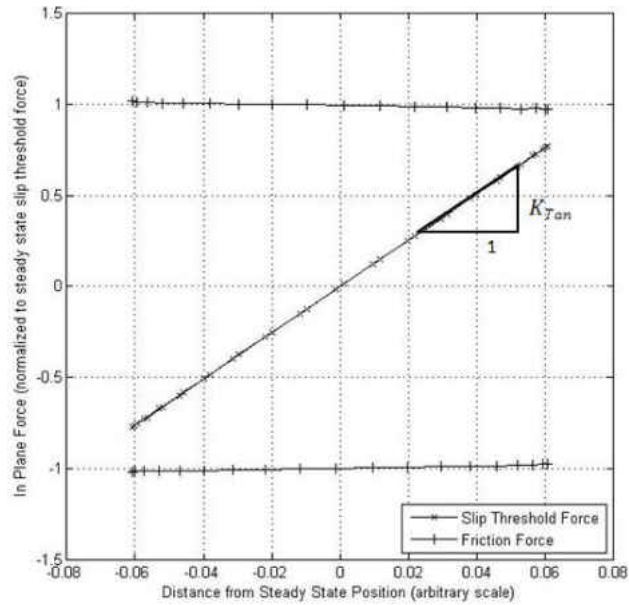


Figure 18: Friction force vs. distance from steady state position

The mechanics of transition to slip condition are illustrated in Figure 19. Values of in plane friction force and slip threshold are shown over the full cycle of oscillation for two increasing values of $\bar{\gamma}$.

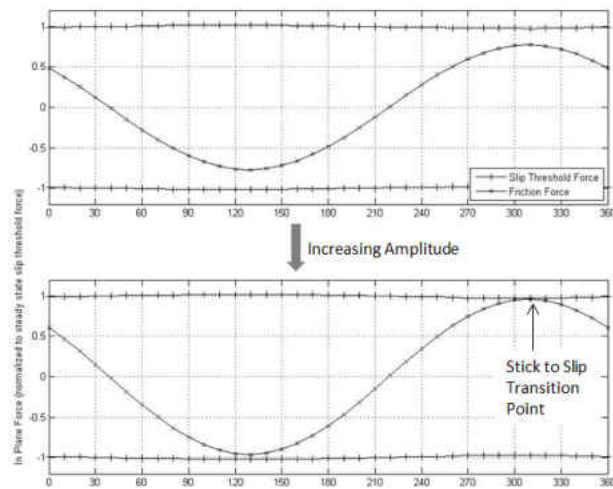


Figure 19: Transition from stick to slip condition

Top plot in this figure corresponds to a value of $\bar{\gamma}$ that equation 31 remains valid throughout the cycle. In plane friction force oscillates between the bounds of slip threshold but never reaches them. In this case, work dissipation is zero and all energy is stored and released elastically due to contact tangential stiffness. Bottom plot corresponds to a value of $\bar{\gamma}$ that in plane friction force becomes equal to the threshold force at a particular phase angle. It must be noted that threshold force itself varies through the cycle due to change in contact normal load but variations are not appreciable at this amplitude. The variation in threshold force is the reason intersection point at 130° phase angle in Figure 19 appears farther than intersection point at 310° phase angle.

At amplitudes larger than slip threshold, slip mode shape is used for evaluation of relative motion, contact force and work dissipation. Relative motion with slip mode shape features much larger in plane motion and slightly different tilt in axis of elliptical trajectory as shown in Figure 20 (a). Distance s in equation 23 is now (with slip motion) calculated to each end of the elliptical orbit, which corresponds to the outer corners of hysteresis loop shown in Figure 20 (b).

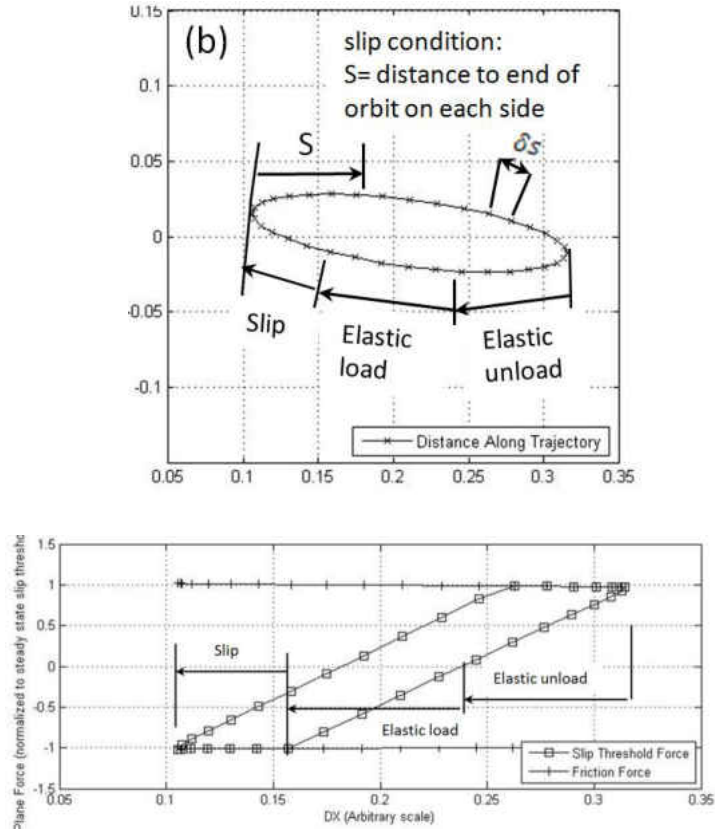


Figure 20: (a) In plane trajectory with slip mode shape, (b) Hysteresis loop

With cascade operating in slip mode shape and formation of hysteresis loop with positive enclosed area, energy dissipation due to friction damping initiates as discussed in section 3.4.4.

3.4.4 Work Dissipation Due To Friction

Next step in the algorithm shown in Figure 14 is to determine work dissipation over one full cycle of vibration. Work dissipation for a given value of $\bar{\gamma}$ is calculated by using the corresponding contact friction force and relative displacement between adjacent shroud tips. In a numerical scheme and with consideration of variable forces, incremental work dissipation at each time step is computed using the friction force at current time step and incremental displacement relative to previous time step.

$$\Delta W_l = F_{Fri} \cdot \delta s \quad (32)$$

Note that only incremental work during slip portion of the cycle results in net work dissipation since incremental energy stored elastically during stick portion of the cycle will be released on the reverse (unload) side of the hysteresis loop. This is because prior to slip initiation relative contact tangential displacement is assumed to be fully elastic (according to simplified Coulomb friction model). Total per cycle work dissipation is calculated by integrating (or summing up in a discrete numerical domain) the incremental work dissipation during slip condition over the full cycle. This summation can be shown to be equivalent to the area enclosed within the hysteresis loop.

$$W_{pc_fri} = \sum_{l=0}^N \{ \sigma \cdot \Delta W_l \} \quad (33)$$

Parameter σ is used as slip indicator where:

$$\sigma = \begin{cases} \mathbf{0} & , s. K_{Tan} < \mu \cdot F_{Norm} \\ \mathbf{1} & , s. K_{Tan} \geq \mu \cdot F_{Norm} \end{cases} \quad (34)$$

The above process is repeated for multiple values of $\bar{\gamma}$ to numerically determine work dissipation versus amplitude function, as further discussed in section 4.2.

3.4.5 Equivalent Log-Decrement Damping

Work exchange in flutter analysis is typically normalized to kinetic energy of the system associated with the mode shape of interest to evaluate resulting log-decrement damping. It is assumed in this process that all of system kinetic energy is associated with the dominant single mode motion associated with flutter. This assumption is only valid during a flutter event when the associated flutter mode shape becomes the dominant response of the system.

With non-viscous damping, log decrement damping is amplitude dependent and cannot be assumed constant as with linearized damping. However work exchange and kinetic energy of the system over one cycle of vibration can be approximated using average cycle amplitude with reasonable accuracy if change in amplitude between multiple cycles is relatively small (i.e., systems with low damping such as

turbomachinery cascades). Therefore while log-decrement damping is amplitude dependent and can change over multiple cycles, it is assumed constant over one cycle in this dissertation. Symbol β is used to express amplitude dependent log-decrement damping exponent which is differentiated from constant log-decrement damping represented by symbol δ .

Non-viscous damping over one cycle is therefore obtained by normalizing frictional work dissipation during a single cycle by kinetic energy associated with the same cycle.

$$\beta_{fri} = - \frac{W_{pc_fri}}{4 Ke} \quad (35)$$

Kinetic energy is associated with mass matrix and modal velocity vector, and for period motion it can be expressed as:

$$Ke = \frac{1}{2} \{\dot{\eta}\} [M] \{\dot{\eta}\}^T = \frac{1}{2} (\bar{\gamma})(\omega_n) \{\varphi\} [M] (\bar{\gamma})(\omega_n) \{\varphi\}^T \quad (36)$$

Since mass normalized mode shapes are used in all work per cycle calculations, kinetic energy associated with the mode shape by itself (without a scale factor) is equal to:

$$\{\varphi\} [M] \{\varphi\}^T = \mathbf{1} \quad (37)$$

Therefore log-decrement damping corresponding to a single cycle is:

$$\beta_{fri} = - \frac{W_{pc_fri}}{2 (\bar{\gamma} \omega_n)^2} \quad (38)$$

3.5 System Response with Nonlinear Damping

With consideration of mechanical work dissipation within the system, net energy exchange of the system is calculated using three major contributors according to equation 19: aerodynamic, viscous, and non-viscous (friction related) work exchange or dissipation. Aerodynamic and viscous component of work per cycle can be determined using currently available methods. Friction work dissipation is evaluated numerically as a function of amplitude using the method developed in section 3.4

$$W_{pc_fri} = f(\bar{\gamma}) \quad (39)$$

Equation 19 can be normalized by system kinetic energy to obtain total system log decrement damping, noting that total system damping is non-constant and amplitude dependent similar to friction damping.

$$\beta_{tot} = \delta_{aer} + \delta_{vis} + \beta_{fri} = - \frac{W_{pc_tot}}{4.K_e} \quad (40)$$

To obtain the exponential component of the system response with amplitude dependent damping, a numerical solution method is developed by creating a number of time series arrays for time dependent response variables. Time is scaled to natural period of oscillation so each entry in the time series corresponds to one cycle. Starting from the time of initial perturbation ($t=0$), number of vibration cycles of the cascade cn can be expressed as:

$$cn = integer\left(\frac{\omega_n t}{2\pi}\right) \quad cn = 1, \dots N_{cyc} \quad (41)$$

In this pseudo-time domain, values of β_{fri} and β_{tot} are considered constant over one cycle as discussed in section 3.4.6. Starting from an initial condition of amplitude α_0 , average amplitude of each cycle is designated as $\bar{\alpha}[cn]$. Total work exchange of the system, kinetic energy, and total system damping are evaluated for present cycle based on its average amplitude, and values are collected in numerical series where each entry corresponds to a single cycle.

$$\beta_{tot}[cn] = - \left(\frac{W_{pc_tot}}{4.K_e} \right) [cn] \quad (42)$$

Here, $\beta_{tot}[cn]$ is total system log decrement exponent that is valid only for cycle cn and its instantaneous sign is a measure of increase or decrease in kinetic energy and amplitude of next cycle. It is normalized values of all work input into the system and dissipation within the system based on the amplitude of current cycle.

Amplitude of next cycle is calculated using definition of log-decrement exponential function:

$$\bar{\alpha}[cn + 1] = \bar{\alpha}[cn] \cdot e^{\beta_{tot}[cn]} \quad (43)$$

With the amplitude of next cycle known, this process of evaluating work exchange, kinetic energy and amplitude of next cycle can be repeated until a converged value of amplitude is reached, or until irreversible divergence is observed indicating cascade instability. Stability evaluations are further discussed in section 4.3 with results of case study.

Figure 21 shows the flow diagram for determining cyclic amplitude numerical series, using HCF limit as an upper bound for a viable design. If total system damping becomes zero at some amplitude, cascade is stabilized and the amplitude will converge to a constant value which is known as LCO.

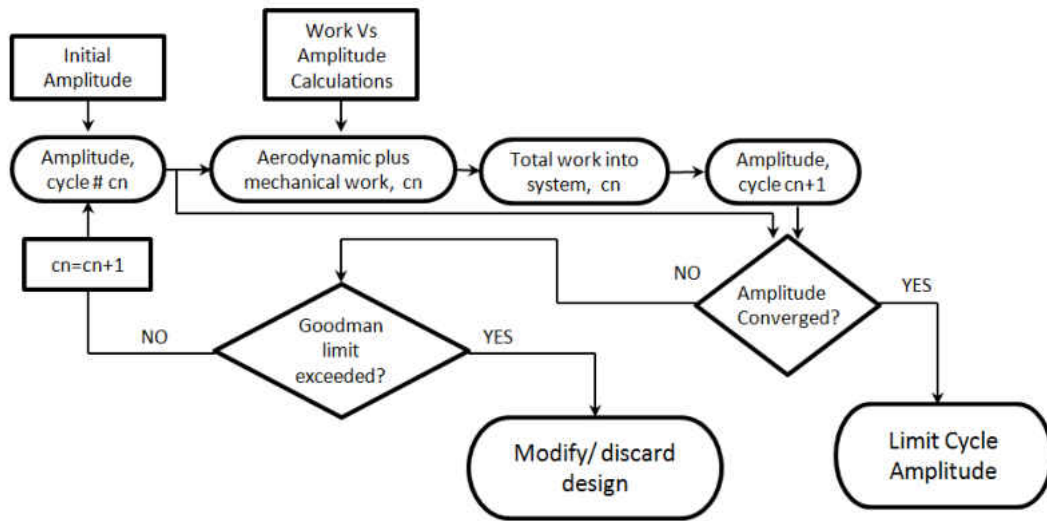


Figure 21: Algorithm for determining system response and stability

Since $\bar{\alpha}[cn]$, $\beta_{tot}[cn]$ and $\beta_{tot}[cn]$ are single dimension arrays, their calculations are computationally efficient. Amplitude of many cycles can be calculated efficiently and with consideration of all relevant contributors to determine system stability starting from an initial condition.

Total system response for a system with nonlinear friction damping is therefore as follows:

$$\{\eta\} = \{\eta_{sta}\} + \bar{\alpha}[\text{integer}(\frac{\omega_n t}{2\pi})] \{\varphi\} e^{i\omega_n t} \quad (44)$$

Figure 22 shows response of the cascade with only linear damping (-1.4% aerodynamic plus 0.6% viscous) and total damping (-0.8% linear plus frictional values from case study in section 4). It can be seen that while linear damping shows unstable response (sum of aerodynamic and viscous damping is slightly negative), friction damping can stabilize the system when amplitude becomes large enough for contact to transition to slip and initiate work dissipation.

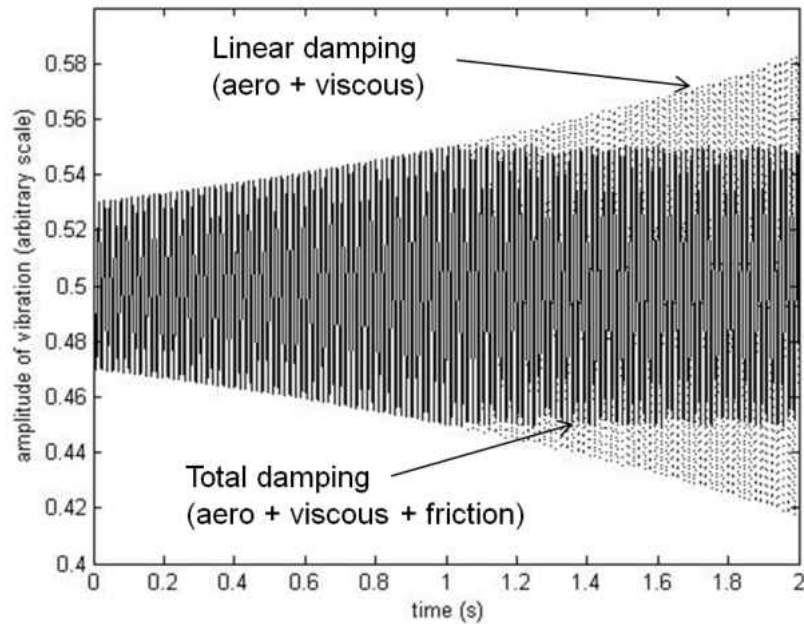


Figure 22: System response with linear damping and total damping

3.6 Cascade Stability

For a system with negative aerodynamic damping, the most unstable nodal diameter of vibration is the one with least (most negative) aerodynamic damping [41]. Therefore stability calculation with total system damping can be limited to this one nodal diameter with most negative aerodynamic damping. This nodal diameter is identified in aerodynamic work analysis, and it is of most concern because it will be excited before all others. Total work into the system (or normalized work represented by log-decrement damping) associated with this nodal diameter determines cascade stability. Sign of total system damping can be used to determine stability. However, since log-decrement damping is itself a variable based on

amplitude and time in a nonlinear system, change in its sign must also be considered when determining overall stability. This concept will be demonstrated in section 4.3 with the case study.

CHAPTER FOUR: FINDINGS

Practical application of this analytical framework is demonstrated in this section by conducting case study of a last stage turbine blade of an IGT engine. This blade (see Figure 5) was recently redesigned for an upgrade package [77] and is used for the computational domain in present dissertation.

Findings and results of the analysis are shown in sections 4.1 through 4.5. Due to proprietary nature of the case study, design information is considered confidential. Therefore arbitrary or scaled units are shown in all graphs, except for calculated values of nonlinear mechanical damping which is the primary contribution of present dissertation to science of flutter prediction. These values are actual damping values that are calculated for this particular blade design, and they can be used in peer review studies to compare with other blade designs.

4.1 Application to IGT Blade

A cyclic sector of the disk and the blade with periodic boundary condition is used in this case study to minimize computational cost while enforcing conditions of cascade nodal diameter.

Despite the need for computational efficiency, a large scale and detailed FE model of the blade is created to accurately simulate mode shape of the complex geometry and contact pattern with available computational tools. The sector model consists of about 1.1M DOF and 120 contact elements along the contact face to properly evaluate contact pressure distribution and force.

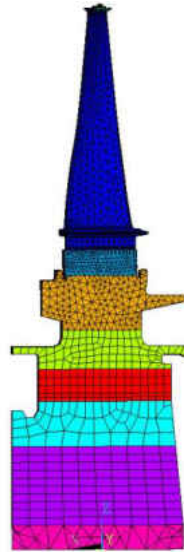


Figure 23: FEM model of one blade/disk sector

Three step solution process in section 3.4.2 is used to obtain three components of the response: static response under operational loads, modal response from frequency domain analysis, and contact force response from a post-modal contact solution in time domain. Numerical values of contact parameters (μ and K_{Tan}) are used consistently among all solution steps to properly simulate contact force and condition. Exact determination of these values, especially at high temperature, is often a challenge and is recommended for future research. Values measured in high temperature rig tests in [48] are used in present dissertation in absence of direct laboratory measurements.

For the first solution step, time domain static solution is obtained under operational condition with steady state loads such as centrifugal and thermal loads. Nonlinear effects of gaps are analyzed in this step, as an iterative matrix inversion method is used to ramp loads and converge on a solution after multiple iterations. Due to influence of contact normal load on work dissipation, this is a necessary step in any meaningful analysis.

Second solution step consists of modal analysis to determine natural frequencies and mode shapes of the rotating cascade with prestressed stiffness matrix from first solution step. Using a duplicate sector, real and imaginary natural mode shapes are obtained for the sector model. Real and imaginary mode shapes

are then combined together with periodic boundary condition corresponding to the nodal diameter of interest to expand a time domain representation of frequency domain solution. Expanded mode shape for second family (first torsion) sixth nodal diameter mode is shown in Figure 24. While only a sector model is solved, full cascade representation is shown for visualization purpose using graphical methods. Displacement scaling is used in this figure to show excessive deformation, as the amplitude of vibration is arbitrary at this point.

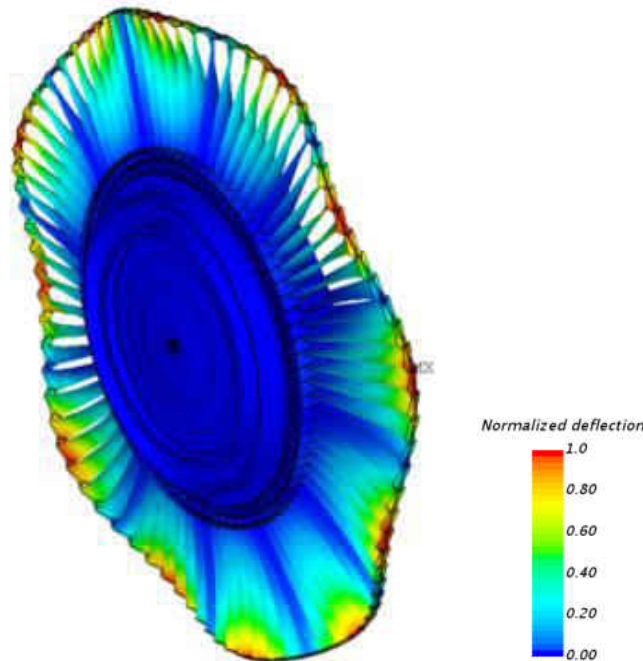


Figure 24: First torsional sixth nodal diameter mode shape of the coupled cascade with shrouds interlocked under operating loads

Aerodynamic work per cycle calculations are performed next using commercially available CFD solver with HBM and flutter analysis capability. Despite advances in analytics and computational power, this step is still the bulk of computational time associated with flutter analysis. This step is part of current analytical work flow so computational expense is expected and tolerated. Work per cycle is calculated with known amplitude, and log-decrement damping is determined from equation 13. This aerodynamic log-decrement is assumed to be constant (amplitude independent). Exact values of calculated aerodynamic

damping are not disclosed due to confidential nature of this information. General pattern of variations with nodal diameter are shown in Figure 25.

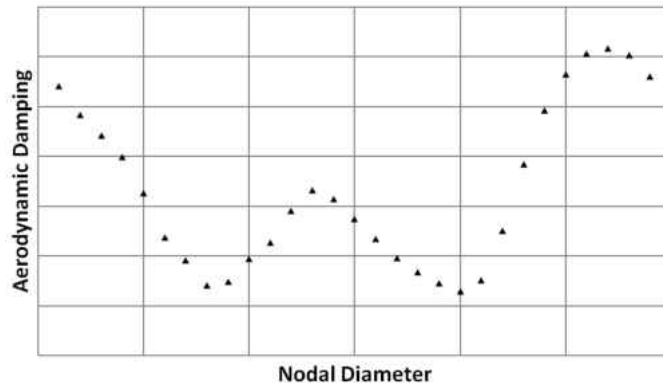


Figure 25: Typical aerodynamic log-decrement damping vs. nodal diameter

Viscous damping is material dependent and can be measured from ping testing results using half power width or other common methods. However such measurements are usually at room temperature and high temperature values are not available at this time. An estimated value of 0.6% log-decrement damping is used in present dissertation as an example of a realistic value.

Nonlinear friction damping is calculated according to section 3.4.4. In plane components of relative motion with multiple values and with two mode shapes corresponding to stick and slip conditions are shown in Figure 26 .

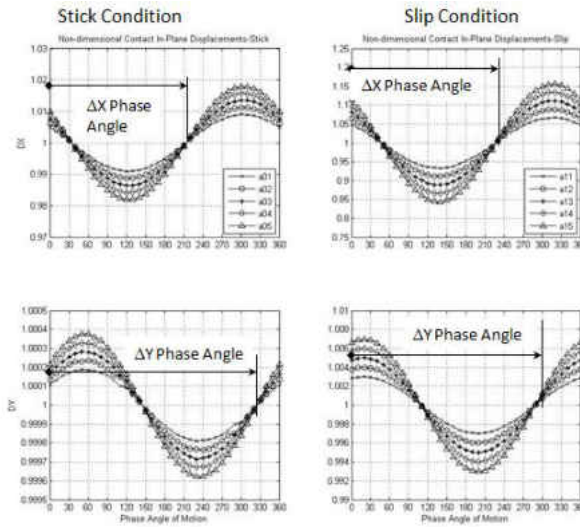


Figure 26: In plane relative motion for multiple values of $\bar{\gamma}$

Out of plane component of motion and contact normal force over full interface area are shown in Figure 27. Highly nonlinear geometric effects such as cubic stiffening can be seen in contact normal force with increasing amplitudes.

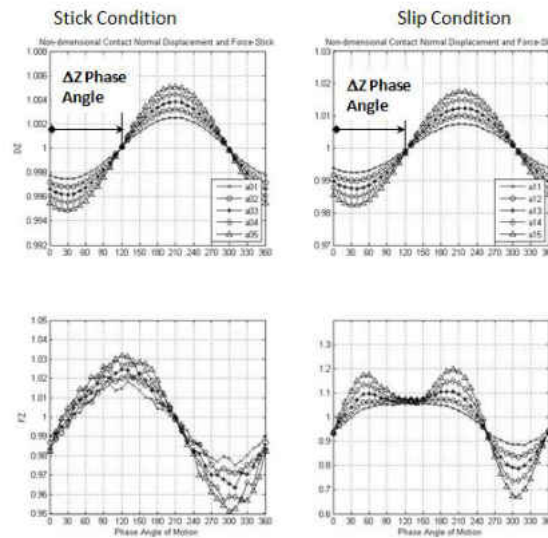


Figure 27: Out of plane motion and contact normal load for multiple values of $\bar{\gamma}$

Normal load is varying during the cycle which is included in the calculation of slip threshold force. Transition from stick to slip occurs when in plane friction force exceeds slip threshold force at any phase angle of the cycle. For friction damping to be present, the amplitude must raise to a large enough value to exceed slip threshold of the friction joint. Trajectory of relative motion changes as mode shape switches from fully stick condition to slip motion with larger amplitudes. Contact relative displacement is calculated relative to static position with stick condition and relative to end of each orbit in slip condition as shown in Figure 17 and Figure 20.

After slip threshold is exceeded, hysteresis loop forms and energy is dissipated by friction work during the slip portion of the cycle. Mode shape is switched to slip mode shape for further calculations.

4.2 Nonlinear Damping Results

Incremental work dissipation during each sub step of solution step 3 is evaluated next according to equation 32. Figure 28 (a) shows friction force and slip threshold force during the full cycle of vibration for a given amplitude. Figure 28 (b) shows the incremental in-plane distance δs relative to previous time step. Net work dissipation occurs only during the slip portion of the cycle as discussed in 3.4.5. Incremental work shown in Figure 28 (c) is the product of friction force F_{fri} , incremental distance δs , and slip condition indicator σ . This plot shows that incremental work is highly nonlinear over the cycle as numerical values of parameters change at each time step increment.

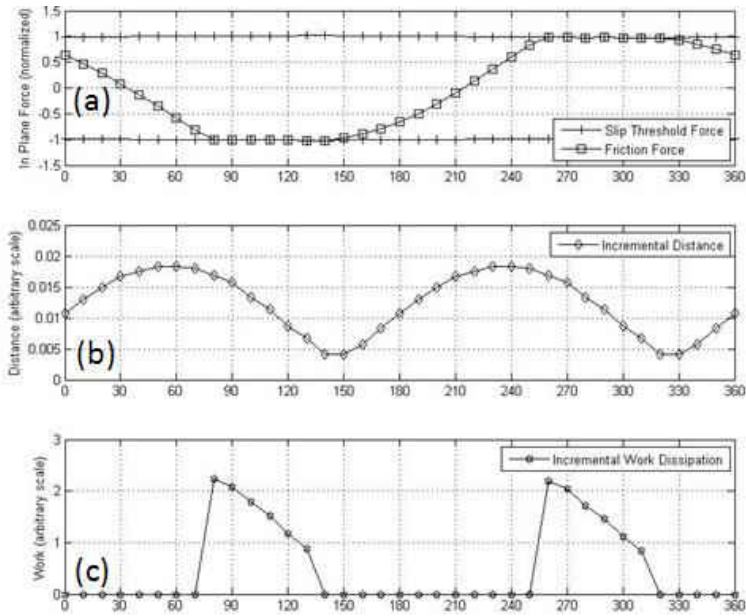


Figure 28: (a) Friction force (b) Incremental distance (c) Incremental work dissipation with small amplitude

With larger amplitude, influence of variable normal load becomes more pronounced, and slip portion of the cycle becomes larger time span of the full cycle. With work dissipation occurring over larger time span of the cycle, slope of work dissipation increases in addition to its value (see Figure 31). However, increase in slope due to this effect is limited to a certain amplitude range. With even larger amplitudes when work dissipation occurs over most of the cycle, no further slope increase is observed related to this effect.

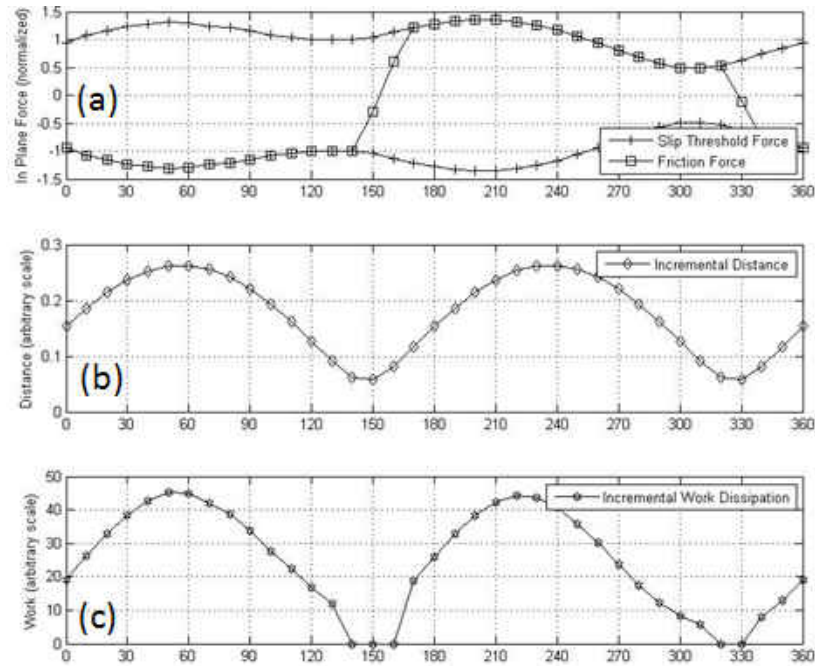


Figure 29: (a) Friction force (b) Incremental distance (c) Incremental work dissipation with large amplitude

To further illustrate the increase in enclosed area of hysteresis loop and work dissipation as the amplitude increases, Figure 30 shown the hysteresis loop for three increasing values of $\bar{\gamma}$ on the same axis of abscissas. Figure 30(a) corresponds to an amplitude post but near slip initiation condition, where hysteresis loop is narrow and slip only occurs on a limited portion of the cycle. Figure 30(b) corresponds to medium amplitude, where slip occurs on most of the cycle but variations in normal load are still insignificant. Figure 30(c) corresponds to relatively large amplitude within the range of study where variations in normal load start to influence the shape and enclosed area of the hysteresis loop.

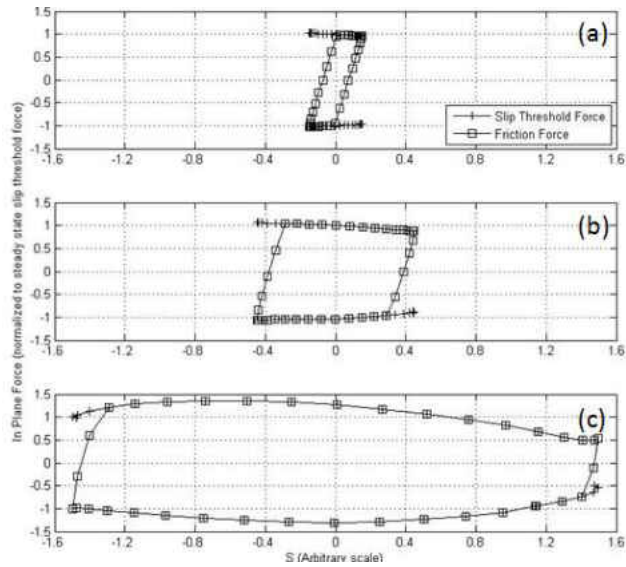


Figure 30: Hysteresis loop for (a) Small (b) Medium (c) large amplitudes

Work dissipation associated with friction is calculated by integrating (or summing up in a discrete computational domain) incremental work dissipation over the full cycle. This process is repeated for multiple amplitudes to obtain work dissipation as a function of amplitude, as shown in Figure 31 for the particular blade design studied here. Units are scaled in this graph due to confidential nature of design information.

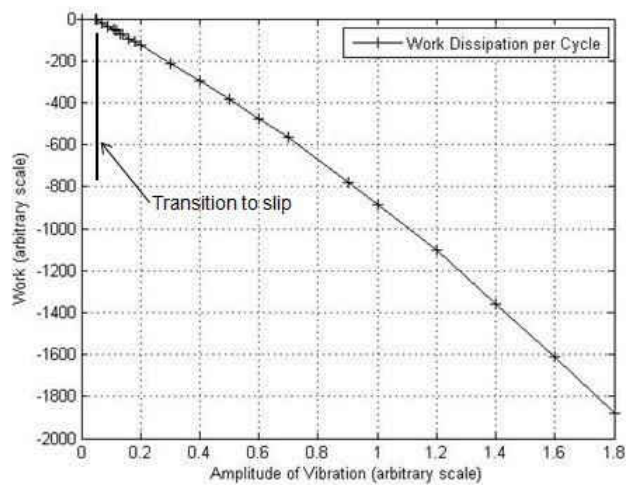


Figure 31: Non-viscous or frictional work per cycle as a function of amplitude

Change in work dissipation slope can be seen in the above figure. With increase in amplitude and slip occurring over larger time span of the cycle, slope of work dissipation increases gradually. However, increase in the slope due to this effect is limited to a certain amplitude range. With even larger amplitudes when slip occurs over most of the cycle, no further slope increase is observed related to this effect.

Work per cycle is normalized to kinetic energy (assumed to be primarily associated with flutter mode shape) to obtain log-decrement damping as a function of amplitude. This graph is shown in Figure 32. Transition from stick to slip condition and mode shape is shown in this graph as the amplitude where friction dissipation begins after friction force exceeds threshold. In reality, there is some frictional damping prior to this transition amplitude due to micro-slip effects which are not considered in this dissertation. Therefore damping through transition region will have a shallower slope in reality than shown here. This plot also shows that frictional damping after slip initiation is a nonlinear function of amplitude, and it declines with higher amplitude as kinetic energy of the cascade increases at a faster rate than work dissipation.

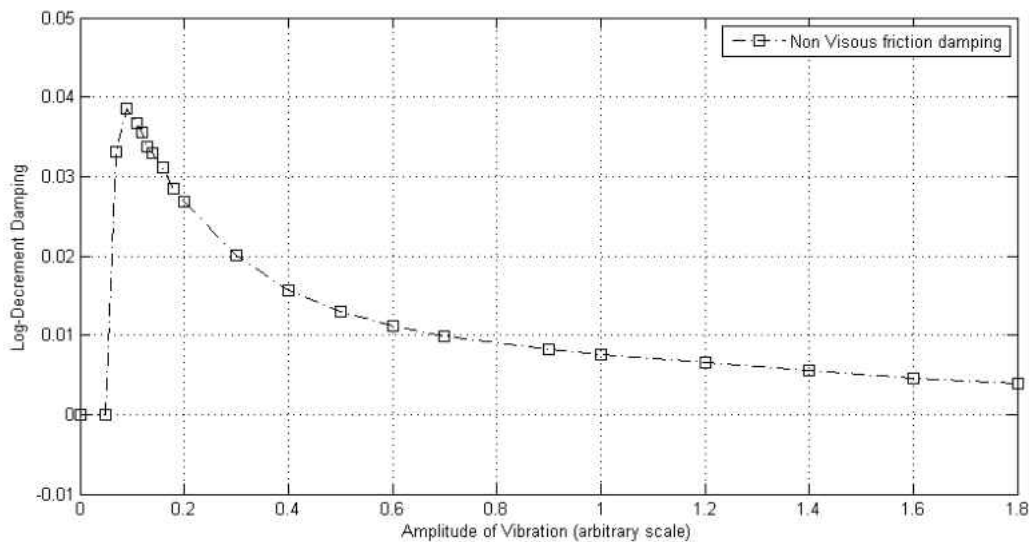


Figure 32: non-viscous mechanical damping as a function of amplitude

This nonlinear function of non-viscous mechanical damping versus amplitude is used for system stability analysis, as discussed in section 4.3.

4.3 Stability Prediction

For a system with negative aerodynamic damping, the most unstable nodal diameter of vibration is the one with least (most negative) aerodynamic damping [41] and it can be identified in aero-elastic damping versus nodal diameter plot. Stability calculation can be limited to this one nodal diameter with the least negative aerodynamic damping because this is the nodal diameter that will be excited before all others. Total work (sum of aerodynamic and mechanical work) into the system associated with this nodal diameter (represented by log-decrement damping) determines cascade stability. If the sign of total work into the system changes with increase in amplitude, it must also be considered.

To fully visualize total system damping as a function of amplitude, all components of total log-decrement damping for the most unstable nodal diameter are shown in Figure 33. Hypothetical values of -1.4% and 0.6% are used respectively for aerodynamic and viscous damping, along with non-viscous damping curve from Figure 32.

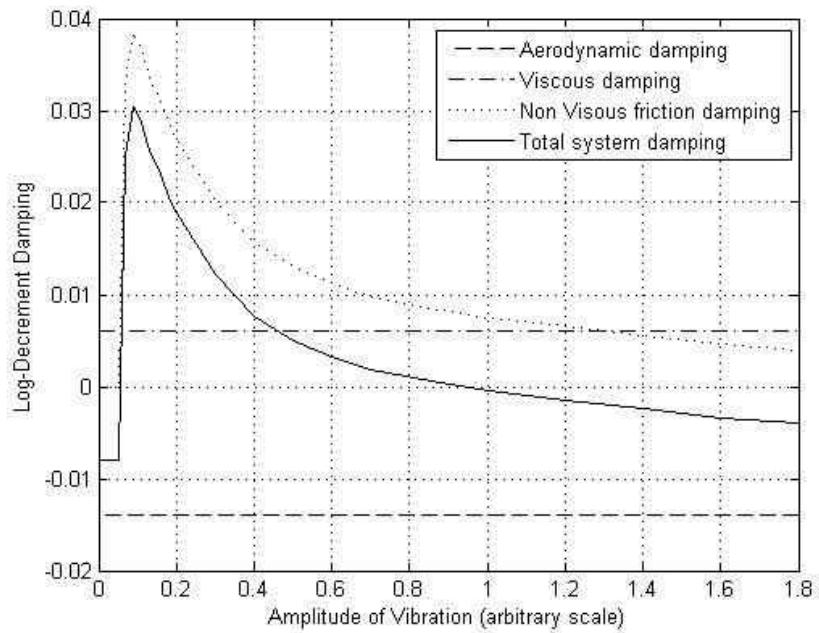


Figure 33: Total system damping as a function of amplitude

Based on visual examination of total damping curve, cascade stability can be divided into three distinct cases depending on aerodynamic damping:

A) For an aerodynamically stable cascade (with positive aerodynamic damping): total system damping is always positive therefore such cascade is always stable.

B) For an aerodynamically unstable cascade with high level of negative aerodynamic damping where total system damping is negative at all amplitudes (i.e., -5% or more negative in this example): total system damping is always negative therefore such cascade is always unstable.

C) For an aerodynamically unstable and frictionally damped system: Aerodynamic damping is slightly negative so total system damping is initially negative but changes sign with increasing amplitude. In this case, a small perturbation can be stabilized after it reaches certain amplitude to maintain a balance between aerodynamic excitation and mechanical dissipation.

Stability characteristics of shrouded cascades with case C are further illustrated in Figure 34. Based on the amplitude of initial excitation, the stability map is divided into three regions. HCF limit on vibratory stress (which is proportional to amplitude) is shown in this figure as the maximum amplitude of practical interest.

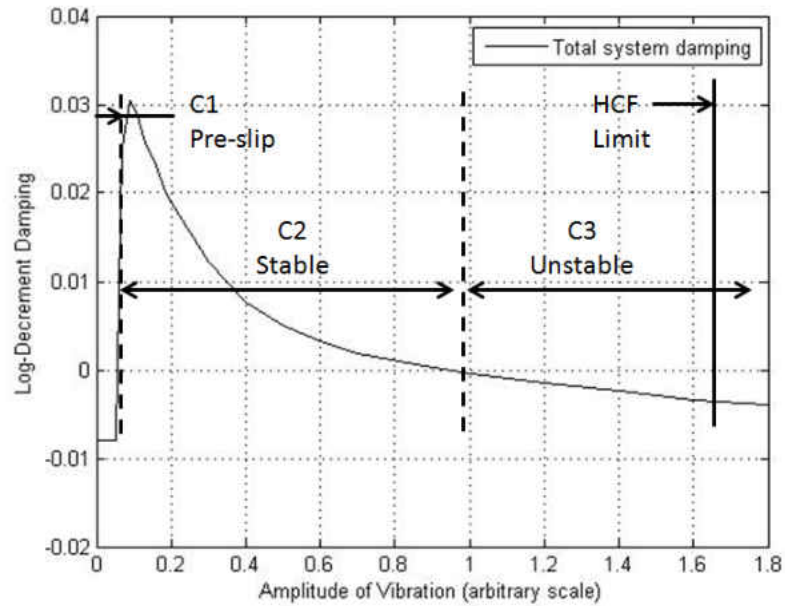


Figure 34: Cascade stability map for case C

Cascade stability in each region is determined from both sign of log-decrement damping associated with initial perturbation, and potential future change in sign of log-decrement damping associated with time history of system response and increase in amplitude. Each region is discussed below, depending on the amplitude of initial perturbation.

C1) this region represents a small initial perturbation, where shroud contact with the initial amplitude remains in stick condition. Since all relative motion between in-contact shroud tips is linear and proportional to tangential stiffness, area under hysteresis loop is zero which indicates no frictional work dissipation. Total system damping is negative; therefore amplitude increases with each cycle while the cascade remains in this region. However this region is not interpreted as globally unstable because it is bound by a stable region as amplitude increases and friction joint begins to slip.

C2) this region represents post slip region where negative aerodynamic damping is stabilized by combination of viscous and non-viscous mechanical damping. This region is stable and any perturbation initiating in this amplitude range will die out progressively over multiple cycles until it reaches lower bound amplitude immediately after slip initiation, where friction damping is at its peak. This is where the steady

state response maybe expected as a LCO. However if sources of perturbations are continuous (as a result of random vortex shedding of upstream components for example) system response may be higher than the stable LCO due to constant excitation. System is fully damped and stable with any amplitude in this region.

C3) this region is post slip and with larger perturbation amplitude where combination of viscous and friction damping due to decrease in the latter is not sufficient to overcome aerodynamic excitation. This region is unstable therefore if any initial perturbation is large enough to cause such amplitude it will lead to exponentially growing motion and immediate cascade failure.

Time domain system response for each region is shown in Figure 35. It is noted that for the range of variables used in this study (-1.4% aerodynamic, 0.6% viscous, non-viscous from Figure 32, $\omega_n \approx 400$ Hz) system response can be determined in as few as 500-1000 cycles or 1-2 seconds.

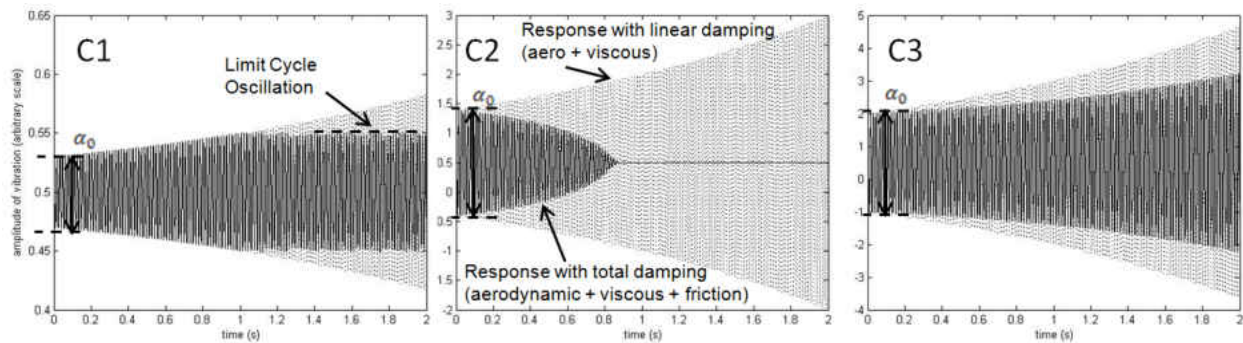


Figure 35: Cascade response with perturbation amplitude in C1, C2 and C3 sub-cases

4.4 Trade Studies

Results of parametric studies are presented in this chapter to demonstrate change in stability map as a function of most significant parameters which are aerodynamic damping, tangential stiffness of the contact surfaces, and coefficient of friction. This information is useful in evaluating stability margin with range of observed or calculated parameters.

System stability region for three different aerodynamic damping values are shown in Figure 36. These values are hypothetical and in the upper range of values of interest in the industry. Viscous log-

decrement damping value of 0.6% and non-viscous friction damping values from Figure 32 are used for this graph. It can be seen that stability region shrinks with decreasing aerodynamic damping as expected. Therefore, as aerodynamic excitation increases, progressively smaller perturbations have the potential to cause global instability and cascade failure. If aerodynamic damping becomes more negative than sum of viscous and non-viscous damping at any amplitude, such cascade is fully unstable and any perturbation will lead to immediate build-up of amplitude and cascade failure (case B).

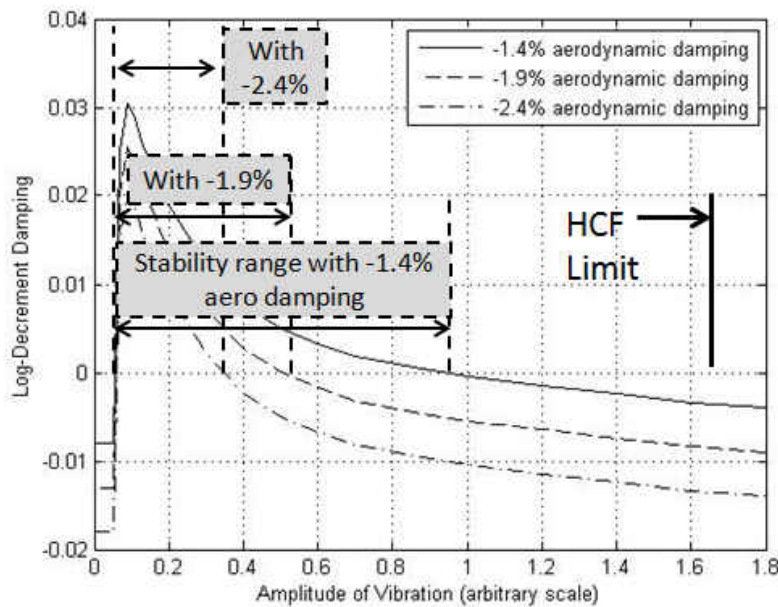


Figure 36: Total system damping with three aerodynamic damping values

Another influencing factor that effects friction damping and therefore total system damping is tangential stiffness of contact surfaces. System stability map for three different values of tangential stiffness is shown in Figure 37. Contact tangential stiffness influences slip threshold distance and therefore the boundary between C1 and C2 regions. It also influences mode shape and relative motion between adjacent shroud tips. Friction damping curves at constant amplitude increase as tangential stiffness decreases because relative contact displacement in the mode shape increases with softer constraint, resulting in more work dissipation. Natural frequencies are also slightly affected by change in tangential stiffness.

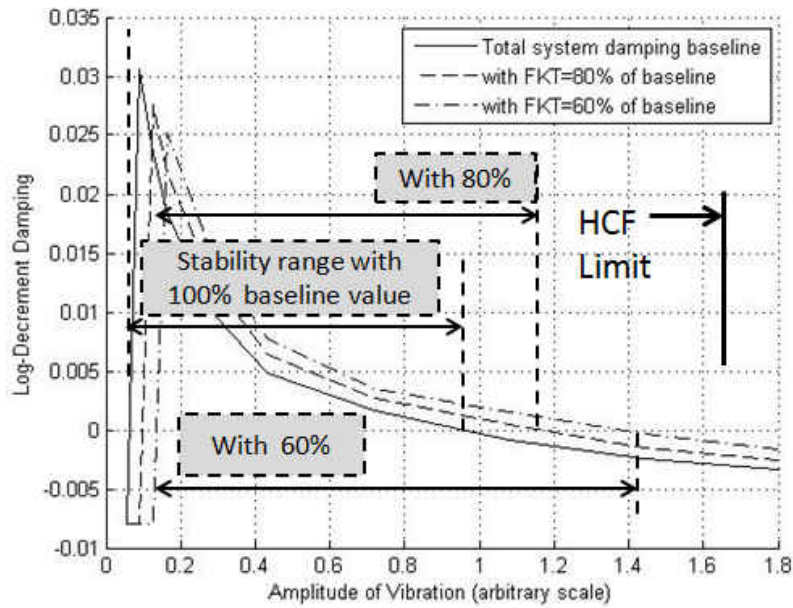


Figure 37: Total system damping with three tangential stiffness values

Finally, system stability map with varying values of friction coefficient is shown in Figure 38. Friction coefficient affects both transition to slip and friction damping therefore its increase has a stabilizing effect by shifting the boundary between regions C2 and C3 to higher amplitudes. This will increase the limits of initial perturbation that can be stabilized.

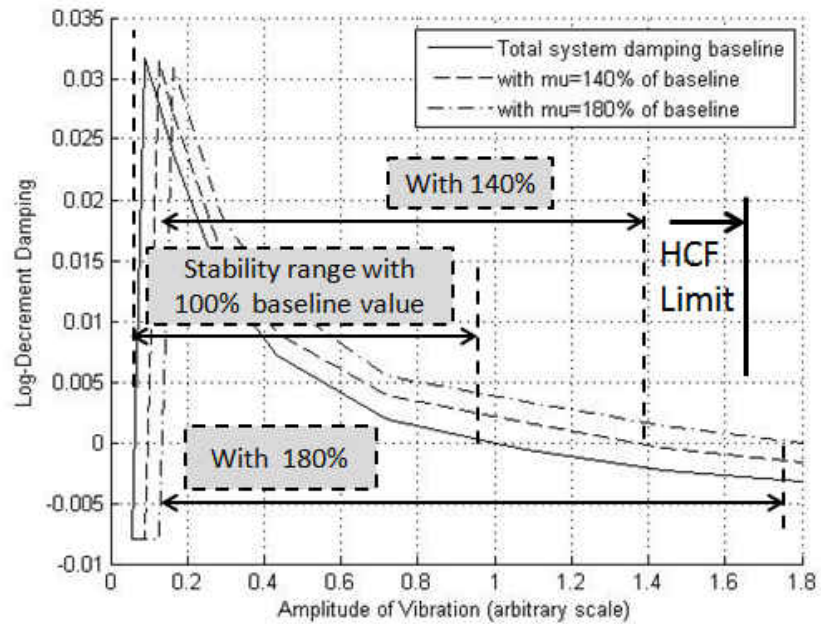


Figure 38: Total system damping with three coefficient of friction values

4.5 Engine Test and Data Analysis

The blade utilized in present case study was recently designed as part of an upgrade program to allow increase in turbine mass flow, and it exhibited negative aerodynamic damping for some nodal diameters. To ensure flutter free operation, tip timing data was obtained for the purpose of design validation after installation of subject blades in a commercially operating IGT [77]. Multiple probes around the cascade were used as shown in Figure 39 for identification of mode shape and traveling wave of response.

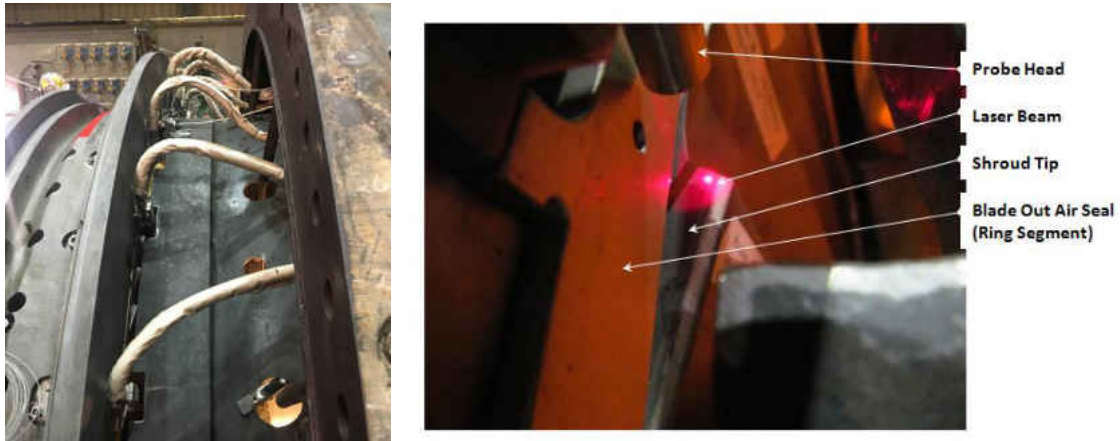


Figure 39: Tip timing instrumentation with multiple probes around the cascade

Observed response was mostly composed of low engine order rotor umbrella modes and engine order response of multiple upstream and downstream counts and differences in counts. An example of response of various traveling waves over time is shown in Figure 40. Flutter response of significant amplitude was not observed in the operating envelop of the engine for any nodal diameter, therefore cascade design proved successful. However, no affirmative data to establish boundary between stable and unstable operation was obtained due to lack of an organized, flutter related response.

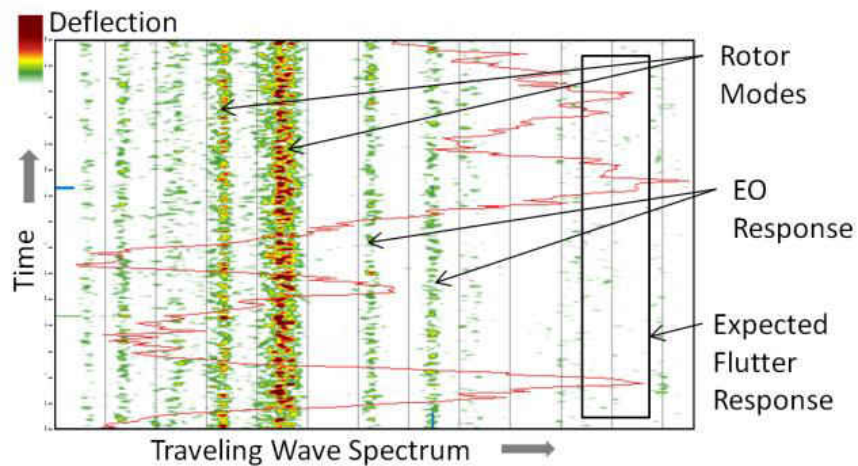


Figure 40: Cascade response at maximum power

It must also be noted that in an engine test only combined effects of aerodynamic and mechanical damping can be evaluated as the total energy in (or out) of the cascade. Neither aerodynamic nor

mechanical damping can be measured independently due to lack of detailed surface pressure instrumentation. Therefore to determine mechanical damping at flutter condition following information is required:

- i) Aerodynamic damping must be calculated through analysis at the operating condition where flutter becomes an issue, which is typically associated with maximum mass flow through the cascade which occurs during steady state operation at full load and fully open IGV angle.
- ii) Total system damping must be known at the same operating condition. Total system damping during steady state operation is only known when it becomes zero at the onset of flutter initiation. This condition was not observed during the validation testing campaign of the case study due to lack of flutter instability within the designated operating envelope of the engine.

With these limitations in mind, results of present study were compared to engine measurements as described below. Transition amplitude to slip condition was calculated using normal contact force predicted by analytical models and baseline contact parameters from [48]. This transition amplitude is shown as a red dotted line in Figure 41 along with time domain response of the cascade operating at the highest mass flow rate and output power of the engine.

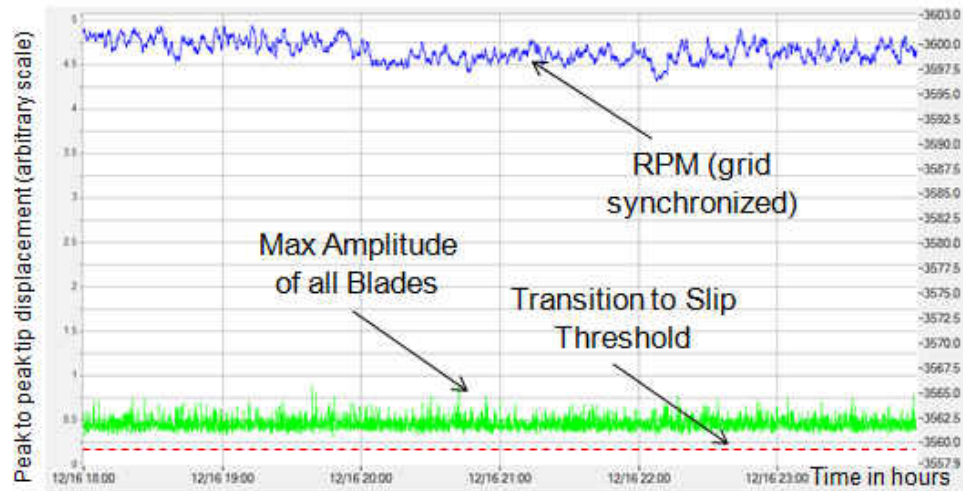


Figure 41: Cascade time domain response

Observed amplitude at this operating condition is higher than boundary line between C1 and C2 regions as predicted by the model using baseline contact parameters, indicating cascade is vibrating in slip condition and energy dissipation due to friction is taking place. However, majority of the observed vibration amplitude was due to other factors such as engine order excitation which may be present independent of flutter response.

Frictional damping of the cascade is determined using observed amplitudes from engine test as shown in Figure 42. While exact values of engine amplitudes and aerodynamic damping of the cascade are confidential, it can be stated that total system damping (aerodynamic plus mechanical) always remained positive with margin for any observed amplitude within the operating envelop. This is consistent with stable operation of the cascade under maximum mass flow condition which is evident in cascade time domain response shown in Figure 41.

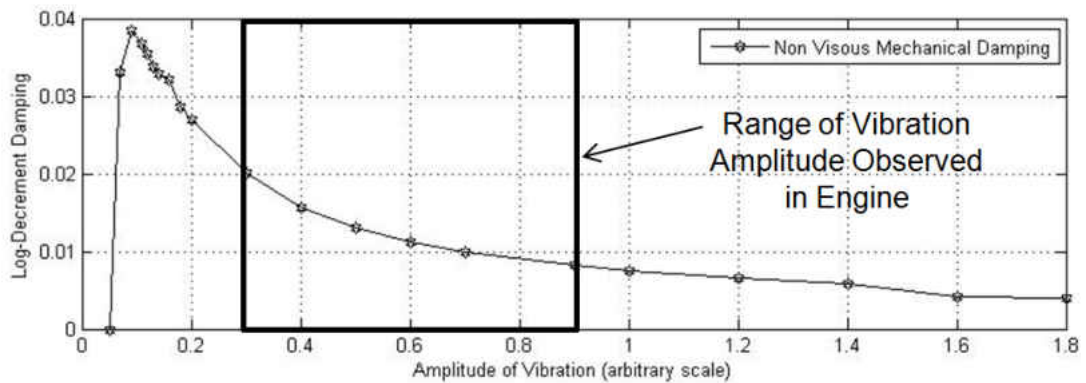


Figure 42: Frictional damping with observed engine amplitude

Operating in slip condition with small relative movement is consistent with physical condition of the contact surfaces after removal from engine, as shown in Figure 43.



Figure 43: Contact surface condition after removal from engine

Further validation of the damping calculations was conducted according to a reviewer’s suggestion on engine data during start up transients. Since transients which occur during rotor spool up are not associated with high mass flow through the engine, they are not considered flutter prone operating points. However cascade damping can be calculated from observed displacement data and frequency response spectrum of blades. Calculated damping can be compared with measured damping to validate the analytical

method for damping calculation, provided all analytical steps are conducted in operational conditions corresponding to engine operation at the time of crossing.

Three distinct crossings were observed during testing, and the method is applied to all three to compare with experimental data. For each crossing, blade operating conditions are different resulting in specific contact normal load and mode shape. First, nodal diameter and frequency of resonance are identified from engine data. A quasi-static condition is assumed based on engine RPM, estimated engine mass flow and blade operating temperature. Solution step 1 is performed at this quasi-static condition and contact normal load is calculated based on nonlinear contact solution.

Solution step 2 is performed next using pre-stressed stiffness matrix to obtain frequency and mode shape corresponding to observed nodal diameter in engine data. Contact tangential stiffness value is adjusted to match predicted frequencies of all crossings to observed data with reasonable accuracy. Remaining steps in the analytical method are repeated to calculate damping values at observed engine amplitudes. A viscous damping log-decrement value of 0.6% (approximately 0.1% c/c_{cr}) is added to calculated friction damping values to obtain total system damping. These damping values are compared to log-decrement damping values in observed data, which are calculated from best fit of tip timing data for each blade to a SDOF model. Mean damping values as well as min-max values are shown in Figure 44, along with calculated values with two different tangential stiffness assumptions.

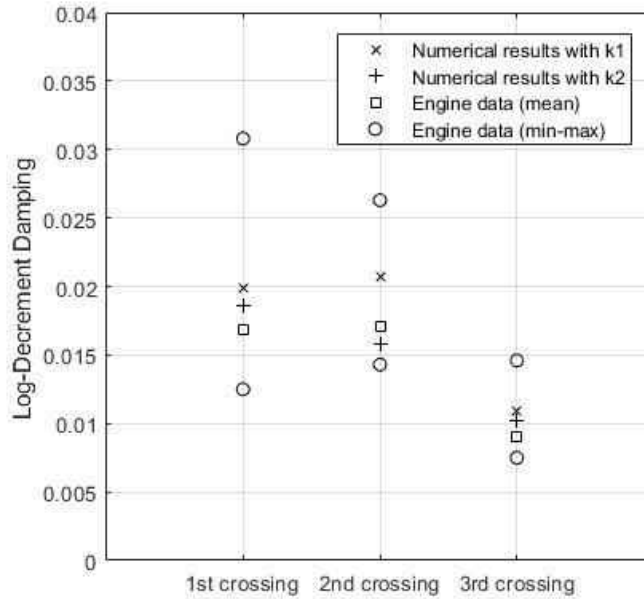


Figure 44: Comparison of numerical results with experimental data

Calculated results show good correlation with mean observed values, and are within range of observed values although there is large variation in data due to packet type response and localized excitations. Table 1 shows the error between calculated and observed mean damping values for both tangential stiffness assumptions.

Table 1: Percentage difference between numerical results and mean engine data

Crossing	Results with k1	Results with k2
1st	0.21%	0.08%
2nd	0.36%	-0.13%
3rd	0.19%	0.12%

Further comparison with engine data using case study of an actual flutter event in engine or large scale rotating rig can be used to further assess the damping method in a flutter application. This objective is not in alignment with the scope of a cascade design for a commercial program as the design and analytical efforts are typically intended to prevent flutter not cause it. However, previous cascade designs that have

encountered flutter in an engine can be analyzed using this method in case of availability of design configuration and operating condition corresponding to flutter event.

CHAPTER FIVE: CONCLUSION

In this dissertation an analytical framework for flutter analysis of shrouded cascade has been developed by extending the energy method to include work dissipation as a result of relative motion and nonlinear friction force at shroud tip contacts. This framework combines existing methods of flutter analysis with additional novel methods summarized in section 5.1 to determine nonlinear frictional damping in a self-excited application and overall stability characteristics of shrouded cascade.

Implementation of this framework is demonstrated on a large scale model of an actual IGT blade, and it indicates significant but amplitude dependent stabilizing effect of friction damping. Parametric studies are conducted to evaluate influence of various parameters. Comparison with limited engine data shows that total system damping remained positive for all observed amplitudes, and cascade remained stable as expected and observed. Due to lack of flutter related response of the test bed, however, transition between stable to unstable operation could not be established. Recommendations for future research in flutter prediction of shrouded cascade are presented in section 5.2 including high temperature measurements of contact parameters.

5.1 Dissertation Contributions

Underlying physical phenomenon that causes flutter can be summarized as the energy (or work) extraction by the structure from the fluid, and its accumulation in the structure in form of kinetic energy. In case of the undesirable condition of aerodynamically unstable cascade (with negative aerodynamic damping for at least one nodal diameter), the balance between aerodynamic excitation and dissipation through mechanical damping determines cascade stability. In current state of art flutter analysis, there is no method available to evaluate mechanical damping due to complications associated with nonlinear friction force.

A major contribution of present dissertation to the science of flutter is that it provides a novel method for quantifying the amount of mechanical damping and associated work dissipation in a flutter application with shrouded cascades. A hybrid, three-step solution method is developed to use best aspects of time and frequency-domain solutions for computational efficiency and capability to accurately determine nonlinearity and other shrouded cascade complexities. Prior hybrid and HBM solution methods are not adequate for this application because they do not account for the influence of static forces due to operational conditions, which plays a substantial role in flutter response of shrouded cascades. Prior time domain only methods are not practical with large scale models due to lack of computational efficiency.

Each solution method in proposed framework is selected optimally for computational efficiency and accurately predicting nonlinear friction related parameters. This framework utilizes all influencing parameters that have aerodynamic and structural impact and creates detailed information regarding motion, frequency, and contact load information over the full cycle of vibration. Effects of contact nonlinearity and transition from stick to slip condition are included as this nonlinear transition affects system mode shapes and friction damping. Shroud contact load variations during cycle of vibration are also included in the analysis by utilizing full motion of contact surfaces associated with mode shape.

Another contribution of this dissertation is to recognize the influence of the static component of response on mechanical damping and overall stability of the cascade. Cascade response is formulated as the product of a small time scale periodic component and a large time scale exponential component, in addition to a static (zero frequency) component which has a critical role in determining the exponential component as it impacts contact normal load and work dissipation.

Another contribution of present dissertation is to expand energy based methodology to include frictional work dissipation associated with vibrating motion of flutter and determine overall response characteristics of the cascade. Exchange of information between multiple domains is used to couple all equations and solve iteratively based on an efficient, energy based method and converge on a global flutter

condition that satisfies all constraints and requirements. This global flutter condition includes prevailing mode shape and nodal diameter of the cascade, corresponding frequency and amplitude of the motion, and amplitude trends which determine cascade stability.

Contributions from present dissertation are combined with existing methods to create analytical framework shown in Figure 45 for comprehensive solution to flutter problem in shrouded cascade applications. The new components of the framework are an addition to the existing structural dynamics and aerodynamic work interaction analyses that are routinely performed in the industry. Implementation of the new components enables evaluation of nonlinear friction damping and cascade stability with inclusion of amplitude dependent mechanical damping. New computational steps are computationally efficient and only add a small computational cost since they are performed only on one nodal diameter of the cascade (the most unstable).

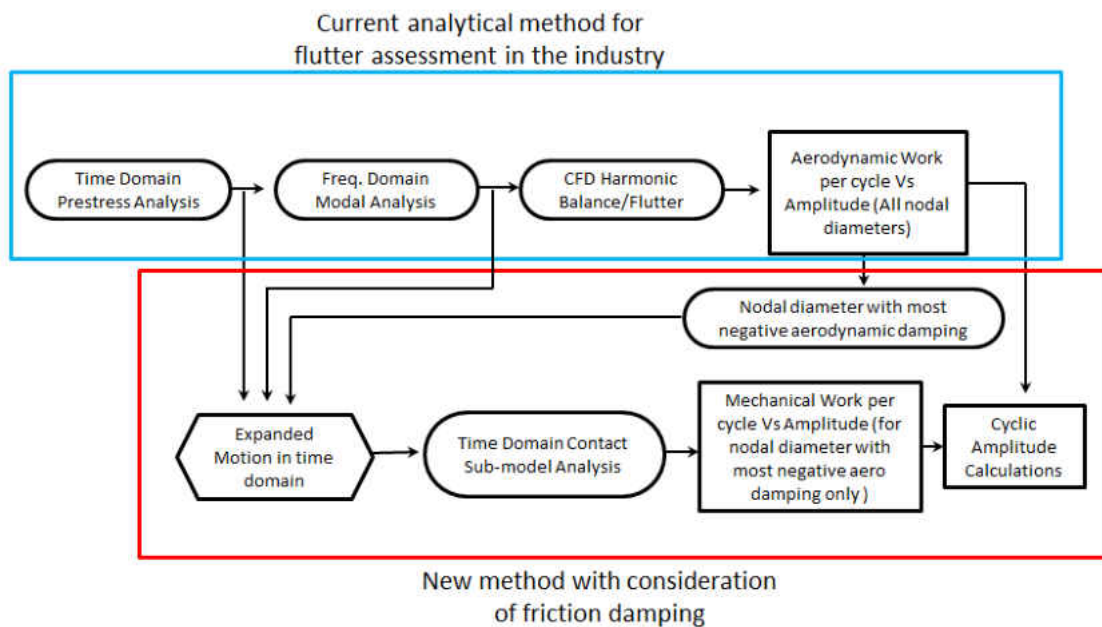


Figure 45: Novel aspects of flutter analysis framework

This framework enables prediction of cascade stability with better accuracy than currently possible with present state of the art analytical tools. For an aerodynamically unstable cascade, mechanical damping

has stabilizing effects. Stability map can be established based on calculated values of total system damping (both aerodynamic and mechanical) versus amplitude. Stability characteristics of cascade can be determined from the stability map and amplitude of initial perturbation. System response may comprise a logarithmically declining, logarithmically increasing, or steady limit cycle oscillations based on amplitude of initial perturbation.

Finally, trade studies are conducted to illustrate the effects of various influencing parameters. These studies show that variations in contact parameters can have important implications on cascade response and stability, and they must be considered in calculation of stability margin.

5.2 Future Research

Further experimental testing and comparison of data with analytical models is required for shrouded cascade although obtaining meaningful experimental data is often the most difficult aspects of flutter research. Full recreation of flutter condition in a rig remains a challenge and only engine operation provides true representative environment, considering that centrifugal loads, thermal conditions, steady and unsteady aerodynamic loads, and nonlinear friction forces all contribute to and influence this complex aero-elastic phenomenon. It can be argued that no rig can be so sophisticated as to mimic all aspects of an actual rotating cascade under full operational loads (centrifugal, thermal and steady state aerodynamic loads with maximum mass flow), therefore an actual engine remains the only fully representative environment for validation. Major obstacle in using engine as a test bed is that almost without exception engine hardware is designed NOT to flutter, therefore if design is successful goal of research is not satisfied and vice versa. Instrumentation data of future designs and engine tests can be used to further compare with stability prediction of analytical framework for aerodynamically unstable cascades that are stabilized by mechanical damping. Prior instrumentation data of cascades that have encountered flutter failure in the past can also

be used to further populate stability prediction map by re-analyzing these cascades using present analytical framework and comparing with engine data.

Further recommendation for research in flutter stability of shrouded cascades is experimental measurement of high temperature values for contact parameters. As demonstrated by trade studies, these parameters are highly influential in determining overall cascade stability yet only limited data is available in public domain.

Using experimentally measured values of contact parameters and response amplitude in the engine during a flutter event, the value of transition amplitude from stable to unstable operation can be established. This is the exact instance when total system damping becomes zero and aerodynamic damping and mechanical damping become equal. By evaluating aerodynamic damping with analysis, mechanical damping can be determined. This is practically the only way to validate a fully representative shrouded cascade flutter model, since neither aerodynamic excitation nor friction work dissipation are directly measurable and only their combined effect can be observed through cascade response in a fully representative environment.

Another item of interest for future research is study of sensitivities of the non-viscous mechanical damping to shroud design parameters such as contact angle and cold assembly gap that influence blade untwist and contact normal load.

LIST OF REFERENCES

- [1] V. Struhal, "Uebereinebesondere Art der Tonerregung (On an unusual sort of sound excitation)," *Annalen der Physik und Chemie*, vol. 3rd series, no. 5 (10), p. 216–251, 1878.
- [2] F. M. White, *Fluid Mechanics*, Third Edition, New York: McGRAW-HILL, INC., 1994.
- [3] T. Theodorsen, "General Theory of Aerodynamics Instability and," Langley, VA, 1935.
- [4] J. R. Write and J. E. Cooper, *Introduction to Aircraft Aeroelasticity and Loads*, Chichester: John Wiley and Sons Ltd, 2007.
- [5] A. R. Collar, "The Expanding Domain of Aeroelasticity," *Journal of the Royal Aeronautical Society*, vol. 51, pp. 1-34, 1947.
- [6] A. J. Scalzo, J. M. Allen and R. J. Antos, "Analysis and Solution of a Nonsynchronous Vibration Problem in the Last Row Turbine Blade of a Large Industrial Combustion Turbine," *Journal of Engineering for Gas Turbines and Power*, vol. 108, pp. 591-598, October 1986.
- [7] J. D. Jeffers and C. E. Meece, "F100 Fan Stall Flutter Problem Review and Solution," *Journal Aircraft*, vol. 12, pp. 350-357, 1975.
- [8] D. S. Whitehead, "Force and Moment Coefficients for Vibrating Aerofoils in Cascade," Technical Report R&M 3254, British ARC., 1960.
- [9] F. Lane, "System Mode Shapes in the Flutter of Compressor Blade Rows," *Journal of Aeronautical Sciences*, vol. 23, pp. 54-66, 1956.
- [10] F. O. Carta, "Coupled Blade-Disk-Shroud Flutter Instabilities in Turbojet Engine Rotors," *Journal of Engineering for Power*, pp. 419-425, Jul. 1967.
- [11] M. F. Platzer and F. O. Carta, "AGARD Manual on Aeroelasticity in Axial-Flow Turbomachines, Vol 1 Unsteady Turbomachinery Aerodynamics," Seine, France, 1987.

- [12] A. Bolcs and T. Fransson, "Aeroelasticity in Turbomachines: Comparison of Theoretical and Experimental Cascade Results," Switzerland, 1986.
- [13] A. Khalak, "A Framework for Flutter Clearance of Aeroengine Blades," *Journal of Engineering for Gas Turbines and Power*, vol. 124, pp. 1003-1010, Oct. 2002.
- [14] J. Waite and R. Kielb, "Physical Understanding and Sensitivities of Low Pressure Turbine Flutter," *Journal of Engineering for Gas Turbines and Power*, vol. 137, pp. 012502-1-01502-9, Jan. 2015.
- [15] M. Nowinski and J. Panovsky, "Flutter Mechanisms in Low Pressure Turbine Blades," *Journal of Engineering for Gas Turbines and Power*, vol. 122, pp. 82-88, Jan. 2000.
- [16] J. Panovsky and R. Kielb, "A Design Method to Prevent Low Pressure Turbine Blade Flutter," *Journal of Engineering for Gas Turbines and Power*, vol. 122, pp. 89-98, Jan. 2000.
- [17] R. Kielb, J. Barter, O. Chernycheva and T. Fransson, "Flutter of Low Pressure Turbine Blades With Cyclic Symmetric Modes A Preliminary Design Method," *Journal of Turbomachinery*, vol. 126, pp. 306-309, Apr. 2004.
- [18] J. J. Waite and R. E. Kielb, "The Impact of Blade Loading and Unsteady Pressure Bifurcations on Low-Pressure Turbine Flutter Boundaries," in *ASME TurboExpo*, Montreal, Canada, 2015.
- [19] T. Rice, D. Bell and G. Singh, "Identification of the Stability Margin Between Safe Operation and the Onset of Blade Flutter," *Journal of Turbomachinery*, vol. 131, pp. 011009-1-011009-10, January 2009.
- [20] R. E. Bartels and A. I. Sayma, "Computational Aeroelastic Modelling of Airframes and Turbomachinery: Progress and Challenges," *Phil. Trans. R. Soc. A*, vol. 365, pp. 2469-2499, 2007.
- [21] H. Thermann and R. Niehuis, "Unsteady Navier-Stokes Simulation of a Transonic Flutter Cascade Near-Stall Conditions Applying Algebraic Transition Models," *Journal of Turbomachinery*, vol. 2006, no. July, pp. 474-483, July 2006.

- [22] J. G. Marshall and M. B. Giles, Some Applications of a Time Linearized Euler Method to Flutter & Forced Response in Turbomachinery, T. H. Fransson, Ed., Kluwer Academic Publishers, 1998.
- [23] M. Jocker, A. Kessar and T. H. Fransson, "Comparison of Models to Predict Low Engine Order Excitation in a High Pressure Turbine Stage," in *10th International Symposium on Unsteady Aerodynamics, Aeroacoustics, and Aeroelasticity in Turbomachines*, 2003.
- [24] W. Ning and L. He, "Computation of Unsteady Flows Around Oscillating Blades Using Linear and Nonlinear Harmonic Euler Method," *Journal of Turbomachinery*, vol. 120, no. July, pp. 508-514, July 1998.
- [25] R. Srivastava, M. A. Bakhle, T. G. J. Keith and G. Stefko, "Aeroelastic Stability Computations For Turbomachinery," Cleveland, OH, 2001.
- [26] J. Marshall and M. Imregun, "A Review of Aeroelasticity Methods with Emphasys on Turbomeachinery Applications," *Journal of Fluids and Structures*, vol. 10, pp. 237-267, 1996.
- [27] D. M. Vogt and T. H. Fransson, "A New Turbine Cascade for Aeromechanical Testing," in *The 16th Symposium on Measuring Techniques in Transonic and Supersonic Flow in Cascades and Turbomachines*, Cambridge, UK, 2002.
- [28] C. E. Meinzer, S. L. Bittner, S. Schmitt, R. E. Kielb and J. R. Seume, "Design of a Single Stage Turbine for the Quantification of Aerodynamic Damping," in *ASME Turbo Expo*, Montreal, Canada, 2015.
- [29] I. McBean, K. Houringan, M. Thompson and F. Liu, "Prediction of Flutter of Turbine Blades in a Transonic Annular Cascade," *Journal of Fluids Engineering*, pp. 1053-1058, 2005.
- [30] V. Gnesin, L. Kolodyazhnaya and R. Rzaǰkowski, "Coupled Aeroelastic Oscillations of a Turbine Blade Row in 3D Transonic Flow," *Journal of Thermal Science* , vol. 10, no. 4, pp. 318-324, 20011.

- [31] R. Rzaḱowski and V. Gnesin, "3-D Inviscid Self-excited Vibrations of a Blade Row in the Last Stage Turbine," *Journal of Fluids and Structures*, vol. 23, pp. 858-873, 2007.
- [32] V. I. Gnesin, L. V. Kolodyazhnaya and R. Rzaḱowski, "A Numerical Modeling of Stator-Rotor Interaction in a Turbine Stage with Oscillating Blades," *Journal of Fluids and Structures*, vol. 19, pp. 1141-1153, 2004.
- [33] V. Carstens, R. Kemme and S. Schmitt, "Coupled Simulation of Flow-Structure Interaction in Turbomachinery," *Aerospace Science and Technology*, vol. 7, pp. 298-306, 2003.
- [34] K. C. Hall, J. P. Thomas and W. S. Clark, "Computation of Unsteady Nonlinear Flows in Cascades Using a Harmonic Balance Technique," *AIAA Journal*, vol. 40, no. 5, pp. 879-886, May 2002.
- [35] R. Srivastava, M. A. Bakhle, T. G. J. Keith and G. Stefko, "Aeroelastic Analysis of Turbomachinery; Part I- Phase Lagged Boundary Condition Methods," *International Journal of Numerical Methods for Heat & Fluid Flow*, vol. 14, no. 3, pp. 366-381, 2004.
- [36] L. He, "Fourier Methods for Turbomachinery Applications," *Progress in Aerospace Sciences*, vol. 46, pp. 329-341, 2010.
- [37] M. I. Platzer and F. O. Carta, "AGARD Manual on Aeroelasticity in Axial-Flow Turbomachines, Vol 2 Structural Dynamics and Aeroelasticity," Seine, France, 1988.
- [38] A. Carrella and D. J. Ewins, "Identifying and quantifying structural nonlinearities in engineering applications from measured frequency response functions," *Mechanical systems and Signal Processing*, vol. 25, pp. 1011-1027, 2011.
- [39] O. O. Bendiksen and G. Seber, "Fluid-Structure Interactions with both Structural and Fluid Nonlinearities," *Journal of Sound and Vibration*, vol. 315, pp. 664-684, 2008.

- [40] R. Corral, J. M. Gallardo and C. Martel, "A Conceptual Flutter Analysis of a Packet of Vanes Using a Mass-Spring Model," *Journal of Turbomachinery*, vol. 131, no. April, pp. 021016-1-021016-7, April 2009.
- [41] C. Martel, R. Corral and R. Ivaturi, "Flutter Amplitude Saturation by Nonlinear Friction Forces: Reduced Model Verification," *Journal of Turbomachinery*, vol. 137, pp. 041004-1-041004-8, Apr. 2015.
- [42] C. A. Coulomb, "Theorie des machines simple (Theory of simple machines)," Bachelier, Paris, 1821.
- [43] P. R. Dahl, "A Solid Friction Model," The Aerospace Corporation, 1968.
- [44] E. P. Petrov and D. J. Ewins, "Generic Friction Models for Time-Domain Vibration Analysis of Bladed Disks," *Journal of Turbomachinery*, vol. 126, no. January, pp. 184-192, January 2004.
- [45] E. P. Petrov and D. J. Ewins, "Analytical Formulation of Friction Interface Elements for Analysis of Nonlinear Multi-Harmonic Vibrations of Bladed Disks," *Journal of Turbomachinery*, vol. 125, no. April, pp. 364-371, April 2003.
- [46] D. Peric and D. R. Owen, "Computational Model for 3-D Contact Problems with Friction Based on the Penalty Method," *International Journal for Numerical Method in Engineering*, vol. 35, pp. 1289-1309, 1992.
- [47] J. C. Simo and T. A. Laursen, "An Augmented Lagrangian Treatment of Contact Problems Involving Friction," *Computers and Structures*, vol. 42, pp. 97-116, 1992.
- [48] C. Schwingshackl, E. P. Petrov and D. J. Ewins, "Measured and Estimated Friction Interface Parameters in a Nonlinear Dynamic Analysis," *Mechanical Systems and Signal Processing*, vol. 28, pp. 574-584, 2012.

- [49] E. P. Petrov and D. J. Ewins, "Effects of Damping and Varying Contact Area at Blade-Disk Joints in Forced Response Analysis of Bladed Disk Assemblies," *Journal of Turbomachinery*, vol. 128, no. April, pp. 403-410, April 2006.
- [50] E. P. Petrov and D. J. Ewins, "Method for Analysis of Nonlinear Multiharmonic Vibrations of Mistuned Bladed Disks With Scatter of Contact Interface Characteristics," *Journal of Turbomachinery*, vol. 127, no. January, pp. 128-136, January 2005.
- [51] C. Schwingshackl, E. P. Petrov and D. Ewins, "Effects of Contact Interface Parameters on Vibration of Turbine Bladed Disks with Underplatform Dampers," *Journal of Engineering for Gas Turbines and Power*, vol. 134, no. March, pp. 032507-1-032507-8, March 2012.
- [52] M. Allara, "A Model For the Characterization of Friction Contacts in Turbine Blades," *Journal of Sound and Vibration*, vol. 320, pp. 527-544, 2009.
- [53] J. H. Griffin, "Friction Damping of Resonant Stresses in Gas Turbine Engine Airfoils," *Journal of Engineering for Power*, vol. 102, pp. 329-333, April 1980.
- [54] A. Sinha and J. H. Griffin, "Effects of Static Friction on the Forced Response of Frictionally Damped Turbine Blades," *Journal of Engineering for Gas Turbines and Power*, vol. 106, pp. 65-69, January 1984.
- [55] C. Breard, J. S. Green, M. Vahdati and M. Imregun, "A Non-linear Integrated Aeroelasticity Method for the Prediction of Turbine Forced Response with Friction Dampers," *International Journal of Mechanical Sciences*, vol. 43, pp. 2715-2736, 2001.
- [56] A. I. Sayma, M. Vahdati and M. Imregun, "An Integrated Nonlinear Approach for Turbomachinery Forced Response Prediction. Part I: Formulation," *Journal of Fluids and Structures*, vol. 14, pp. 87-101, 2000.

- [57] M. Vahdati, A. I. Sayma and M. Imregun, "An Integrated Nonlinear Approach for Turbomachinery Forced Response Prediction. Part II: Case Studies," *Journal of Fluids and Structures*, vol. 14, pp. 103-125, 2000.
- [58] E. P. Petrov and D. J. Ewins, "Advanced Modeling of Underplatform Friction Dampers for Analysis of Bladed Disk Vibration," *Journal of Turbomachinery*, vol. 129, pp. 143-150, 2007.
- [59] E. Cigeroglu, N. An and C. H. Menq, "Forced Response Prediction of Constrained and Unconstrained Structures Coupled Through Frictional Contacts," *Journal of Engineering for Gas Turbines and Power*, vol. 131, no. March, pp. 022505-1-022505-11, March 2009.
- [60] J. Griffin, W.-T. Wu and Y. EL-Aini, "Friction Damping of Hollow Airfoils: Part I-Theoretical Development," *Journal of Engineering for Gas Turbines and Power*, vol. 120, pp. 120-125, January 1998.
- [61] Y. M. EL-Aini, B. K. Benedict and W.-T. Wu, "Friction Damping of Hollow Airfoils: Part II- Experimental Verification," *Journal of Engineering for Gas Turbines and Power*, vol. 120, pp. 126-130, January 1998.
- [62] J. H. Griffin and A. Sinha, "The Interaction Between Mistuning and Friction in the Forced Response of Bladed Disk Assemblies," *Journal of Engineering for Gas Turbines and Power*, vol. 107, pp. 205-211, January 1985.
- [63] A. Sinha, J. Griffin and R. E. Kielb, "Influence of Friction Dampers on Torsional Blade Flutter," *Journal of Engineering for Gas Turbines and Power*, vol. 108, pp. 313-318, April 1986.
- [64] A. Sinha and J. H. Griffin, "Effects of Friction Dampers on Aerodynamically Unstable Rotor Stages," *AAIA Journal*, vol. 23, no. 2, pp. 262-270, 1985.

- [65] R. Srivastava, M. A. Bakhle, T. G. J. Keith and D. Hoyniak, "Aeroelastic Analysis of Turbomachinery; Part II- Stability Computations," *International Journal of Numerical Methods for Heat & Fluid Flow*, vol. 14, no. 3, pp. 382-402, 2004.
- [66] I. Lee, S. Shin and Y. Kim, "Mistuned Bladed Disk Forced Vibration Analysis Based on Standing Wave Formulation," *Aerospace Science and Technology*, vol. 24, pp. 275-282, 2013.
- [67] A. V. Srinivasan and D. G. Cutts, "Dry Friction Damping Mechanisms in Engine Blades," *Journal of Engineering for Power*, vol. 105, pp. 332-341, April 1983.
- [68] C. H. Menq, J. H. Griffin and J. Bielak, "The Influence of a Variable Normal Load on the Forced Vibration of a Frictionally Damped Structure," *Journal of Engineering for Gas Turbines and Power*, pp. 300-305, April 1986.
- [69] B. D. Yang and C. H. Menq, "Modeling of Friction Contact and Its Application to the Design of Shroud Contact," *Journal of Engineering for Gas Turbines and Power*, vol. 119, pp. 958-963, October 1997.
- [70] B. D. Yang, J. Chen and C. H. Menq, "Prediction of Resonant Response of Shrouded Blades with Three Dimensional Shroud Constraints," *Journal of Engineering for Gas Turbines and Power*, vol. 121, pp. 523-529, July 1999.
- [71] J. Chen and C. H. Menq, "Periodic Response of Blades Having Three Dimensional Nonlinear Shroud Constraints," *Journal of Engineering for Gas Turbines and Power*, vol. 123, pp. 901-906, October 2001.
- [72] E. Bazen, J. Bielak and J. H. Griffin, "An Efficient Method for Predicting the Vibratory Response of Linear Structures with Friction Interfaces," *Journal of Engineering for Gas Turbines and Power*, vol. 108, pp. 633-640, October 1986.

- [73] J. H. Wang and W. K. Chen, "Investigation of the Vibration of a Blade with Friction Dampers by HBM," *Journal of Engineering for Gas Turbines and Power*, vol. 115, pp. 294-299, April 1993.
- [74] T. M. Cameron and T. H. Griffin, "An Alternating Frequency/Time Domain Method for Calculating the Steady-State response of Nonlinear Dynamic Systems," *Journal of Applied Mechanics*, vol. 56, pp. 149-154, March 1989.
- [75] J. Guillen and C. Pierre, "An Efficient, Hybrid, Frequency-Time Domain Method for the Dynamics of Large-Scale Dry-Friction Damped Structural Systems," in *17th Biennial Conference on Mechanical Vibration and Noise*, Las Vegas, NV, 1999.
- [76] S. Patil, L. Zori, P. Galpin, J. C. Morales and P. Godin, "Investigation of Time/Frequency Domain CFD Methods to Predict Turbomachinery Blade Aerodynamic Damping," in *ASME TurboExpo*, Seoul, South Korea, 2016.
- [77] A. Torkaman, G. Vogel, S. Fiebiger, D. Dietrich and R. Washburn, "GAS TURBINE CYCLE UPGRADE AND VALIDATION FOR HEAVY DUTY INDUSTRIAL MACHINES," in *Proceedings of ASME Turbo Expo 2017*, Charlotte, NC, USA, 2017.